

# Effects of fentanyl on the cortical activity of neonates

---

Timo Vehviläinen

# Effects of fentanyl on the cortical activity of neonates

**Timo Vehviläinen**

Thesis submitted in partial fulfillment of the requirements for  
the degree of Master of Science in Technology.  
Otaniemi, Day Month 2019

Supervisor: Prof. Lauri Parkkonen  
Advisors: Prof. Sampsu Vanhatalo  
PhD. Anton Tokarev

**Aalto University  
School of Science  
Master's Programme in Life Science Technology**

**Author**

Timo Vehviläinen

**Title**

Effects of fentanyl on the cortical activity of neonates

**School** School of Science**Master's programme** Life Science Technology**Major** Human Neuroscience & Technology**Code** SCI3601**Supervisor** Prof. Lauri Parkonen**Advisors** Prof. Sampsa Vanhatalo, PhD. Anton Tokariev**Level** Master's thesis    **Date** November 25<sup>th</sup> 2019    **Pages** 69    **Language** English**Abstract**

**Background** Fentanyl is a widely used analgesic in neonatal intensive care, but its full effects on cortical activity have been left largely uninvestigated. The target of this thesis was to use statistical analysis of computational electroencephalography (EEG) features to identify any short-term effects of fentanyl on the brain state of neonates.

**Methods** EEG recordings from 15 neonate subjects treated with fentanyl (0.5–2 µg/kg) were examined in a single-arm trial, using a set of 9 different analytic features measuring power, spectral density, nestedness, synchrony in transients and power between brain areas, fractal dimensions, and continuity of the signal. Changes in these features within the first 10min post-drug period were evaluated for significance using visual inspection of time trends, Wilcoxon signed-rank testing, and testing for correlation (Spearman's  $\rho$ ) between individual baselines and changes in feature values.

**Results** Testing for correlation between individual baselines and feature changes revealed significant ( $p < 0.05$ ) and negative correlation ( $\rho < -0.5$ ) in peak-to-peak amplitudes and general power levels over all measured frequency ranges ([1–30] Hz) in the right hemisphere and parietal areas. We also observed declining of power coupling in all brain areas. These effects started from 3–4min after fentanyl administration and lasted for the duration of the experiment. Transient nestedness of [3–8] Hz frequencies showed lessening in the right hemisphere immediately after administration, lasting for the duration of the experiment. Other features measured showed no significant changes in correlation values. Time trend inspection and Wilcoxon signed-rank testing displayed no discernible effects.

**Conclusions** Fentanyl causes general lessening of the EEG signal in neonates shortly after administration in multiple brain areas, and weakens overall power correlation. We found the usage of individualistic & statistical baseline assignment and baseline-to-change correlation testing to be crucial for determining of these effects. This might be due to the method's tolerance towards non-linear effects on non-negative features and missing data.

**Keywords** electroencephalography, fentanyl, drug, neonate, analgesic

**Tekijä**

Timo Vehviläinen

**Työn nimi**

Fentanylin vaikutukset vastasyntyneiden aivotoimintaan

**Korkeakoulu** Perustieteiden korkeakoulu**Maisteriohjelma** Life Science Technology**Pääaine** Human Neuroscience & Technology**Koodi** SCI3601**Valvoja** Prof. Lauri Parkkonen**Ohjaajat** Prof. Sampsa Vanhatalo, FT Anton Tokariev**Työn laji** Diplomityö**Päiväys** 25.11.2019**Sivuja** 69**Kieli** englanti**Tiivistelmä**

**Taustatietoa** Fentanylin kokonaisvaltaisia vaikutuksia aivotoiminnan eri tasoihin ei ole kartoitettu, vaikka fentanyilia käytetään jatkuvasti kipulääkkeenä mm. vastasyntyneiden teho-osastolla. Tämän työn tarkoituksesta on selvittää, miten fentanylin vaikutukset ovat laskennallisesti havaittavissa vastasyntyneiden aivosähkökäyrästä (EEG).

**Tutkimusmenetelmät** 15:n poikkileikkaustutkimussa fentanyyllilla hoidetun vastasyyneen ( $0.5\text{--}2 \mu\text{g/kg}$ ) aivosähkökäyrästä laskettiin yhdeksän ominaista arvoa, joiden avulla mitattiin amplitudia, taajuustiheyttä, signaalien pesiytyvyyttä, lyhytaikaisten ilmiöiden samanaikaisuutta, taajuusvoimakorrelatiota aivoalueiden välillä sekä signaalien fraktaaliulottuuksia ja jatkuvuutta. Näiden arvojen muutoksienvilistä tilastollista merkityksellisyyttä mitattiin ensimmäisen 10:n minuutin aikana fentanyyllilla lääkitsemisestä. Näissä mittauksissa käytettiin datan visuaalista arvointia sekä Wilcoxonin merkityjen sijalukujen testiä ja Spearmanin korrelaatiokerrointa yksilöllisten pohja-arvojen ja arvomuutoksen välillä.

**Tulokset** Pohja- ja muutosarvojen välillä havaittiin merkitsevä ( $p < 0.05$ ) ja negatiivista ( $\rho < -0.5$ ) korrelatiota niin huipusta-huippuun amplitudissa kuin voiman spektrin heydessä kaikilla mitatuilla kaistataajuuksilla ([1–30] Hz) oikeassa aivopuoliskossa sekä pääläenlohkossa. Kaikilla aivoalueilla havaittiin myös keskinäisen taajuusvoimakorrelaation vähemistä. Vaikutukset alkivat n. 3–4min lääkityksen alkamisen jälkeen, ja kestivät kokeen loppuun saakka. Lyhytaikaisten aaltojen pesiytyvyydessä havaittiin ale-nemista [3–8] Hz:n taajuuksilla oikeassa aivopuoliskossa heti lääkityksen alettua, mikä jatkui kokeen loppuun saakka. Muissa arvoissa ei havaittu merkitsevä korrelatiota. Datan visuaalinen tarkistelu eikä Wilcoxonin merkityjen sijalukujen testikään tuottanut merkitseviä tuloksia.

**Johtopäätökset** Fentanyl aiheuttaa vastasyntyneissä yleistä EEG-signaalin vähemistä useilla aivoalueilla, vähentäen myös yleistä voimataajuuskorrelatiota. Tutkimuksemme mukaan yksilöllisten sekä tilastollisesti määritettyjen pohja-arvojen käyttö parantaa vertailutestien voimaa. Tämä saattaa johtua puuttuvien arvojen sivuuttamisen ja epä-lineaaristen vaikutusten löytämisen hyödyllisyystä.

**Avainsanat** aivosähkökäyrä, fentanyl, lääkeaine, vastasyntynyt, analgeesi

# Preface

I wish to thank my advisors Sampsa Vanhatalo & Anton Tokarev at BABACenter for all the support and guidance they have provided me with towards the successful completion of this thesis, bringing a most formative period of my life to a satisfying and meaningful finale.

My most heartfelt gratitude belongs to all the wonderful people sharing the ride alongside me, including my friends at The Polytech Choir, Teekkarispeksi and Inkubio; my many families away from home. It is thanks to all the music, camaraderie and unabashedly good times we've shared, that I can say my twenties were more than mere living.

# Contents

<b>Abstract</b>	ii
<b>Tiivistelmä</b>	iii
<b>Preface</b>	iv
<b>Contents</b>	v
<b>1. Introduction</b>	1
<b>2. Background</b>	2
2.1 The Neonatal Intensive Care Unit . . . . .	2
2.2 Fentanyl . . . . .	2
2.3 Electroencephalography . . . . .	3
2.4 Analysis of EEG data . . . . .	4
2.5 Neonatal EEG . . . . .	6
<b>3. Materials &amp; Methods</b>	8
3.1 The data set & montage construction . . . . .	8
3.2 Pre-processing . . . . .	10
3.3 Data epoching . . . . .	12
3.4 Computational features & methods . . . . .	13
3.4.1 Activation Synchrony Index . . . . .	14
3.4.2 Weighted Phase Lag Index (wPLI) . . . . .	16
3.4.3 Nestedness Coefficient . . . . .	18
3.4.4 Power Spectral Density & Cross Power Spectral Density	19
3.4.5 Multifractal Detrended Fluctuation Analysis . . . . .	20
3.4.6 Amplitude-integrated EEG . . . . .	23
3.4.7 Range-EEG . . . . .	23
3.4.8 Suppression Curve . . . . .	23

3.5	Statistical analysis . . . . .	24
3.5.1	Absolute time trend . . . . .	26
3.5.2	Baseline assignment & Relative time trend . . . . .	26
3.5.3	Wilcoxon signed-rank test . . . . .	28
3.5.4	Baseline–delta correlation & Spearman’s rank-order correlation . . . . .	31
<b>4.</b>	<b>Results</b>	<b>36</b>
4.1	Artifact percentage . . . . .	36
4.2	Time trends . . . . .	36
4.3	Wilcoxon signed-rank . . . . .	36
4.4	baseline–delta correlation . . . . .	37
<b>5.</b>	<b>Discussion</b>	<b>39</b>
5.1	General observations . . . . .	39
5.2	Technical limitations and strengths . . . . .	40
5.3	Future prospects . . . . .	41
<b>6.</b>	<b>Conclusions</b>	<b>42</b>
	<b>Bibliography</b>	<b>43</b>
	<b>A. Statistical Analysis Results</b>	<b>48</b>
	<b>B. Artifact Percentage Table</b>	<b>68</b>

# Symbols & Abbreviations

## Symbols

$\tau$	Time lag
$j$	Imaginary unit
$P_\tau(a, b)$	Joint probability
$\theta(a, b)$	Phase difference
$E$	Expected value
$\sum$	Sum
$W$	Sum of ranked values
$R$	Sum of ranks
$F_q(s)$	Fluctuation function
$D(q)$	q-order singularity dimension
$H(q)$	q-order Hurst component
$h(q)$	q-order singularity exponent
$\sigma$	Standard deviation
$r$	Pearson's correlation coefficient r
$\rho$	Spearman's rank-order correlation coefficient rho
$\Delta$	Delta values

## Abbreviations

aEEG	Amplitude-integrated Electroencephalography
APT	Artifact Percentage Threshold
ASI	Activation Synchrony Index
BL	Baseline epoch
CA	Conceptual Age
cPSD	Cross Power Spectral Density
CRA	Chronological Age a.k.a. legal age
DFA	Detrended Fluctuation Analysis
EDTF	Energy-Weighted Temporal Dependency Function
EEG	Electroencephalography
FDR	False Discovery Rate
FE	post-drug epoch feature value
FFT	Fast Fourier Transform
fMRI	Functional Magnetic Resonance Imaging
FWER	Familywise Error Rate
GA	Gestational Age
GPCR	G-Protein–Coupled Receptor
Hz	Hertz
IBI	Inter-Burst Interval
IQR	Inter-Quartile Range
LI	Lower 5 <sup>th</sup> Index
MFdfa	Multifractal Detrended Fluctuation Analysis
MOP	$\mu$ -Opioid Receptor
NICU	Neonatal Intensive Care Unit
NC	Nestedness Coefficient
PLI	Phase Lag Index
PLV	Phase Locking Value
PSD	Power Spectral Density
rEEG	Range-Electroencephalography
REST	Reference Electrode Standardization Technique
SAT	Spontaneous Activity Transient
SC	Suppression Curve
wPLI	Weighted Phase Lag Index

# 1. Introduction

Preterm birth complications continue to be a globally leading cause of child mortality in infants under the age of 5, responsible for around 1 million deaths each year [1]. The quality of care for these cases and for otherwise ill full-term babies in neonatal intensive care units keeps rising. But even as child mortality rates keep dropping, more and more children are being admitted to intensive care [2]. This increases demand for more comprehensively understanding the effects of neonatal care to the child.

Many of the treatment methods in the neonatal intensive care unit are physiologically stressful for the infant. Consequently, they are often treated with drugs to produce anesthesia and/or analgesia in order to improve comfort and success rate of various procedures. Fentanyl, an agonist to the  $\mu$ -opioid receptor, is a strong analgesic that is used often for its relatively rapid onset and half-life, as well as reduced adverse effects on pulmonary and hemodynamic function compared to similar drugs [3]. Despite its ubiquitous use, targeted studies towards the effects of fentanyl on the cerebrocortical activity of human neonates have been limited to just a few methods of inquiry.

The aim of this study was to investigate the existence of detectable short-term effects caused by intravenous fentanyl administration in a set of 9 computational features extracted from neonate EEG signal. The data included four-channel EEG data from 15 human neonate subjects, which were treated with fentanyl before undergoing painful treatment. The last 5 minutes of EEG data before drug administration were used for baseline calculations, and the first 10 minutes after administration were scoured for any noticeable changes in several modes of statistical inquiry.

Both Samuli Suvisto's and Juulia Jaatela's theses titled "Effects of Dexmedetomidine on the cortical activity of neonates" and "Computational features of neonatal EEG monitoring after asphyxia" were used as a baseline and roughly followed for the applicable parts when carrying out the studies for this thesis. [4, 5].

## 2. Background

This section introduces general knowledge in the purview of this study. This includes information about neonatal care, properties of fentanyl, and basics of both neonatal and general electroencephalography analysis.

### 2.1 The Neonatal Intensive Care Unit

The Neonatal Intensive Care Unit (NICU) specializes in treating and monitoring newly-born critically ill or premature infants. Reasons behind the neonate requiring intensive care include difficulties in breathing, infections or birth defects, neurological disorders, labor complications or problems caused by the mother's disease [6].

Due to the stress caused by treatment procedures, it is standard practice for the infant in a non-emergency case to be medicated preceding the procedure. Commonly used medications include various mixtures of sedatives, analgesics, anesthetics and muscle relaxants. The use of these medications ensures comfort, attenuates the risk of adverse physiological consequences and reduces both the number of attempts and the time required for successful procedures. [7, 8]

### 2.2 Fentanyl

Opioids are very commonly used in the modern NICUs [9]. Fentanyl is a strong synthetic opioid, that is used by itself as an analgesic and with other drugs as an anesthetic. Fentanyl is able to be administered in many ways via transdermal patches, oral tablets, transnasal sprays or intravenous injections [10]. Like other opioids of its ilk, fentanyl functions by activating opioid receptors located in the central and peripheral nervous system. Fentanyl specifically targets a G-protein-coupled receptor (GPCR) called the  $\mu$ -opioid receptor (MOP). The activation of these receptors initiates a chain reaction inside the synaptic nerve, which results

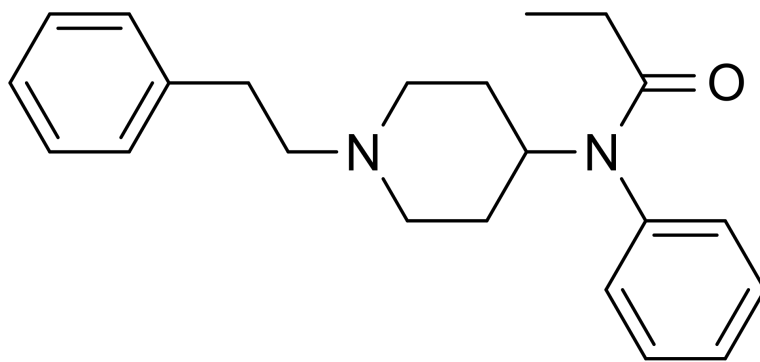


**Figure 1.** A diagram of the chemical structure of fentanyl.

in inhibition of nerve activity. [11–13].

Fentanyl is a preferred drug in the NICU due to the relatively rapid rise and fall in its effectiveness when using small doses intravenously [14]. Fentanyl is 50–100 times stronger than morphine—another commonly used analgesic opioid—which allows for it to be used in quantities of micrograms ( $\mu\text{g}$ ) instead of milligrams (mg) [15, 16]. Although study results differ, fentanyl has in some cases been shown to have lesser adverse side-effects when compared to morphine in terms of hypotension, decreased gastrointestinal motility and myocardial depression. [17–20]

A diagram of the chemical structure of fentanyl can be seen in Figure 1.

### 2.3 Electroencephalography

Electroencephalography (EEG) is a non-invasive method for measuring brain activity in the cerebral cortex by recording microvolt-sized ( $\mu\text{V}$ ) fluctuations of electrical potential on the scalp. These potentials originate from a large number of post-synaptic action potentials in the outer-most brain tissue, which—when positioned spatially close together, directionally parallel and are temporally synchronized—summate into a potential that is strong enough to be detected on the scalp with electrodes via volume conduction through the skin, the skull and other obstructing layers. As volume conduction occurs radially from the each source, the signal recorded by each electrode is a spatially weighted sum of the electrical activity within its vicinity. Depending on how close adjacent electrodes are to each other, the same source can also affect measurements in multiple electrodes. [21, 22]

The fluctuations recorded at each position are recorded in comparison to a common, electrically neutral reference. Typically used physical references include the vertex of the head, the nose, and the ears. Virtual referencing methods are also possible, such as reference electrode standardization technique (REST) or infinity reference technique. [23]

Although effects of noisy volume conduction can be lessened with various signal analysis methods, the spatial resolution of EEG is limited by the number of electrodes used. However, its temporal sampling resolution is one of the best among methods in neuro-imaging, reaching real-time detail in the millisecond (ms) range. [24]

While the number of electrodes used can vary depending on the situation, their placement usually follows an international 10–20 system, where electrodes are placed with the help of anatomic landmarks found in the skull. This accommodates for differences in head sizes and shapes. An illustration of the 10–20 system can be found in Figure 2. [25, 26]

## 2.4 Analysis of EEG data

Through its uniquely defined location, each electrode provides a different perspective view into the electric landscape of the brain. Full EEG is data is the combined collection of all these data stream channels, each of which is named after its respective electrode in the 10–20 system.

The form of the signal in each channel is a time series waveform of electric potential. Methods of EEG analysis usually focus on three main components of this time series: frequency, amplitude and phase. Moreover, because of the unpredictable and stochastic nature of the signal, analytic descriptions are determined by statistically analysing its general characteristics over some time period of arbitrary length. This is to produce figures that are roughly statistically comparable to each other despite the inherent randomness. Several established parametric and non-parametric methods exist for the purposes of extracting useful interpretations from EEG data, such as connectivity and rhythm. [27]

The EEG signal includes information from across the whole frequency spectrum. Only a part of the spectrum, however, is thought to contain clinically useful information pertaining to neuroelectrical sources. For analytic purposes, the EEG frequency spectrum is conventionally divided roughly into the frequency bands described in Table 1.

Amplitudes measured within a normal adult EEG signal lie typically in the range of [10–100]  $\mu\text{V}$  [28]. Neonatal EEG amplitudes can reach multiple hundred  $\mu\text{V}$ .

The appearance of artifacts are common in clinical EEG. An artifact is any electrical potential recorded by an electrode which does not originate in the brain. The true source of these artifacts may be either physiological or non-physiological. Physiological artifacts are caused by non-neurological functioning of

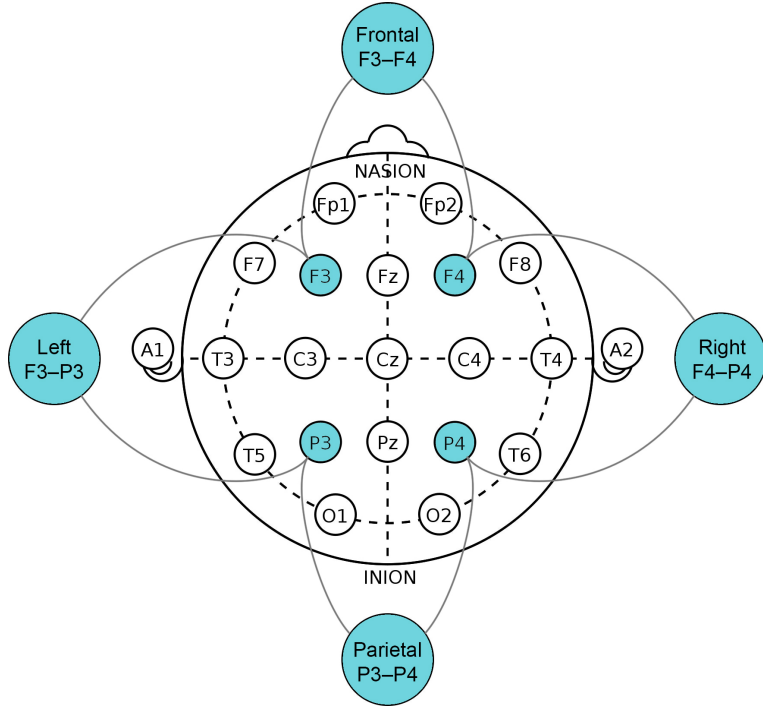


**Figure 2.** An illustration of the 10–20 system of electrode placements. The four monopolar electrode channels and four bipolar channel montages used in this study are highlighted in blue.

Frequency band [Hz]	band name
~[0.1–4]	delta ( $\delta$ )
~[0.4–8]	theta ( $\theta$ )
~[8–13]	alpha ( $\alpha$ )
~[14–40]	beta ( $\beta$ )
>~40	gamma ( $\gamma$ )

**Table 1.** Conventional nomenclature for the different frequency bands discussed in EEG literature [28]. Exact frequency boundaries vary slightly in use.

the human body, such as muscle or eye movement and cardiovascular activity. Non-physiological artifacts are caused by electromagnetic fields outside the subject's body. These fields may originate almost anywhere, most commonly from objects touching the electrode, power lines, other medical equipment or from general movement in the environment. These artifacts can also be categorized by their duration into either transient or continuously persistent types. [29–31]

Previous analysis has proven EEG signal attributes to be sensitive towards being modulated by drugs, visibly e.g. via increased power in specific frequency bands and depression of background activity [32]. Fentanyl specifically has been shown to slow down the EEG signal in adults, decreasing power in the  $\alpha$ -band and increasing it in the  $\delta$ -band [33, 34].

## 2.5 Neonatal EEG

The neonatal brain—and the preterm brain to an even greater extent—has analytic characteristics that distinguish it from the adult brain. The connectivity of the brain is at its highest in the first weeks of the post-natal period, with approximately 100 billion neurons and 100 trillion connections between them [35]. The organization of neuronal networks is regulated by a cortical zone unique to the pre-natal & natal stage in brain development called the subplate, which disappears after the neonatal stage [36].

Due to the dynamic nature of cortical development, neonatal brain measurements are often parameterized in terms of the baby's gestational age (GA, defined as the time between conception and birth), chronological age (CRA, defined as the time between birth and measurement) and/or conceptional age (CA, defined as GA plus CRA). When interpreting neonatal EEG, it is generally assumed that the immature brain develops similarly relative to its CA whether in utero or ex utero. This allows for qualitative comparison of EEG results from prematurely born babies with CRA of a few weeks and full-term babies with CRA of few days. [37]

The signature characteristic of a normal EEG signal of the prenatal stage is the presence of so-called spontaneous activity transients (SAT), also known by many other names such as "spindles", "beta-delta complexes" or "brushes" [37].

SATs manifest themselves in the signal as large ( $> 100\mu\text{V}$ ) and fast ([15–30] Hz) oscillatory bursts nesting in slower frequencies ([0.1–4] Hz) and lasting multiple seconds [38]. They are believed to be caused by processes integral to correct development of connections between brain areas. As CA increases, SATs become more synchronous across the brain while also getting more infrequent, eventually disappearing completely. The degree of SAT synchrony can also be used to

determine REM-sleep states (most synchronous) from non-REM sleep states (least synchronous). [39]

Because fluctuations in the density of SATs are visually very apparent, neonatal EEG signal is often parsed as a landscape of discontinuous periods (high SAT density) inter-mixed with increasing periods of continuity (little to no SATs) as the baby matures. Discontinuous periods are further qualitatively judged by measuring gaps of time between consecutive SATs, or so-called inter-burst intervals (IBI). IBIs have been shown to get smaller during cortical development. [40]

### **3. Materials & Methods**

This section includes an introduction to the data, as well as to the methods used for assessing the effects of fentanyl on neonates. The entire process pipeline consists of five separate stages:

1. All the required channel montages are constructed from the original EEG data.
2. The acquired montages are cleaned and pre-processed to avoid erroneous effects in the further stages.
3. After cleaning, the data montages are split into smaller time periods, or epochs.
4. Multiple different computational analytic features are calculated from the epochs.
5. The acquired sets of features are statistically tested in order to determine whether the introduction of fentanyl causes any changes in the brain.

These stages are detailed in subsections 3.1–3.5. A full overview of the processing pipeline is illustrated in Figure 3. All processing was implemented in MATLAB 2019a.

#### **3.1 The data set & montage construction**

The data consisted of four-channel EEG recordings of 15 neonates that were under 28 days old (CRA), and was collected in a single-arm trial at Lund University between the dates from September 18<sup>th</sup> 2012 to November 12<sup>th</sup> 2014. The subjects were administered with pre-diluted 5 µg/ml fentanyl ampoules preceding a painful procedure. The procedure in question was either light skin breaking procedure (anticipated medium pain), or one of tracheal intubation or pleural drainage (anticipated strong pain).

Those treated with the light skin breaking procedure received fentanyl with a

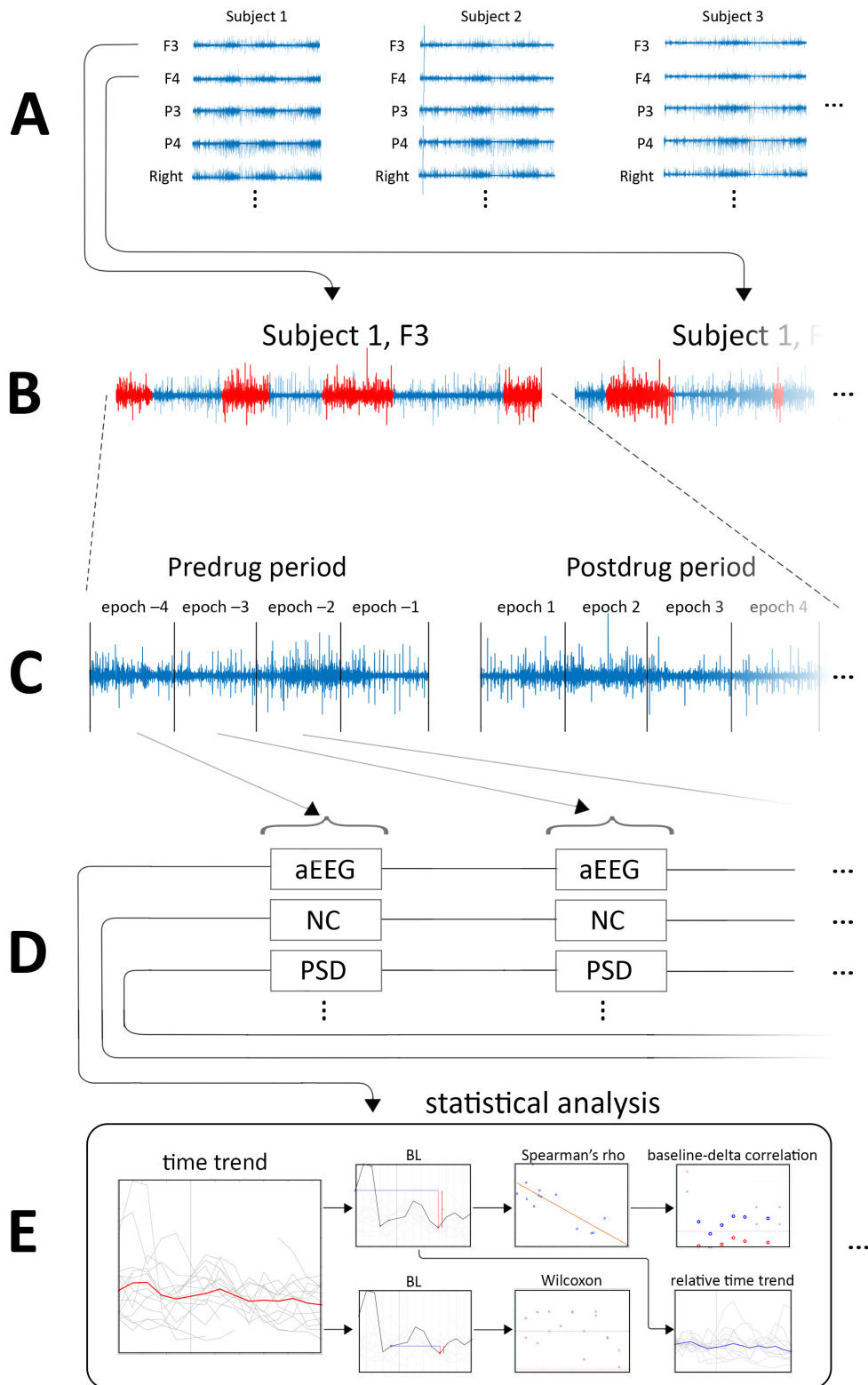


**Figure 3.** This flowchart illustrates the entire analysis process for this thesis. Starting with the original data (**A**) that is divided into 8 different channel montages, we first go through artifact removal and other pre-processing(**B**, illustrated in more detail in Figure 4). Next, we divide each recording into pre-drug and post-drug periods, and further into epochs of a designated duration (**C**). From these epochs, we calculate various different features (**D**), which together with the same features from different epochs make up a feature continuum. Finally, we perform statistical analysis and timeline inspections on these feature continuums of the data (**E**, illustrated in more detail in Figure 9).

dose of  $0.5 \mu\text{g}$  per kilogram of bodyweight, administered over 1 minute, starting at 3-5 minutes before the procedure. Subjects treated with either tracheal intubation or pleural drainage received fentanyl with a dose of  $2 \mu\text{g}/\text{kg}$ , administered over 10 minutes just before the start of the procedure. Repeated doses or complementary analgesics were administered according to the pain assessment and clinical judgement of the clinicians involved.

Most of the subjects had at least 30 minutes of recorded EEG-signal before drug administration, with the exception of one who had less than 14 minutes of recorded pre-drug data. All of the subjects had at least 2 hours of post-drug EEG signal recorded after drug administration.

The four EEG channels recorded were:

- Left frontal channel F3
- Right frontal channel F4
- Left parietal channel P3
- Right parietal channel P4

The location of these electrodes on the scalp is illustrated in Figure 2. All four channels shared a frontal mid-line point as their reference. All recordings had a sampling frequency of 250 Hz.

In addition to these four monopolar channels, the following four additional bipolar channel montages were constructed as a subtraction of two of the monopolar channels:

- F3–P3 (Left hemisphere)
- F4–P4 (Right hemisphere)
- F3–F4 (Frontal lobe)
- P3–P4 (Parietal lobe)

This resulted in a total of 8 EEG signals per subject. This stage represents the A-section of Figure 3.

### 3.2 Pre-processing

Most of the recordings were visually determined to include artifacts. The periods with a heavy concentration of artifacts were annotated by hand for each monopolar channel. The data was also treated with an automated pre-processing pipeline,

which detected any samples exceeding an absolute value of  $\pm 1000 \mu\text{V}$  as artifacts. Samples included in either the hand-picked or auto-detected artifact regions were set to 0. Then the signals were globally band-pass-filtered to a range of [0.2–30] Hz. Artifact removal was done before filtering in order to prevent envelope edge effects, which might introduce new ringing artifacts. If a given sample was considered corrupted in a monopolar electrode channel, it was also marked as corrupted in all of the bipolar montages in which that electrode was a constituent.

The band-passing was implemented with a 5<sup>th</sup> order Butterworth 0.2 Hz high-pass filter and a 7<sup>th</sup> order Butterworth 30 Hz low-pass filter, which were filtered in both forward and reverse direction to avoid phase shifting. The signal was mirrored on both sides before filtering to avoid edge effects, and the reflections were removed after filtering.

The effects of artifact removal and filtering represent section B of Figure 3, and are illustrated with more detail in Figure 4.

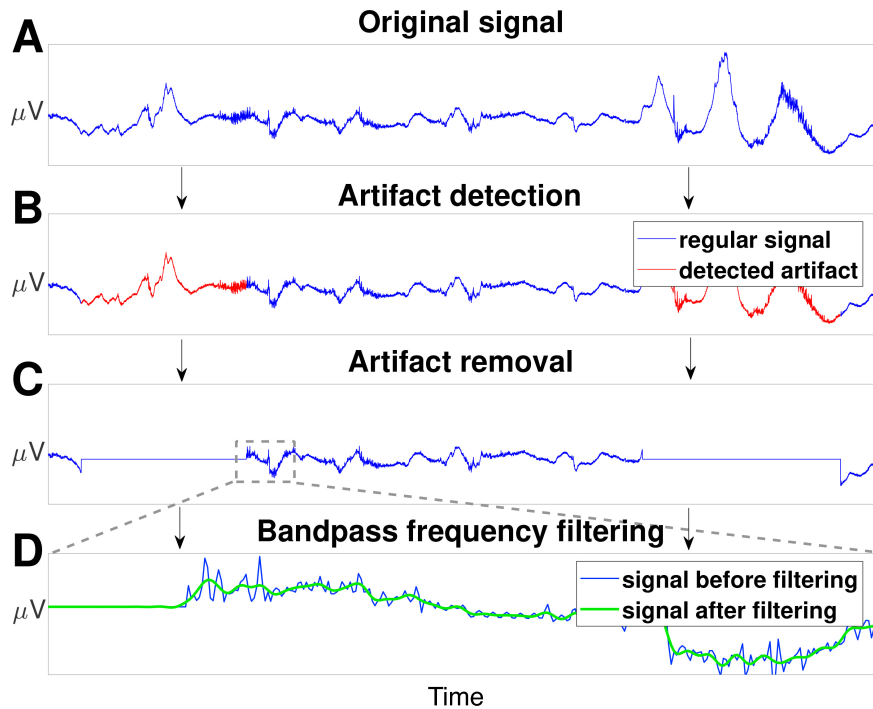


**Figure 4.** This image illustrates the process of pre-processing and cleaning the data. From the original data (**A**), areas are marked as artifacts, both by hand and via an automatic amplitude gate (areas marked with red in **B**). These areas are removed from consideration by setting them to zero (**C**). Finally, the data is band-passed into a range of [0.2–30] Hz. A magnified picture displays the smoothing effect of high-pass filtering the data (**D**).

### 3.3 Data epoching

Each channel recording was divided into two time periods at the point of fentanyl administration:

1. a pre-drug time period before fentanyl administration
2. a post-drug time period after fentanyl administration

These time periods were further divided into 2-minute sized epochs, with 1 minute of overlap between adjacent epochs. A simplified version of this (without the overlapping) is illustrated in the C-section of Figure 3. Any remainder data left over from this procedure was discarded either from the beginning of the pre-drug time period or from the end of the post-drug time period.

Because the goal of this study was to examine mainly the short-term effects of fentanyl, the data was trimmed to include only the last 5 pre-drug epochs and the first 10 post-drug epochs, concentrating attention on a 30-minute period around the moment when fentanyl was first administered.

### 3.4 Computational features & methods

A selection of 9 computational features were calculated for each epoch of EEG data. Depending on the feature, these calculations were done for each channel separately, a subset of all the channels, or as a combination of some of the channels. For some of the features, the data was further filtered into multiple band-passed versions before feature calculation. The full lists of channel selections and filters for each feature are listed in Table 2.

The features used can be roughly categorized into three groups in terms of what they are measuring:

1. Features measuring synchrony:

- **Activation Synchrony Index (ASI)** for amplitude-amplitude correlation,
- **Weighted Phase Lag Index (wPLI)** for phase-phase correlation, and
- **Nestedness Coefficient (NC)** for phase-amplitude correlation.

2. Feature measuring power-based effects:

- **Power Spectral Density (PSD)** and
- **Cross Power Spectral Density (cPSD)** for spectral analysis,
- **Amplitude-integrated EEG (aEEG)** and
- **Range-EEG (rEEG)** for peak-to-peak measurement

3. Other miscellaneous features:

- **Multifractal Detrended Fluctuation Analysis (MFDFA)**,
- **Suppression Curve (SC)**

This feature extraction represents the D-section of Figure 3. In subsections 3.4.1–3.4.8, all the computational features are introduced in a more detailed manner.

Some epochs of data were deemed too artifact-heavy to produce reliable results for feature computation. However, some of the features used are more sensitive to

artifact disturbances than others. For this reason, each of the different features was also assigned an artifact percentage threshold (APT). For each epoch of feature calculation, if the ratio of samples marked as artifacts exceeded that feature's APT, calculation for that epoch was omitted. The selected APTs are listed in Table 2.

### 3.4.1 Activation Synchrony Index

Activation synchrony index (ASI) is a feature originally developed by Räsänen and colleagues [41] for measuring inter-hemispheric synchrony, which has been shown to increase with neonatal age and decrease with different brain disorders. Although originally designed for inter-hemispheric synchrony measurement, ASI can be used to measure amplitude-amplitude correlation between any two EEG signals. ASI quantifies the co-occurrence of SATs between the signals by statistically computing the time delay between their quantized amplitude envelopes [41].

The signals were pre-processed following the work of Räsänen and colleagues [41]:

- First the the signals were band-passed to a range of [1.5–20] Hz and down-sampled to 50 Hz.
- A 1<sup>st</sup> order finite impulse response high-pass filter was applied to emphasize higher frequencies related to SATs.
- Fast Fourier Transform (FFT) was used to compute the amplitude envelopes of the two signals. A Hamming window with a width of 2 seconds and step size of 0.1 seconds was used for the FFT.

An energy envelope was computed as the sum of amplitudes of frequency bins between the [1.5–25] Hz range. The energy envelopes were then quantized into 8 different amplitude levels, following Räsänen et al. [41] and Koolen et al. [42, 43]. This was done to decrease the joint probability space of amplitude value combinations, and was accomplished by assigning each sample to its nearest cluster, as determined by a standard k-means algorithm. This resulted in two sequences corresponding to the two input signals.

To measure the dependency between the quantized energy envelopes, an Energy-Weighted Temporal Dependency Function (EDTF) was implemented. EDTF is a mutual information-based metric that measures the overall (non-logarithmic) statistical dependencies across all possible discrete signal state pairs at different relative temporal lags between the signals of interest, weighting the degree of statistical coupling of each state pair by the amount of signal energy associated

Feature	Montages	Frequency bands [Hz]	APT [%]	Values per epoch
ASI	F3–P3			
	F4–P4			
	F3–F4	1.5–20	20	5
	P3–P4			
	Left–Right			
wPLI	F3–P3	0.25–3		
	F4–P4	3–8	10	16
	F3–F4	8–15		
	P3–P4	15–30		
NC	F3	3–8		
	F4	8–15	10	12
	P3	15–30		
	P4			
PSD	All 8 channels	1–3		
		3–8	50	32
		8–15		
		15–30		
cPSD	F3–P3	1–3		
	F4–P4	3–8	50	20
	F3–F4	8–15		
	P3–P4	15–30		
	Left–Right			
aEEG (mean & IQR)	All 8 channels	2–15	50	16
rEEG (mean,IQR & LI)	All 8 channels	0.2–30	50	24
MFdfa (width, height, peak, tail)	All 8 channels	0.2–30	1	32
SC	Whole brain as 1 channel	0.2–30	50	1

**Table 2.** A summary table of the channel montages, frequency bands and artifact percentage thresholds (APT) used for calculation of each of the different features. Monopolar channels refer to channels F3,F4,P3 and P4. Also, the amount of total feature values calculated for each epoch is noted. It is the product of combinations for all the montages, frequency bands and possible sub-features used for that feature.

with these states. EDTF is calculated with the following formula:

$$\text{EDTF}(\tau) = \sum_{ij} E(a_i)E(b_j) \frac{P_\tau(a_i, b_j)^2}{P(a_i)P(b_j)} \quad (3.1)$$

where  $P_\tau(a_i, b_j)$  denotes the joint probability of observing level  $a$  in the first channel and level  $b$  in the second channel when the second signal is delayed by  $\tau$  seconds relative to the first signal. Essentially, the EDTF computes the signals' average deviation from statistical independence when one is delayed from the other. The contribution of each variable pair is weighted by the product of the signal amplitudes  $E(a_i)$  and  $E(b_j)$ , ensuring emphasis on high-energetic parts of the signal over background activity.

We then compare the values of EDTF around  $\tau = 0$  to the rest of the range, since a synchronous brain is assumed to be represented by a clear maximum EDTF value when lag is zero. This is achieved by first normalizing all the EDTF values to a relative range by subtracting the global minimum EDTF value from all EDTF values:

$$\text{EDTF}_{\text{norm}}(\tau) = \text{EDTF}(\tau) - \min\{\text{EDTF}(x), x \in [-5, 5]\} \quad (3.2)$$

Finally, ASI is calculated as the ratio of the normalized EDTF value at  $\tau = 0$  divided by the mean EDTF over the entire range. In this study a range of  $\tau = [-5, 5]$  seconds was used:

$$\text{ASI} = \frac{\text{EDTF}_{\text{norm}}(\tau = 0)}{\frac{1}{101} \sum_{\tau=-5s}^{5s} \text{EDTF}_{\text{norm}}(\tau)} \quad (3.3)$$

This ratio describes the magnitude of coupling between the signals without any delay compared to the coupling with delay. A higher ASI value corresponds to higher synchrony between the two channels measured.

In this study, five different montage pairs were used to calculate ASI, resulting in five ASI values calculated for each epoch. Synchrony was compared between intra-hemispheric monopolar channels F3–P3 and F4–P4, as well as between the inter-hemispheric monopolar channels F3–F4 and P3–P4. In addition, a measure of synchrony between full hemispheres was measured by computing ASI between the Left and Right bipolar montages. APT for ASI was set to 20%.

### 3.4.2 Weighted Phase Lag Index (wPLI)

Phase-locking or phase synchrony is a measure of how much the phase difference between two signals changes over time. A higher phase locking value means that

the phase difference between these signals stays fixed. This principle is illustrated in Figure 5. Phase synchrony is regarded as a sign of functional interaction between two distinct areas of the brain [44]. One method for measuring phase synchrony is known as the phase locking value (PLV). PLV uses the phases of signals to estimate their phase covariance, and is computed with the following equation:

$$\text{PLV} = \frac{1}{N} \left| \sum_{n=1}^N e^{j\theta(t,n)} \right| \quad (3.4)$$

where  $N$  is the number of samples,  $j$  is the imaginary unit and  $\theta(t, n)$  is the phase difference between the two signals.

PLV was first introduced by Lachaux and others [45]. It was further developed by Stam and colleagues [46] into a new measure called phase lag index (PLI), which estimates phase correlation using the imaginary component of the cross-spectrum. This corrects for disadvantages such as volume conduction, noise and use of common reference. The noise tolerance of PLI was further improved upon by Vinck and colleagues [47] by introducing weighted PLI (wPLI), which gives the PLI values weight depending on the magnitude of the imaginary component. When the phase difference between the two signals is close to either 0 or  $\pi$  radians where the imaginary component is 0, noise may flip the cross-spectra over the real axis, turning phase lags into leads and vice versa. Weighting these areas less makes wPLI less sensitive to noise. This difference between PLI and weighted PLI is illustrated in Figure 6. To overcome the problem of sample-size bias, Vinck and colleagues [47] proposed a metric called de-biased wPLI.

The first step when computing de-biased wPLI is the computation of the imaginary components of the cross-spectrum. After the imaginary components have been computed, they are averaged to one value. The average is then normalized by the magnitudes of the imaginary components. This results in the following equation:

$$\text{wPLI} = \frac{\sum_{j=1}^N \sum_{k=j+1}^N W_{j,k} d(X_j, X_k)}{N(N-1)\bar{W}} \quad (3.5)$$

where  $W_{j,k} \equiv |\Im(X_j)\Im(X_k)|$  is the weight,  $d(X_j, X_k) \equiv \text{sign}(\Im(X_j))\text{sign}(\Im(X_k))$ ,  $\bar{W}$  is the normalized weight and  $\Im(X)$  is the imaginary component of the cross-spectrum of the respective signal. [47]

In this study, wPLI was calculated between channel combinations F3–P3, F4–P4, F3–F4 and F4–P4. wPLI was calculated for four different band-passed versions of the data: [0.25–3] Hz, [3–8] Hz, [8–15] Hz and [15–30] Hz. These four channel combinations and four frequency bands resulted in 16 wPLI values being computed

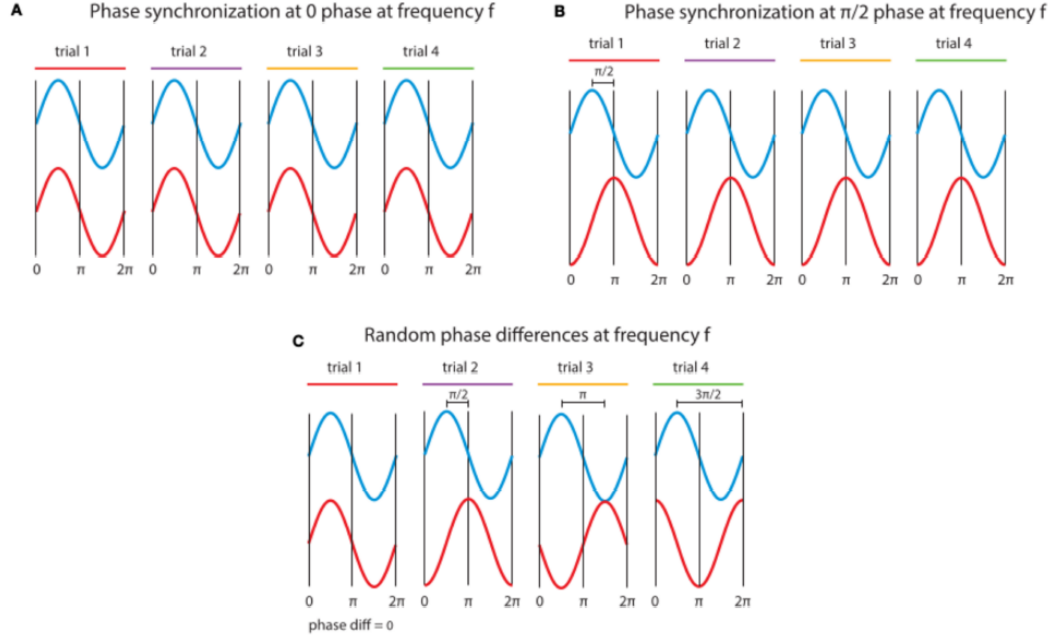


**Figure 5.** This figure shows examples of three different cases of phase synchrony between two signals. In **A**, both signals have the same phase and more importantly, the phase difference between the two signals doesn't change at all between trials. In this example there is perfect phase synchrony. In **B**, there is an initial phase difference of  $\frac{\pi}{2}$  between the signals, but synchrony is still perfect since this difference stays constant through all trials. In **C**, the difference between signal phases varies from one trial to the next, so there is no synchrony. Figure modified from Bastos and Schoffelen [48]

for each epoch of EEG data.

### 3.4.3 Nestedness Coefficient

Nestedness Coefficient (NC) is a feature used to measure the coupling between the phase of a low-frequency component and the amplitude of another higher-frequency component within one signal. When NC is high, it means that these two attributes are highly correlated with each other [38]. These occurrences are observed in neonate SATs [49]. They are thought to represent the coordination of spatially overlapped networks with different functionalities [50, 51]. This phase-amplitude coupling is illustrated in Figure 7.

Practically this is done by first filtering out two band-passed versions of the signal, one slower than the other. Then the amplitude envelope of the faster signal is extracted with the complex magnitude of its Hilbert Transform. The phase synchrony of this envelope is then calculated with respect to the phase of the slower signal, as in Equation 3.4.

For this study, the slower signal was bandpassed to a range of [0.2–0.6] Hz for all scenarios, while three different versions were chosen for the faster frequency band:

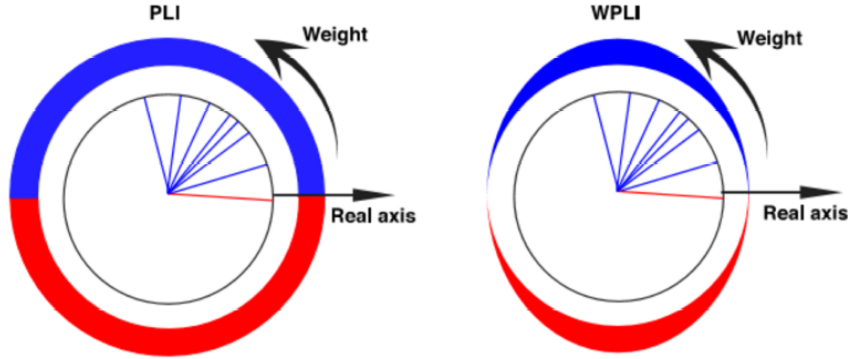


**Figure 6.** Comparison between PLI and wPLI. All cross-spectra are weighted equally by PLI and assigned a value of either +1 or -1 depending on which side of the real axis it lies. Phase lead has a value of +1 and is illustrated in blue, while phase lag has a value of -1 and is illustrated in red. In wPLI, the cross-spectra are weighted by the magnitude of their imaginary components. Cross-spectra that are close to the imaginary axis (phase difference close to  $\pm\frac{\pi}{2}$ ) contribute more than cross-spectra close to the real axis (phase difference close to 0 or  $\pi$ ). Figure modified from Vinck and colleagues [47]

[3–8] Hz, [8–15] Hz and [15–30] Hz. These three frequency band versions were calculated for all four monopolar channels, resulting in 12 NC values calculated for each epoch.

### 3.4.4 Power Spectral Density & Cross Power Spectral Density

In Power Spectral Density (PSD) the power or energy of a signal is measured as a function of frequency. In this study, PSD was computed using Welch's estimate, in which the time series is divided in to segments with 50% overlap. A segment size of 10 seconds was used. The segments were extracted with a Hamming window, and a periodogram for each segment are obtained by computing the FFT of the segment's auto-correlation function. The PSD value assigned to each segment is the mean of its periodogram. [53].

Cross Power Spectral Density (cPSD) is calculated similarly to PSD, except that

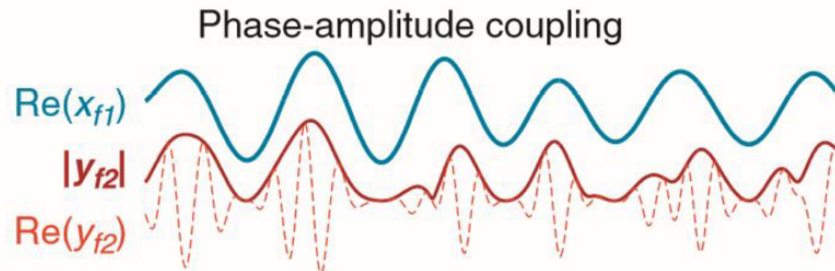


**Figure 7.** Illustration of phase-amplitude coupling. The slower and faster signal are denoted with a blue line and a dashed red line, respectively. The amplitude envelope of the faster signal is marked with a solid red line. Figure modified from Palva and Palva [52].

FFT is computed from the cross-correlation of two signals instead of the auto-correlation of one signal. Unlike in many other studies, where cPSD is used for measuring coherence between two signals similar to wPLI [48], in this study cPSD was used for assessing power per unit frequency shared between two channels. Cross-correlation can be defined as:

$$R_{X_1, X_2}(\tau) = E[X_1(t)X_2(t + \tau)] \quad (3.6)$$

where  $X_1$  and  $X_2$  denote the two signals and  $\tau$  is the time lag between them, and  $E$  is the expected value operator.

Both PSD and cPSD were calculated for the following frequency bands: [1–3] Hz, [3–8] Hz, [8–15] Hz and [15–30] Hz. PSD was calculated from all four monopolar and four bipolar channels, resulting in a total of 32 PSD values calculated per epoch. cPSD was calculated between electrode pairs F3–P3, F4–P4, F3–F4 and F4–P4, as well as between the intra-hemispheric bipolar channels Left–Right. This resulted in 20 cPSD values calculated per epoch.

### 3.4.5 Multifractal Detrended Fluctuation Analysis

Detrended Fluctuation Analysis (DFA) is a time series analysis method for determining the statistical self-similarity and self-affinity of a monofractal signal. A signal is considered monofractal if its fractalities in space and fractalities in time are happening independently from one another. However, if self-repeating patterns are occurring across a multidimensional axis of both time and location, ie. the scaling factor can't be described by a single exponent, the signal is considered to be multifractal. Multifractal Detrended Fluctuation Analysis (MFDFA) is a generalized version on DFA, designed to analyze multifractal signals. It has been shown to differentiate between various pathologies and activities in different areas of the brain [54, 55].

MFDFA consists of the following steps described in the literature [56, 57].

1. A noise-like EEG signal is converted into a random walk signal to obtain a profile. This is done by subtracting the global mean, and then calculating the cumulative sum of the signal:

$$Y(i) \equiv \sum_{n=1}^N (x_n - \bar{x}), i = 1, \dots, N \quad (3.7)$$

Here  $Y$  is the profile of the signal  $x$ ,  $N$  is the number of data points and  $\bar{x}$  is the mean of the signal.

2. The acquired profile is divided into non-overlapping segments with a length of  $s$  data points.
3. A local trend for each segment is computed with least-square fit, and variance for each segment  $v$  is computed with the following equation:

$$F^2(s, v) \equiv \frac{1}{s} \sum_{i=1}^s \{Y[(v-1)s+i] - y_v(i)\}^2, v = 1, \dots, N_s \quad (3.8)$$

4. The fluctuation function of  $q^{\text{th}}$  order is obtained by averaging over all the segments as in Equation 3.9. This thesis used values of  $q$  ranging from  $-5$  to  $+5$  with a step size of  $0.5$ , following the work of Matic and colleagues [58].

$$F_q(s) \equiv \frac{1}{N_s} \sum_{v=1}^{N_s} ([F^2(s, v)]^{q/2})^{1/q} \quad (3.9)$$

5. Steps 2-4 are repeated for different values of segment size  $s$ , in order to determine the dependence between segment size (fractality of a certain time scale) and fluctuation functions  $F_q(s)$ . In this study, time scales ranging from 25 to 1875 samples were used, such that the largest time scale represented  $1/16^{\text{th}}$  of the 2-minute epoch, and the smallest scale of 25 samples was following the instructions of Ihlen et al [57]. Number of different scales used was 19, taken equidistantly from the logarithmic scale between  $\log_2(25)$  and  $\log_2(1875)$ .
6. Finally, the dependence of the fluctuation functions  $F_q(s)$  with respect to the time scales  $s$  were determined. The relationship of the fluctuation functions and time scales is determined by a  $q$ -order Hurst exponent  $H(q)$  as in the following equation:

$$F_q(s) \sim s^{H(q)} \quad (3.10)$$

Because of this, by plotting them together on a logarithmic scale for different values of  $s$  and  $q$ , the slopes of these functions indicate the  $q$ -order Hurst exponents  $H(q)$ . These are used for determining the  $q$ -order singularity exponents  $h(q)$  and the  $q$ -order singularity dimensions  $D(q)$  in the following manner:

$$h(q) = H(q) + qH'(q) \quad (3.11)$$

$$D(q) = q[h(q) - H(q)] + 1 \quad (3.12)$$

The relationship of the obtained variables  $h(q)$  and  $D(q)$  describes the multifractal spectrum of the original signal. We can quantify this relationship by plotting

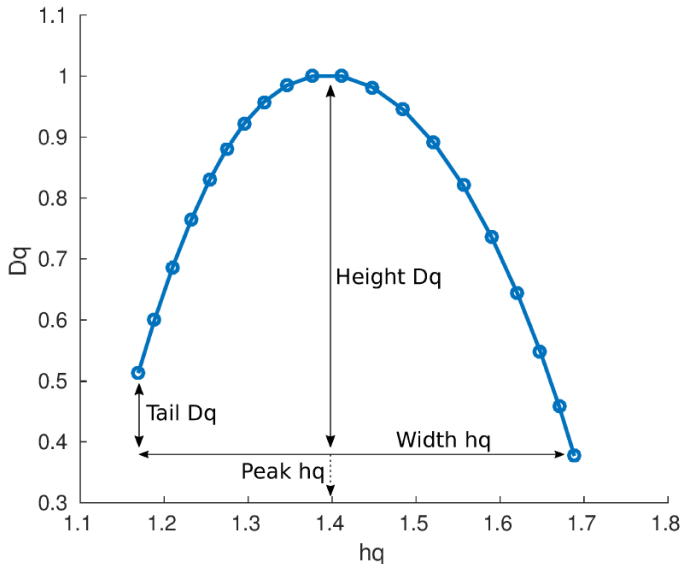


**Figure 8.** An example plot of the multifractal spectrum, along with the four spectrum attributes *width*, *height*, *peak* & *tail*. Figure from Suvisto [4].

them together and extracting measure attributes of the plot. For this study, four attributes were recorded for each multifractal spectrum, measured for each 2-minute epoch of EEG data. These measures were as follows:

- *Width*, defined as the difference between the maximum  $h(q)$  and minimum  $h(q)$  values.
- *Height*, defined as the difference between the maximum  $D(q)$  and minimum  $D(q)$  values. It describes temporal changes in the local Hurst exponents.

Both *width* and *height* describe the size of the spectrum, and were computed following the work of Zorick and Mandelkern [59].

- *Peak*, defined as the singularity exponent  $h(q)$  where the singularity dimension reaches its maximum.
- *Tail*, defined as the difference between the two  $D(q)$  values associated with the smallest and largest values of  $h(q)$ . It was first introduced by Matic and colleagues [58].

An illustration of these attributes, together with an example plot of the multifractal spectrum are shown in Figure 8.

These four attributes were collected for all four monopolar channels and for all four bipolar channels, resulting in a total of 32 MFDFA attribute values collected for each epoch of EEG data.

### 3.4.6 Amplitude-integrated EEG

Amplitude-integrated EEG (aEEG) is a time-compressed measure of peak-to-peak amplitude of an EEG signal. It is used for extended periods of bedside monitoring and evaluation of baseline brain activity. In addition, aEEG has been shown to be a powerful tool in detecting seizures and in monitoring responses to drug therapy and depth of anesthesia. [60–64]

For obtaining aEEG, the frequencies outside a [2–15] Hz range are strongly attenuated, after which the signal is re-scaled and smoothed to better show trending.

For this study, two attributes of the aEEG signal were extracted for each epoch, namely the mean and inter-quartile range (IQR). They are used to estimate the central tendency and variability for aEEG, respectively. These two sub-features for all four monopolar and four bipolar channels resulted in a total of 16 attribute values collected for each epoch.

### 3.4.7 Range-EEG

Range-EEG (rEEG) can be used to complement aEEG, as they are both a type of peak-to-peak amplitude measure. It is used e.g. for automatic detection of IBIs [65]. While aEEG is an underestimation of the true peak-to-peak amplitude due to frequencies below 2 Hz and above 15 Hz being attenuated, rEEG is an overestimate. In rEEG, the signal is divided into 2-second non-overlapping segments, and for each segment the local minimum value is subtracted from the local maximum value. For evaluating the characteristics of rEEG, three attributes of the rEEG signal were extracted for each epoch, namely the mean, IQR, and lower 5<sup>th</sup> percentile (LI). LI of rEEG has been shown to increase with brain maturation and its sudden rises have been correlated with epileptic seizures [61, 63]. These three sub-feature measures collected for all four monopolar and four bipolar channels resulted in a total of 24 attribute values collected per epoch.

### 3.4.8 Suppression Curve

Line length is a feature designed by Esteller and colleagues [66] to act as an demodulator for amplitude and frequency, and is defined as the running sum of the absolute differences between all consecutive samples within a predefined window. This method was further developed by Koolen and colleagues [67] into a feature called Suppression Curve (SC), in order to identify IBIs and extended periods of discontinuous EEG signal. In this study, a 1-second window of 250

samples was used, with a 30-sample overlap between consecutive windows. The line length for a single window segment  $i$  is denoted as  $L(i)$  and calculated as in the following equation:

$$L(i) = \sum_{j=1}^{250-1} |x_{j+1} - x_j| \quad (3.13)$$

where  $x_j$  denotes the  $j^{th}$  sample of the  $i^{th}$  1-second window. To normalize the line length values between 0 and 1, each line length  $L(i)$  is divided with the sum of all the line lengths within an epoch, as in Eq. 3.14

$$L_n(i) = \frac{L(i)}{\sum_i L(i)} \quad (3.14)$$

Since SATs and their subsequent IBIs are usually detected all over the brain at the same time, the line length information from all four monopolar channels is aggregated together by extracting the median over all channels, as in Eq. 3.15.

$$Me\_Ln(i) = \text{median}(L_n(i)) \quad (3.15)$$

Finally, SC for the epoch is defined as the complement of the quotient of the median of all  $Me\_Ln$  values over their mean, as in Eq. 3.16. If the signal is continuous, the mean and median tend to have a smaller difference when compared to a discontinuous signal, resulting in a smaller SC value.

$$SC = 1 - \frac{\text{median}(Me\_Ln)}{\text{mean}(Me\_Ln)} \quad (3.16)$$

This results in one SC value per epoch for the whole brain, representing the amount that the EEG signal is being "suppressed" by interfering SATs.

### 3.5 Statistical analysis

For examining the effect of fentanyl on the features detailed in Section 3.4, four different analytical methods were used. In Figure 3 this stage is referred to in the E-section. A more magnified illustration is seen in Figure 9, and the purpose of this section is to further describe this stage in detail. These four methods defined in subsections 3.5.1–3.5.4 were implemented for each of the 158 combinations of features, electrode montages and frequency bands. This adds up to a total of 632 different plots being produced.

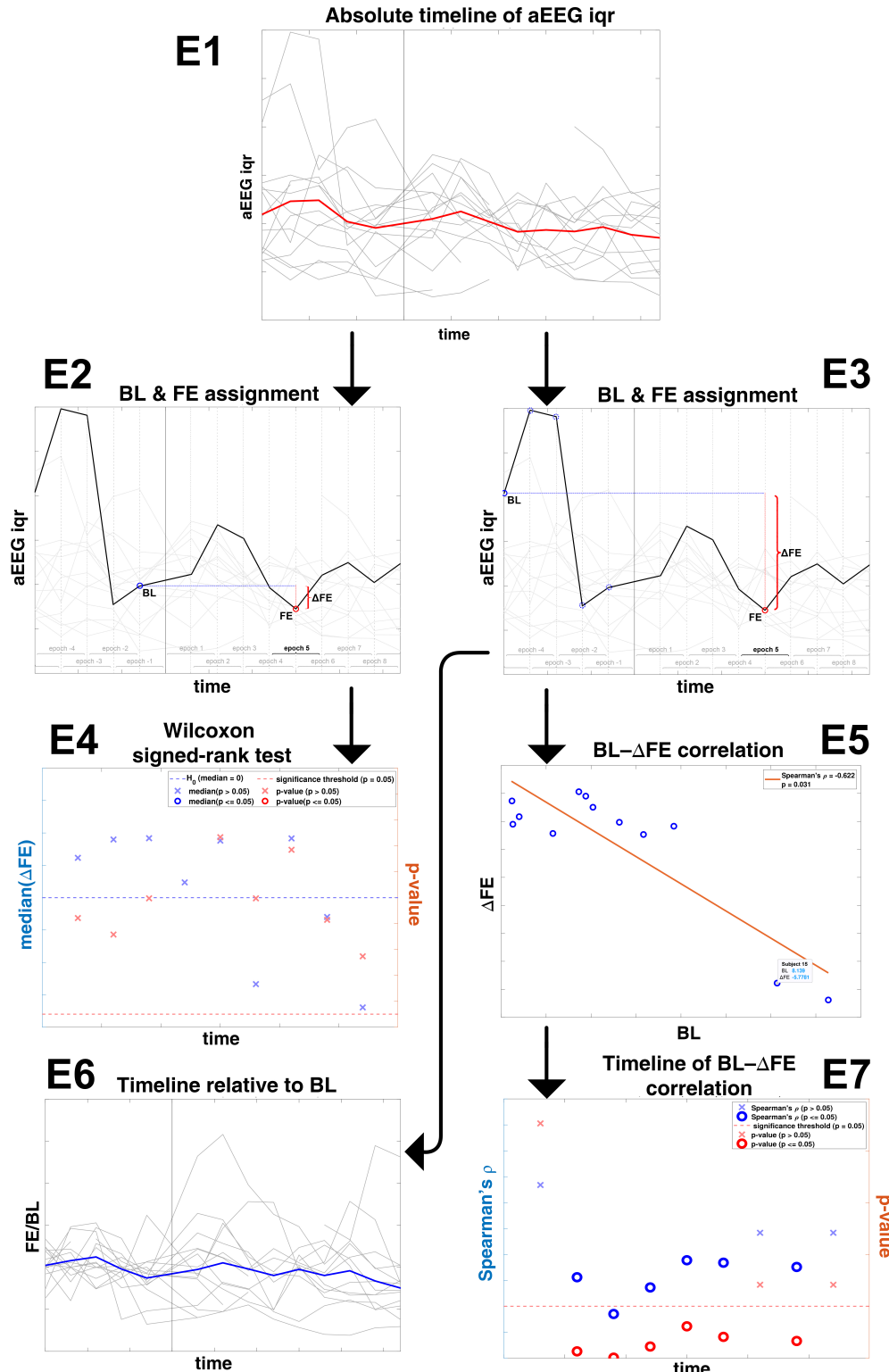


**Figure 9.** Presented here is an overview of the statistical analysis process first introduced in the E-section of Figure 3. First, each set of gathered features is plotted on an absolute timeline (**E1**, magnified version in Figure 10). A baseline assignment method is chosen (**E2**, magnified in Figure 11) and the Wilcoxon signed-rank-test timeline is computed (**E4**, magnified in Figure 14). Another baseline assignment method (**E3**, magnified in Figure 12) is used for both the construction of relative time trends (**E6**, magnified in Figure 13) and also for calculating the timeline for baseline–delta correlation test results (**E5** and **E7**, magnified in Figures 15 & 16 respectively.)

### 3.5.1 Absolute time trend

The simplest and most straightforward way of probing the values received from computational features is to plot them as-they-are on a timeline to try and visually detect any meaningful fluctuations across time.

This method of "eye-balling" the data is intuitively uncomplicated, but is also mathematically less rigorous than other methods, making it less useful for making precise interpretations. Its effectiveness also heavily relies on the expertise of the viewer. However, it can—apart from being an analytically simple place to start from—be helpful in confirming possible findings arrived to by other statistical means.

When visually inspecting the data, key things to look out for are trends that behave similarly across multiple subjects in terms of both direction and timing. We also expect any possibly significant general trends to appear only after fentanyl administration has begun. If a similar observation is made across multiple brain areas, this would lend credence to it being caused by an actual phenomenon instead of randomness.

An example of a collection of absolute feature values being plotted on a timeline is seen in Figure 10.

### 3.5.2 Baseline assignment & Relative time trend

One way to compare feature values before and after fentanyl administration is to choose or construct one value to represent the state of the brain's "normal" activity before the drug has had any effect. Let us call this number the baseline value (BL).

The optimal method for coming up with a good estimation for BL—while an integral topic—is beyond the scope of this thesis. For the purposes of this study, the following two methods for determining BL were arbitrarily chosen:

1. The arguably simplest method for BL assignment is simply to take the last recorded feature value before drug administration as most representative of the brain state before any effects relating to the test condition occurred. That is, we take the feature value in the last pre-drug epoch as our baseline. This method is illustrated in Figure 11.
2. Another intuitive approach to BL assignment is to use either parametric or non-parametric statistical measures in an attempt to collectively represent the pre-drug data history to a further extent than just the latest epoch. In this study, we chose to use the median value of the last five pre-drug epochs as the measure

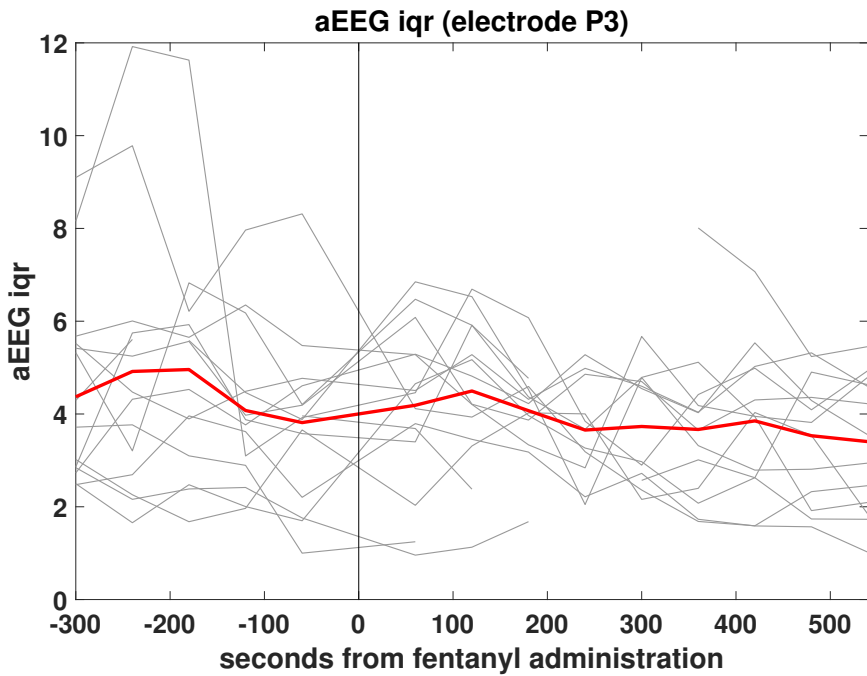


**Figure 10.** Here absolute feature values for each subject are represented against time as gray lines. A timeline of the mean of all the subjects is also represented, with a red line. This is to make it easier to visually spot any synchronized and directionally parallel fluctuations shared across multiple subjects.

for determining the baseline. An illustration of this method is seen in Figure 12.

Once BL has been defined for each subject, we are able to visually examine fluctuations in the feature not just in absolute terms, but also in terms relative to each individual BL. For example, we can devise a plot where the feature values of each subject have been divided by their respective BL. This produces a graph of feature percentages, where the "neutral" BL state of the feature value sits at 100% for every subject.

The advantage of this approach is making the baseline brain state of all the subjects visually more alike on the timeline, which helps in visual inspection of common trends. It also squishes all feature values less than BL into the space between 100% and 0, which might make it easier to spot effects that are proportional to BL instead of being linear in nature. An example of this kind of relative time trend is seen in Figure 13.

Aside from visual inspection, we also want to make more numerical before-and-after comparisons on states of the brain. For this purpose, let the post-drug feature values (FE) in each epoch be separately compared to their respective BL via subtraction. Each comparison yields a difference  $\Delta FE$  representing how similar or dissimilar that epoch is to the BL of that same subject:

$$\Delta FE_{s,e} = FE_{s,e} - BL_s \quad (3.17)$$

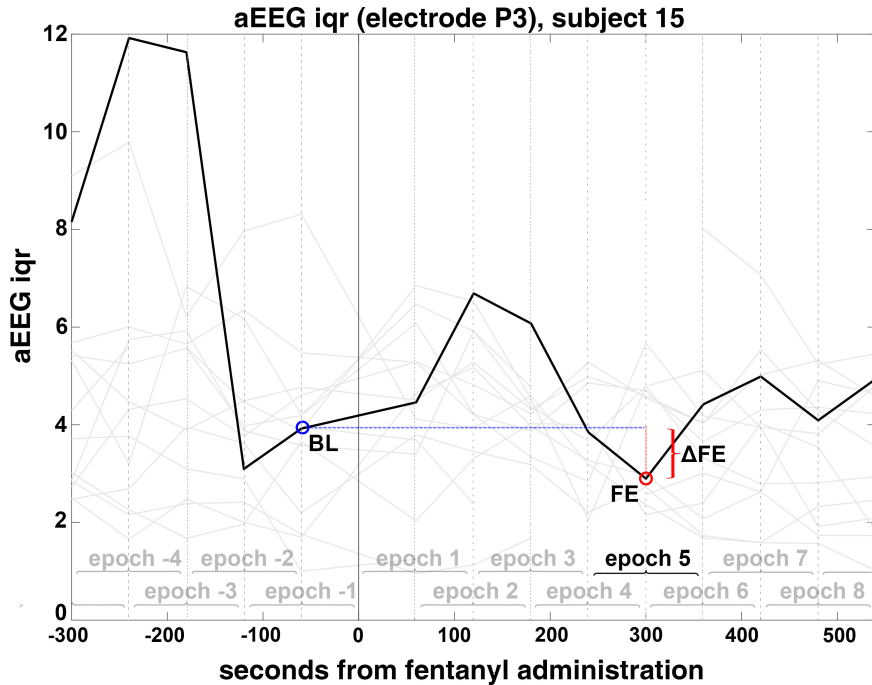


**Figure 11.** An example of determining the baseline (BL) by using the feature value of the last pre-drug epoch. Here presented as an example are the absolute timelines for aEEG IQR values, with one of the subjects highlighted in black. The last pre-drug value is pinpointed by a blue circle. An example of determining  $\Delta FE$  for a given post-drug epoch—as defined in Equation 3.17—is depicted by pinpointing the FE of the 5<sup>th</sup>-epoch with a red circle.  $\Delta FE$  is then defined as the signed vertical difference between FE and BL. Here FE is smaller than BL, so  $\Delta FE$  has a negative sign.

where  $FE_{s,e}$  is the post-drug feature value from subject  $s$  in epoch  $e > 0$ , and  $BL_s$  is the baseline value of subject  $s$ , as defined by one of the two methods described above. This derivation is also visually explained in Figures 11 and 12.

A collective measure (and its significance value) is then constructed from the comparisons over all subjects, representing how similar FEs in that epoch are to their BL in general. In this study, two methods for obtaining this collective measure were used, and they are detailed in subsections 3.5.3 and 3.5.4

### 3.5.3 Wilcoxon signed-rank test

Wilcoxon signed-rank test is statistical test for comparing two sample sets, where each sample has a corresponding pair in the other set. It tests for the null hypothesis that the two sets are originated from underlying models that have the same median, i.e. that the median of their paired differences (in this case the set of  $\Delta FE$  for a given epoch) is zero.

To perform the Wilcoxon signed-rank test, each  $\Delta FE$  in the epoch is first assigned a rank value based its absolute magnitude, with the smallest magnitude being assigned a rank of 1, the second smallest a rank of 2 etc. If there are ties within magnitudes, each of the tied cases is assigned a rank that is the mean of the ranks

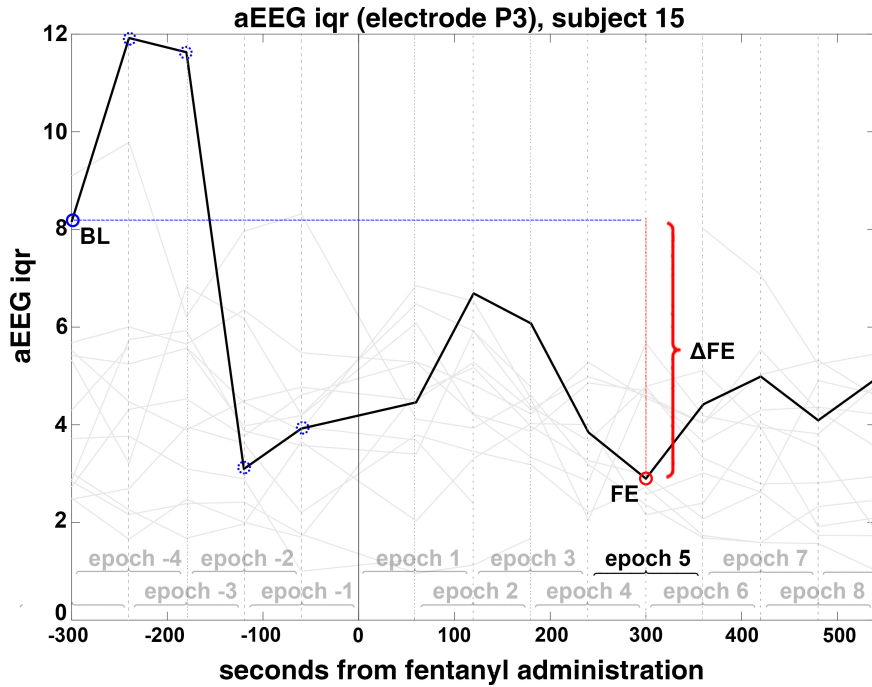


**Figure 12.** Presented here is the statistical method used in this study of determining the baseline (BL) by choosing the median of the last five pre-drug values. From the absolute feature value timeline of one subject (highlighted in black), the last five pre-drug epoch values are highlighted with dashed blue circles, and their median is highlighted with a solid blue circle. Illustrated here in red is also the method for calculating  $\Delta FE$  for a given epoch, which is performed identically to the one presented in Figure 11.

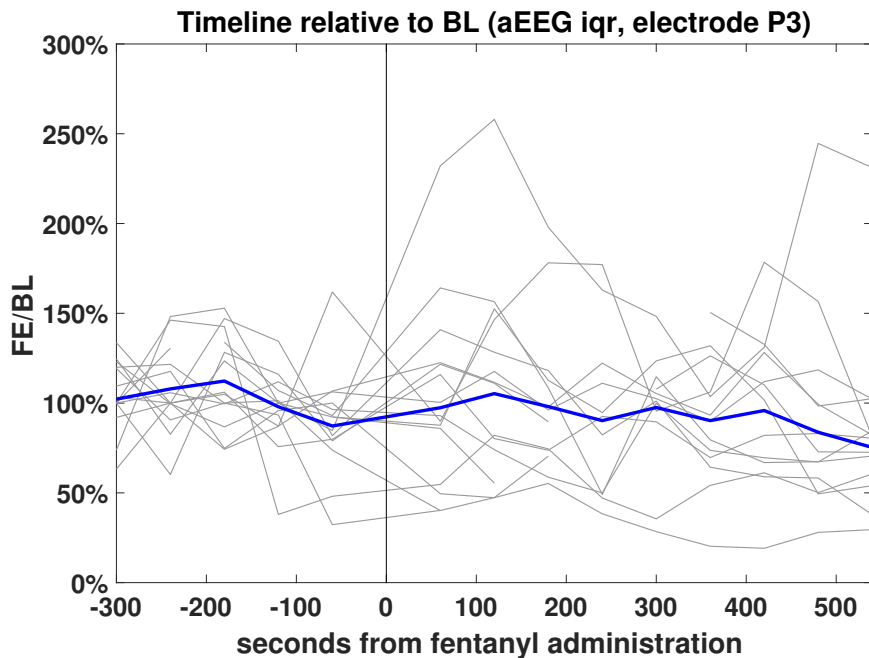


**Figure 13.** For this relative time trend graph, absolute feature values from each epoch were divided by a common baseline (BL). For each subject, their baseline in this case was the median feature value of the last their five pre-drug epochs as defined in Figure 12. The result of this division is presented here as a timeline of percentages, where each subject's BL is set to 100%. The relative timelines of the subjects are represented by gray lines, and their mean is represented by a blue line.

that would be tallied, were there to be no ties. Each rank is also assigned the sign of the  $\Delta F_E$  it was calculated from. An example of this entire process is depicted in the upper section of Table 3.

Next, two intermediate statistics are calculated:

- $S^+$  defined as the absolute value of the sum of all the positively signed ranks
- $S^-$  defined as the absolute value of the sum of all the negatively signed ranks.

From these, the smaller value is chosen and defined as our test statistic  $W$ .

To determine whether our test statistic is significant and whether to reject the null hypothesis, a significance threshold  $\alpha$  is chosen and a (two-tailed)  $p$ -value is calculated. The  $p$ -value represents the likelihood of a similar or more extreme test statistic arising from random data, and the chosen threshold  $\alpha$  represents our maximum allowance for such a random occurrence. In this study, a significance threshold of  $\alpha = 0.05$  was chosen for all tests. This means that, at worst, we expect to get a false rejection of the null hypothesis 1 out of every 20 times we run the test.

For relatively small sample sizes ( $n < 20$ ), the  $p$ -value of our test statistic can be determined via a permutation test, comparing it to the distribution of all possible  $W$ s obtained from all possible permutations of the two original sample sets BL and FE. In practice however, the significance of the test statistic is obtained by comparing it to a reference table of pre-calculated critical values for different sample sizes  $n$  and significance thresholds  $\alpha$ . If the obtained  $W$  is smaller than the critical value, the result is marked significant and the null hypothesis is rejected.

This process is laid out in the lower part of Table 3.

For larger samples ( $n \geq 20$ ), the Central Limit Theorem can be used to approximate the  $p$ -value by stating that the sampling distribution of  $W$  approaches a normal distribution, and calculating a  $z$ -score for it as follows:

$$z = \frac{W}{\sigma_W} \quad (3.18)$$

where  $\sigma_W$  is the standard deviation of  $W$ ,

$$\sigma_W = \sqrt{\frac{n(n+1)(2n+1)}{6}} \quad (3.19)$$

and  $n$  is the number of pairs between sample sets.

This  $z$ -score is then compared to a  $z$ -distribution or a critical value  $Z$  for a given  $\alpha$ , and a  $p$ -value is obtained. If our score is smaller than the critical value, we fail to reject the null hypothesis. [68]

Subject	BL	FE	$\Delta FE$	sign( $\Delta FE$ )	rank(  $\Delta FE$  )	signed rank
1	3.88	4.78	0.90	+	6	6
2	3.57	4.78	1.21	+	7	7
3	4.18	4.69	0.51	+	4	4
4	1.69	2.97	1.28	+	8	8
5	4.76	4.59	-0.17	-	2	-2
6	5.47	5.67	0.20	+	3	3
7	1.75	2.56	0.81	+	5	5
8	8.31	2.36	-5.95	-	10	-10
9	4.60	4.54	-0.06	-	1	-1
10	3.65	2.15	-1.5	-	9	-9
$S^+$	$=  6 + 7 + 4 + 8 + 3 + 5 $			$= 33$		
$S^-$	$=  -2 - 10 - 1 - 9 $			$= 22$		
$W$	$= \min(S^+, S^-)$			$= 22$		
	$W_{crit}(n = 10, \alpha = 0.05)$			$= 5$		$< W$
	$p\text{-value}$			$= 0.57548$		$> \alpha$

**Table 3.** An example of performing the Wilcoxon signed-rank test to a single epoch of 10 feature values. The first 10 rows depict the process of obtaining the signed ranks of each  $\Delta FE$ , one per subject. The next three rows demonstrate the determining of our test statistic  $W$  with the intermediary statistics  $S^+$  and  $S^-$ . The last two rows state the result of our test, namely comparing our obtained  $W$  to a critical value obtained from a reference table for our sample size  $n = 10$  and significance threshold  $\alpha$ . Since our test statistic  $W$  is greater than the critical value and correspondingly the  $p$ -value is greater than  $\alpha$ , we would fail to reject the null hypothesis in this case, i.e. we haven't detected any significant effect on the feature values due to fentanyl.

In this study, we used the last-epoch method depicted in Figure 11 when determining BL for Wilcoxon signed-rank testing.

After performing the test for all the post-drug epochs, a timeline of signed-rank test results can be constructed, as in Figure 14, showing us how  $\text{median}(\Delta FE)$  changes over time.

### 3.5.4 Baseline–delta correlation & Spearman’s rank-order correlation

The effects caused by fentanyl on the feature values might be proportional in nature. That is, the magnitude of change  $\Delta FE$  might be a variable that is dependent of the size of its respective BL. To investigate for this kind of an effect, we perform a baseline–delta correlation test.

To start, we construct a " $\Delta FE$ -vs-BL" plot, such as the one depicted and described in Figure 15. From this plot, we are then able to calculate a correlation coefficient to describe the dependence or independence of the two variables BL &  $\Delta FE$ . In this study, the tool chosen for this task was Spearman’s rank-order correlation coefficient.

Spearman’s rank-order correlation is a variation of Pearson’s correlation coefficient. While Pearson’s correlation measures the magnitude of linear correlation

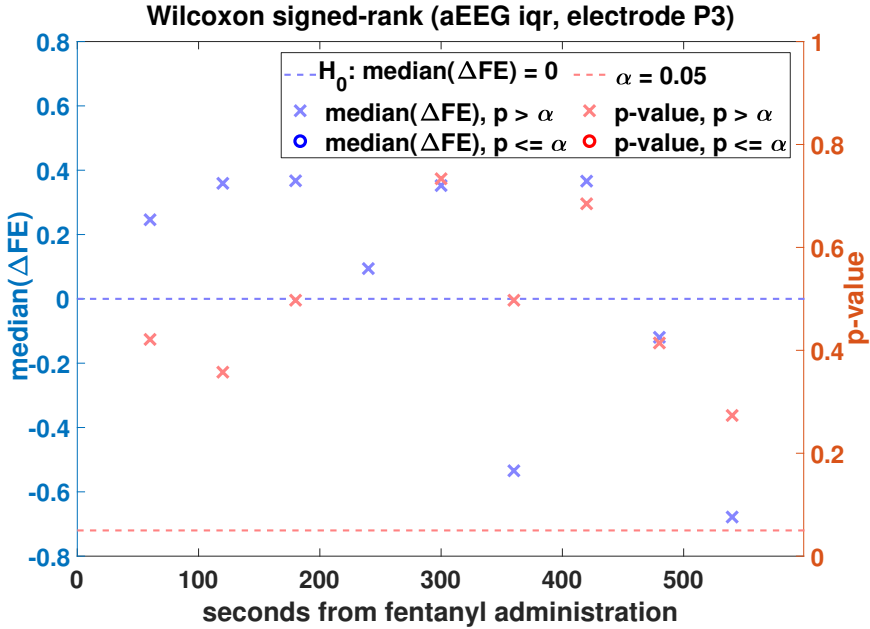


**Figure 14.** Here presented is an example of the Wilcoxon sign-rank test result timeline between feature values in post-drug epochs (FE) and a common baseline (BL) defined as in Figure 11. For each post-drug epoch, the actual median values of  $\Delta FE$  are represented in blue (left y-axis), and the corresponding  $p$ -value for the signed-rank test is represented in red (right y-axis). Insignificant results ( $p > 0.05$ ) are represented with crosses. Any significant results ( $p \leq 0.05$ ) would be presented with circles. Here however, no statistically significant results are present.

between two variables, Spearman's correlation is equipped to detect relationships between variables that are monotonous but not linear, while also being more resistant to outliers [69].

Calculation of Spearman's rho differs from Pearson's  $r$  only in that we use the ranks of the sample sets instead of using the two sample sets themselves. [70].

Given paired data  $(x_1, y_1), (x_2, y_2), \dots, (x_n, y_n)$ , Pearson's  $r$  is defined as

$$r_{xy} = \frac{\sum_{i=1}^n (x_i - \bar{x})(y_i - \bar{y})}{\sigma_x \sigma_y} \quad (3.20)$$

where  $\bar{x}, \bar{y}$  are the sample means, and  $\sigma_x, \sigma_y$  are the sample standard deviations, defined as

$$\bar{x} = \frac{1}{n} \sum_{i=1}^n x_i \quad (3.21)$$

$$\sigma_x = \sqrt{\sum_{i=1}^n (x_i - \bar{x})^2} \quad (3.22)$$

for  $x$ , and analogously for  $y$ .

Derived from Equation 3.20, Spearman's correlation coefficient can be expressed

as follows:

$$\rho = \frac{\sum_{i=1}^n (\text{rank}(x_i) - \overline{\text{rank}(x)})(\text{rank}(y_i) - \overline{\text{rank}(y)})}{\sigma_{\text{rank}(x)}\sigma_{\text{rank}(y)}} \quad (3.23)$$

If there are no ties within the ranks of each sample set, this simplifies into the form

$$\rho = 1 - \frac{6 \sum_{i=1}^n D_i^2}{n(n^2 - 1)} \quad (3.24)$$

where  $D_i = \text{rank}(x_i) - \text{rank}(y_i)$ . [70]

An example calculation of Spearman's rho is presented in Table 4.

Similar to Pearson's  $r$ , Spearman's rho gets values within the interval  $[-1, 1]$ , where  $-1$  denotes perfect negative correlation,  $+1$  denotes perfect positive correlation, and  $0$  denotes no correlation. To calculate the  $p$ -value of a given rho to determine its significance with respect to the size of the data set, we first calculate a  $t$ -value:

$$t = \rho \sqrt{\frac{n-2}{1-\rho^2}} \quad (3.25)$$

where  $n-2$  is the degrees of freedom. Comparing this  $t$ -value to Student's  $t$ -distribution gives us the corresponding  $p$ -value. [71]

As with Wilcoxon's signed-rank test, we can form a timeline of Spearman's correlation coefficients and their  $p$ -values after computing them for all the post-drug epochs for a single feature. A demonstration of such a timeline is seen in Figure 16.

For baseline-delta correlation testing, the BL was defined as in Figure 12. Similarly to the Wilcoxon's signed-rank test, a significance threshold of  $\alpha = 0.05$  was chosen for Spearman's correlation coefficient.

Subject	BL	rank(BL)	$\Delta FE$	rank( $\Delta FE$ )	D	$D^2$
1	3.88	2	0.90	7	-5	25
2	3.72	1	1.06	8	-7	49
3	5.16	10	-0.46	4	6	36
4	2.23	3	0.73	12	-9	81
5	4.62	6	-0.03	5	1	1
6	5.84	8	-0.17	3	5	25
7	2.40	5	0.16	10	-5	25
8	8.13	11	-5.77	2	9	81
9	4.04	4	-0.50	6	-2	4
10	2.25	7	-0.10	11	-4	16
11	3.15	9	-0.42	9	0	0
12	9.27	12	-6.38	1	11	121
$\sum D^2$						= 464
n						= 12
$\rho$		$= 1 - \frac{6.464}{12(12^2-1)}$				= -0.6224
$t$		$= -0.6224 \cdot \sqrt{\frac{12-2}{1-(0.6224)^2}}$				= -2.5146
p-value		Compare $t$ to Student's t-distribution				= 0.03068

**Table 4.** An example of obtaining Spearman's correlation coefficient  $\rho$  and it's corresponding  $p$ -value, using sample sets of BL and  $\Delta FE$  with ( $n = 12$ ). The first 12 rows depict the ranks of the paired sets, their paired differences  $D$  and their square  $D^2$ . The bottom section displays the implementation of Equations 3.24 and 3.25 for the numerical values obtained here.

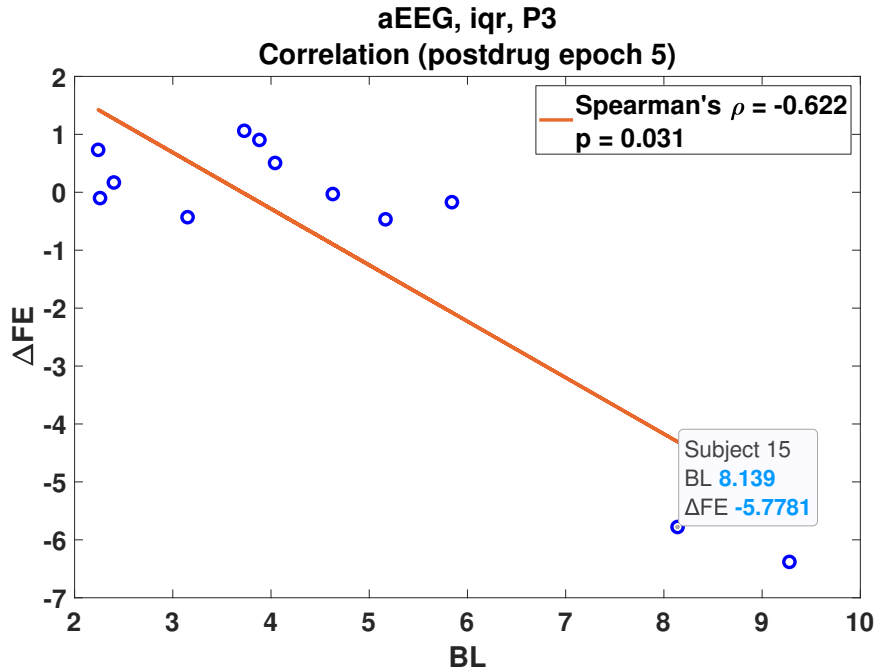


**Figure 15.** An example of the  $\Delta FE$ -vs-BL -plot, for which Spearman's correlation is calculated in baseline–delta correlation testing. The x-coordinates of each point (or subject) is determined by their BL as defined in Figure 12. The y-coordinate is the  $\Delta FE$  of the post-drug epoch in question. For illustrative purposes, the coordinates of a single subject are labeled and a yellow line is drawn to denote the linear regression line of the resulting plot (Spearman's correlation doesn't measure linearity but monotonicity). Here Spearman's correlation is deemed to be quite negative ( $\rho = -0.622$ ) and significant ( $p = 0.031$ ).

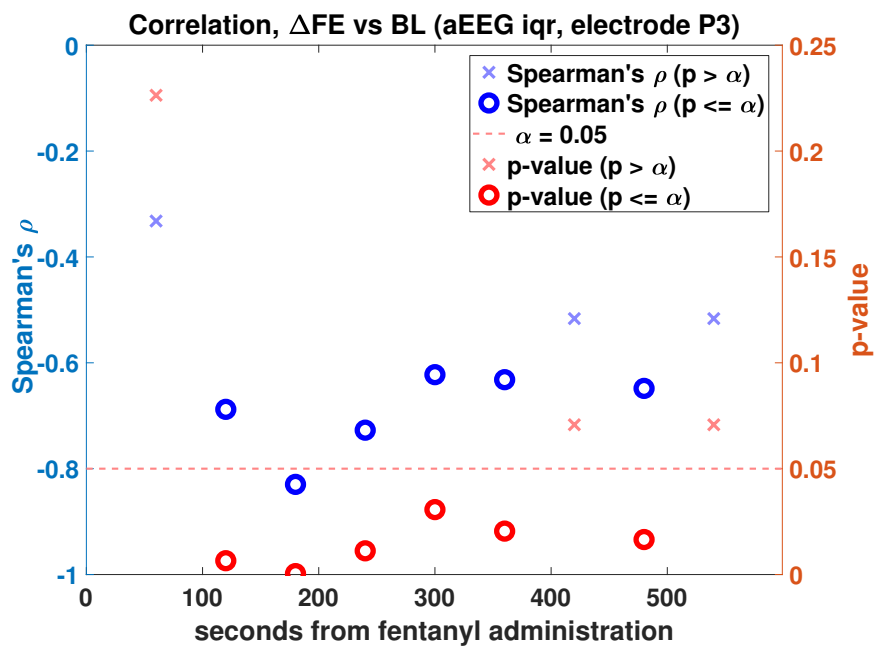


**Figure 16.** A timeline of baseline–delta correlation values for the relative change of feature values ( $\Delta$ FE) in post-drug epochs compared to a common baseline (BL). For each subject, their baseline in this case was defined as the median of the last five pre-drug feature values. For each post-drug epoch, a Spearman’s rho and a corresponding  $p$ -value was calculated in a manner that is displayed in Table 4. Here, the results of those calculations are presented as a timeline, with the correlation coefficients in blue (left y-axis) and their corresponding  $p$ -values in red (right y-axis) for each epoch. Insignificant results ( $p > \alpha$ ) are presented with crosses and significant results ( $p \leq \alpha$ ) are presented with circles.

## 4. Results

This section describes the general summary of the results achieved in the pre-processing stage and statistical analysis stage. A total collection of all the results can be found in Appendix A.

### 4.1 Artifact percentage

Within the examination period used for statistical analysis of short-term effect (last 5 pre-drug epochs and first 10 post-drug epochs), around 57% of all the epochs had less than 1% of artifacts. This means that most epochs were able to be used for calculation in all of the computational features. Around 12% of the epochs within the examination period had more than 50% of artifacts, making them unusable for any feature computation. An example of the artifact percentage profile for a few subjects can be seen in Figure 17, and a full profile of all the subjects' APT is available in Appendix B.

### 4.2 Time trends

None of the absolute time trends, neither absolute nor relative, displayed visually clear changes between pre-drug and post-drug feature values. Fluctuations appeared to be arbitrary throughout all the recordings, excluding some outlier cases.

### 4.3 Wilcoxon signed-rank

None of the Wilcoxon signed-rank timelines showed clear signs of consistent significant effects being present. The few epochs where the null hypothesis was rejected were not corroborated by either spatially or temporally nearby results, and thus were interpreted as false positives. The only place showing 3 temporally

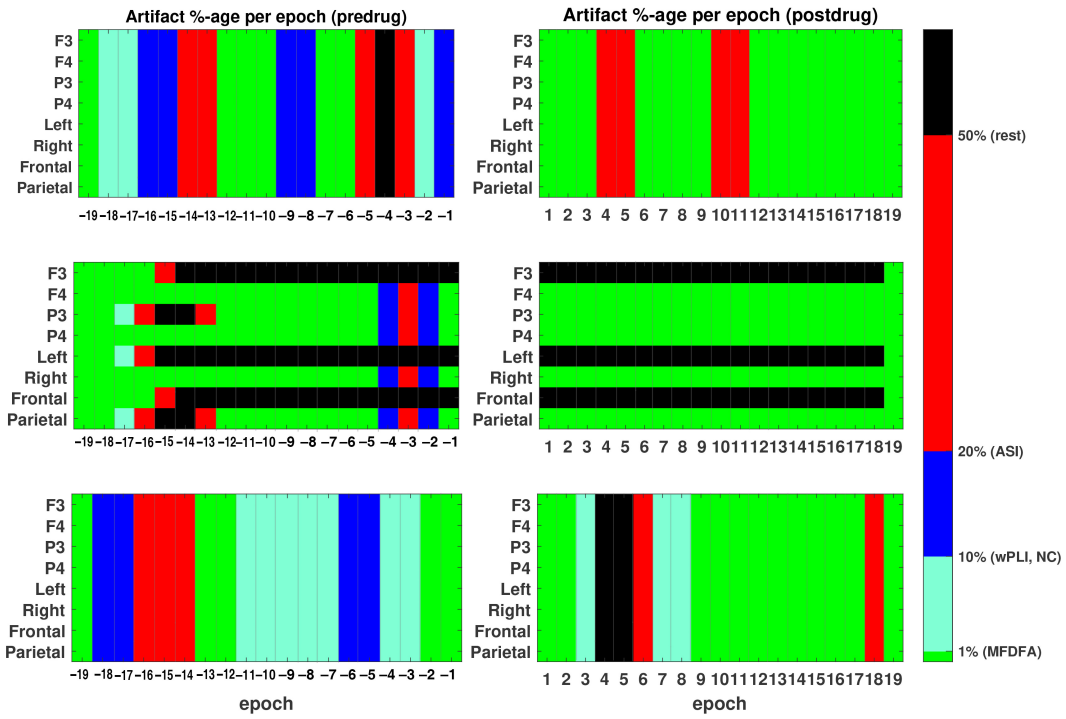


**Figure 17.** Artifact percentages for the first three subjects. This includes 19 pre-drug epochs and 19 post-drug epochs. Only 5 pre-drug and 10 post-drug epochs were used for statistical testing. Each pair of subplots contains the APT information for all 4 monopolar and 4 bipolar channels from one subject. The color ranges of different percentage ranges are explained in the color bar. For example, epochs marked with bright green had less than 1 % of their samples marked as unusable during the preprocessing pipeline.

consecutive rejections of the null hypothesis were seen in the parietal bipolar montage (P3–P4) of aEEG mean feature where  $\text{median}(\Delta\text{FE})$  seemed to be lowered from BL, starting around 200 seconds after fentanyl administration. This result did not replicate in either the P3 or P4 electrode.

#### 4.4 baseline–delta correlation

Most of the features showed no consistently significant correlations in baseline–delta testing. However, there were significant results in some of the measurements. All of the significant results ( $p < 0.05$ ) displayed negative correlation of at least ( $\rho < -0.5$ ). This means that in general, bigger BL values lead into more negative  $\Delta\text{FE}$  values.

**aEEG & rEEG:** For almost all of the sub-features for both aEEG (mean, IQR) and rEEG (mean, IQR, LI) there were trends of significantly negative correlational effects in the F4, P3 & P4 electrodes, which also manifested themselves in the right hemispheric (F4–P4) and parietal (P3–P4) bipolar montages. Only rEEG IQR features failed to show significant results in the F4–P4 montage. These effects started

around 150–300s after the fentanyl administration had been started, except for rEEG LI in the P4 electrode, which started around 400–500s after administration. These effects lasted at least until approximately 600s after administration, which was where the chosen examination period of these short-term effects ended. The correlation was always most negative at around 300s after administration.

**NC:** There was a significant trend of negative correlation in the F4 and P4 electrodes, which started immediately after administration and lasted for the duration of the 600s examination period. This effect was most prominent in the [3–8] Hz frequency range, and slightly visible also in the [8–15] Hz range.

**PSD:** Significant negative correlation trends were detected in all monopolar electrode channels across all frequency bands, although they were less prominent in the F3 channel in all but the [15–30] Hz frequency range. These effects also showed up in the Right and Parietal bipolar channel montages in all frequency bands. They started from approximately 150–200s after drug administration, and lasted mostly throughout the 600s observation period. The correlations were at their most negative around 300s after administration.

**cPSD:** Significant negative correlation trends were present in almost all of the tests across all the bipolar montage pairs and frequency bands. The clarity of the trends varied somewhat between test variables, but the only test that failed to show any significant correlation was the Left–Right montage pair in the [8–15] Hz range. Most other tests showed results similar to PSD, with effects starting either immediately or 150–200s after fentanyl administration, and lasting throughout the 600s measurement period.

**wPLI:** Initial inspection of correlation within wPLI values showed seemingly significant trends in multiple different frequency bands and multiple channel pairings. However, absolute wPLI values often exceeded values that would be realistically produced by effects of real brain synchrony ( $wPLI < 0.6$ ). These results are suspected to be due to remaining artifacts and noise in the data, as wPLI is very sensitive to edge effects and other artifacts that might be produced in the preprocessing stage. Due to this, the correlation results were not considered reliable.

## 5. Discussion

This study provides evidence that fentanyl produces detectable effects in the neonatal brain. These results are discussed below.

### 5.1 General observations

We found fentanyl's effect to be most prominent on features relating to EEG power and amplitude.

The correlation trends in both average rEEG and aEEG point towards a general decline in peak-to-peak amplitude. The correlation values being negative across the board implies, that greater baseline values lead to greater declines. These trends were weakest in the F3 electrode, which contributed to them not showing up in the Frontal and Left bipolar montages. Cortical activity in all other regions was reliably weakened and had less variability. The lowering of IQR-values also aligns with this interpretation, as the variance between signal amplitudes should get increasingly smaller as they tend closer towards zero. General lowering of the lower 5<sup>th</sup> index in rEEG also suggests that the effect is not only dampening towards the biggest amplitude differences, but lessens the signal as a whole.

The general lessening of signal power also concurs our findings with PSD, where we saw decline in all monopolar channels across all frequency ranges. This result differs slightly from studies carried previously on adults, where fentanyl was found to increase power in the  $\delta$ -band [34]. The declines in cPSD values point towards general de-coupling of power levels between brain areas that had previously been correlated, although the transient synchronies seemed to be unaffected in ASI.

The only reliable effect on transient brain synchrony we found was the lessening of  $\theta$ -waves nesting inside  $\delta$ -waves in the right hemisphere, suggesting that these kinds of effects are less prominent.

The fact that none of the aforementioned significant correlation results manifested themselves visibly in either of the time trends or in the Wilcoxon tests

shows, that baseline–delta correlation testing offers additional power towards extracting this type of trend data and should be utilized in future studies of this kind. This result is in concordance with findings in Samuli Suvisto’s thesis [4].

## 5.2 Technical limitations and strengths

The process of artifact removal proved difficult. This is not unusual in EEG studies, but it is most inconvenient when comparing specific time periods across multiple subjects, as this rids us of the freedom to choose well-behaved epochs for study. The appearance of artifacts in different subjects at different times means, that the total group of individuals being compared to each other can change from epoch to epoch, lessening the consistency of chronological comparison. This might also be why the combination of correlation testing against individual baselines ended up giving the best results. Using individual-specific baselines makes across-time comparisons more valid, and statistical testing lessens the impact of the number of subjects changing from epoch to epoch.

The method of choosing BL as the median of 5 pre-drug epochs might also be a better representation of pre-drug brain activity than the last-epoch BL method used in Wilcoxon signed-rank testing. Using only one epoch for BL is more susceptible for there to be a missing value in the BL due to artifacts. One missing BL value makes all of that subject’s FE comparisons for that feature impossible, effectively lessening  $n$  for that entire feature and consequently the power in all tests. When instead choosing BL from among multiple different epochs, it is more likely that at least one of them will have uncorrupted data that can be used.

CA for the subjects was unknown. This makes interpretation of the results more fuzzy, as there might be differences in the way the brain reacts to analgesics depending on CA and the developmental stage of the cortical subplate. One way to correct this would be to better annotate CA or even CRA in the data, making it possible to treat it as another variable. Alternatively—were we to have the luxury of choosing so—it would be most helpful for all the subjects to have a as similar CA as possible.

It should be noted that computing a high number of different  $p$ -values from the same data is susceptible to accumulation of false positives, a.k.a. type I errors. Some of these occurrences are detectable enough with visual inspection; a single epoch showing significant effects in the absence of any other spatially or temporally coinciding test results can logically be induced to likely have been a false alarm. However, type I errors can just as easily accumulate in clusters, obscuring their distinction from true positive results.

One way to lower the false discovery rate (FDR) would be to change significance threshold  $\alpha$  from 0.05 to smaller value such as 0.01. This would make it so that type I errors appear at worst only at a rate of 1 in every 100 tests as opposed to 1 in 20, thus making it less probable for them to group together in a deceptive manner.

Other considerable ways would include using the Benjamini–Hochberg procedure, which is used to prune a number of the largest significant  $p$ -values.

Some neuro-imaging methods like fMRI use familywise error rate (FWER) control methods such as Bonferroni correction, which limits the probability of at least one type I error appearing. These methods, however, are better suited in those fields where the data density is orders of magnitudes larger. If used in short periods of EEG data, their use would instead greatly increase the probability of type II errors (false negatives).

### 5.3 Future prospects

More in-depth statistical studies might be done to more rigorously determine appropriate APT values for the different features, as the numbers used for this study were little more than educated postulations. Other choices for selection of individual baseline values might also be explored, in order to find the most neutral overall comparison to drug-affected periods even when facing missing pre-drug data.

The Matlab pipeline constructed for producing the results in this study is freely available in GitHub with the permission of this thesis's advisors:

<https://github.com/Timo-Vehvilainen/EEG-feature-analysis-pipeline>

## 6. Conclusions

The goal of this thesis was to investigate short-term effects of fentanyl on neonate cortical activity using EEG. A total of 9 different computational features were extracted from four-channel EEG data from 15 subjects both before and after fentanyl administration. The states of these features were inspected for statistically significant changes between pre-drug and post-drug states, using 4 different methods of statistical evaluation.

Results suggest that fentanyl causes general weakening in the amplitude of the EEG signal, which is detectable as the lessening of rEEG, aEEG and PSD values across multiple frequency ranges, especially in the right hemispheric and the parietal brain areas. In addition, we detected de-coupling of previously power-correlated brain areas, and a decrease in nested  $\theta$ -waves. These effects occurred within 3–4 minutes from fentanyl administration. No significant effects relating to transient SAT synchrony between brain areas were found.

We found the most effective statistical method for detecting fentanyl-induced changes to be individualistic baseline–delta correlation testing. This method is most sensitive to effects where the change in feature measurement is proportional to its initial value. More traditional inspection methods such as time trends and Wilcoxon signed-rank testing failed to show discernible effects with our sample size.

The pipeline constructed for this thesis is freely available for usage in further research with fentanyl or other drugs.

# Bibliography

- [1] L. Liu, S. Oza, D. Hogan, Y. Chu, J. Perin, J. Zhu, J. E. Lawn, S. Cousens, C. Mathers, and R. E. Black, “Global, regional, and national causes of under-5 mortality in 2000–15: an updated systematic analysis with implications for the Sustainable Development Goals,” *The Lancet*, vol. 388, no. 10063, pp. 3027–3035, 2016.
- [2] W. Harrison and D. Goodman, “Epidemiologic trends in neonatal intensive care, 2007-2012,” *JAMA Pediatrics*, vol. 169, no. 9, pp. 855–862, 2015.
- [3] C. E. Rosow, J. Moss, D. M. Philbin, and J. J. Savarese, “Histamine release during morphine and fentanyl anesthesia,” *Anesthesiology*, vol. 56, no. 2, pp. 93–96, 1982.
- [4] S. Suvisto, “Effects of Dexmedetomidine on the cortical activity of neonates (Master’s Thesis),” 2018.
- [5] J. Jaatela, A. Tokariev, and N. Stevenson, “Computational features of neonatal EEG monitoring after asphyxia (Master’s Thesis),” 2017.
- [6] E. Martin and T. McFerran, “A Dictionary of Nursing,” in *A Dictionary of Nursing*, p. 275, Oxford University Press, 2008.
- [7] J. W. Ziegler and I. D. Todres, “Intubation of Newborns,” *American Journal of Diseases of Children*, vol. 146, pp. 147–149, 2 1992.
- [8] J. Oei, R. Hari, T. Buttha, and K. Lui, “Facilitation of neonatal nasotracheal intubation with premedication: A randomized controlled trial,” *Journal of Paediatrics and Child Health*, vol. 38, no. 2, pp. 146–150, 2002.
- [9] R. W. Hall, E. Boyle, and T. Young, “Do Ventilated Neonates Require Pain Management?,” *Seminars in Perinatology*, vol. 31, no. 5, pp. 289–297, 2007.
- [10] T. L. Yaksh and M. S. Wallace, “Opioids, Analgesia, and Pain Management,” in *Goodman & Gilman’s The Pharmacological Basis of Therapeutics*, pp. 481–527, New York: McGraw-Hill, 2011.
- [11] M. R. Bruchas and C. Chavkin, “Kinase cascades and ligand-directed signaling at the kappa opioid receptor,” *Psychopharmacology*, vol. 209, no. 2, pp. 137–147, 2010.
- [12] B. N. Dhawan, F. Cesselin, R. Raghbir, T. Reisine, P. B. Bradley, P. S. Portoghese, and M. Hamon, “International Union of Pharmacology. XII. Classification of opioid receptors,” *Pharmacological Reviews*, vol. 48, no. 4, pp. 567–592, 1996.
- [13] R. Al-Hasani and M. R. Bruchas, “Molecular mechanisms of opioid receptor-dependent signaling and behavior,” *Anesthesiology*, vol. 115, no. 6, pp. 1363–1381, 2011.

- [14] K. J. Anand and R. W. Hall, "Pharmacological therapy for analgesia and sedation in the newborn," *Archives of Disease in Childhood: Fetal and Neonatal Edition*, vol. 91, no. 6, pp. 448–453, 2006.
- [15] E. J. Kuip, M. L. Zandvliet, S. L. Koolen, R. H. Mathijssen, and C. C. van der Rijt, "A review of factors explaining variability in fentanyl pharmacokinetics; focus on implications for cancer patients," *British Journal of Clinical Pharmacology*, vol. 83, no. 2, pp. 294–313, 2017.
- [16] A. Mitchell, S. Brooks, and D. Roane, "The premature infant and painful procedures," *Pain Management Nursing*, vol. June, no. 2, pp. 58–65, 2000.
- [17] M. Ayed, V. S. Shah, and A. Taddio, "Premedication for non-urgent endotracheal intubation for preventing pain in neonates," *Cochrane Database of Systematic Reviews*, no. 2, 2017.
- [18] R. W. Hall, S. S. Kronsberg, B. A. Barton, J. R. Kaiser, and K. J. S. Anand, "Morphine, hypotension, and adverse outcomes among preterm neonates: Who's to blame? Secondary results from the NEOPAIN trial," *Pediatrics*, vol. 115, no. 5, pp. 1351–1359, 2005.
- [19] G. Menon, E. M. Boyle, L. L. Bergqvist, N. McIntosh, B. A. Barton, and K. J. Anand, "Morphine analgesia and gastrointestinal morbidity in preterm infants: Secondary results from the NEOPAIN trial," *Archives of Disease in Childhood: Fetal and Neonatal Edition*, vol. 93, no. 5, pp. 362–367, 2008.
- [20] R. W. Hall and R. M. Shbarou, "Drugs of Choice for Sedation and Analgesia in the Neonatal ICU," *Clinics in Perinatology*, vol. 36, no. 2, pp. 215–226, 2009.
- [21] W. O. Tatum et al, "Handbook of EEG Interpretation," in *Handbook of EEG Interpretation*, pp. 1–56, Springer Publishing Company, 2 ed., 2014.
- [22] B. Burle, L. Spieser, C. Roger, L. Casini, T. Hasbroucq, and F. Vidal, "Spatial and temporal resolutions of EEG: Is it really black and white? A scalp current density view," *International Journal of Psychophysiology*, vol. 97, no. 3, pp. 210–220, 2015.
- [23] D. Yao, "A method to standardize a reference of scalp EEG recordings to a point at infinity," *Physiological Measurement*, vol. 22, no. 4, pp. 693–711, 2001.
- [24] R. P. Lystad and H. Pollard, "Functional neuroimaging: a brief overview and feasibility for use in chiropractic research.," *The Journal of the Canadian Chiropractic Association*, vol. 53, no. 1, pp. 59–72, 2009.
- [25] H. Jasper, "The ten twenty electrode system of the international federation," *Electroencephalography and Clinical Neurophysiology*, vol. 52, pp. 3–6, 1999.
- [26] V. L. Towle, J. Bolaños, D. Suarez, K. Tan, R. Grzeszczuk, D. N. Levin, R. Cakmur, S. A. Frank, and J. P. Spire, "The spatial location of EEG electrodes: locating the best-fitting sphere relative to cortical anatomy," *Electroencephalography and Clinical Neurophysiology*, vol. 86, no. 1, pp. 1–6, 1993.
- [27] F. L. da Silva, "Eeg analysis: Theory and practice," in *Electroencephalography: Basic Principles, Clinical Applications and Related Fields-Fifth Edition*, pp. 1199–1231, Baltimore: Williams & Wilkins, 2005.
- [28] E. Niedermeyer, "The Normal EEG of the Waking Adult," in *Electroencephalography: Basic Principles, Clinical Applications and Related Fields*, pp. 149–173, Baltimore: Williams & Wilkins, 1999.

- [29] D. M. White and A. C. Van Cott, "EEG artifacts in the intensive care unit setting," *American Journal of Electroneurodiagnostic Technology*, vol. 50, no. 1, pp. 8–25, 2010.
- [30] E. L. Reilly, "EEG Recording and Operation of the Apparatus," in *Electroencephalography: Basic Principles, Clinical Applications, and Related Fields*, pp. 19–50, Academic Press, 2005.
- [31] A. Kamp, G. Pfurtsscheller, G. Edlinger, and F. L. d. Silva, "Technological basis of eeg recording," in *Electroencephalography. Basic principles, clinical applications and related fields*, pp. 127–138, Williams & Wilkins, 2005.
- [32] G. Bauer and R. Bauer, "EEG, drug effects, and central nervous system poisoning," in *Niedermeyer's Electroencephalography: Basic Principles, Clinical Applications, and Related Fields: Sixth Edition*, pp. 901–922, Williams & Wilkins, 2012.
- [33] P. S. Sebel, J. G. Bovill, A. Wauquier, and P. Rog, "Effects of high-dose fentanyl anesthesia on the electroencephalogram," *Anesthesiology*, vol. 55, no. 3, pp. 203–211, 1981.
- [34] J. C. Scott, K. V. Ponganis, and D. R. Stanski, "EEG quantitation of narcotic effect: The comparative pharmacodynamics of fentanyl and alfentanil," *Anesthesiology*, vol. 62, no. 3, pp. 234–241, 1985.
- [35] S. Ackerman, "The Development and Shaping of the Brain," in *Discovering the Brain*, pp. 86–103, National Academies Press, 1992.
- [36] I. Kostović and N. Jovanov-Milošević, "The development of cerebral connections during the first 20-45 weeks' gestation," *Seminars in Fetal and Neonatal Medicine*, vol. 11, no. 6, pp. 415–422, 2006.
- [37] E. M. Mizrahi, S. L. Moshé, and R. A. Hrachovy, "Normal EEG and sleep: Preterm and term neonates," in *Niedermeyer's Electroencephalography: Basic Principles, Clinical Applications, and Related Fields: Sixth Edition*, pp. 153–162, Williams & Wilkins, 2012.
- [38] S. Vanhatalo, J. Matias Palva, S. Andersson, C. Rivera, J. Voipio, and K. Kaila, "Slow endogenous activity transients and developmental expression of K<sup>+</sup>-Cl<sup>-</sup> cotransporter 2 in the immature human cortex," *European Journal of Neuroscience*, vol. 22, no. 11, pp. 2799–2804, 2005.
- [39] S. Vanhatalo and K. Kaila, "Development of neonatal EEG activity: From phenomenology to physiology," *Seminars in Fetal and Neonatal Medicine*, vol. 11, no. 6, pp. 471–478, 2006.
- [40] M. Hayakawa, A. Okumura, F. Hayakawa, K. Watanabe, M. Ohshiro, Y. Kato, R. Takahashi, and N. Tauchi, "Background electroencephalographic (EEG) activities of very preterm infants born at less than 27 weeks gestation: A study on the degree of continuity," *Archives of Disease in Childhood: Fetal and Neonatal Edition*, vol. 84, no. 3, pp. 163–167, 2001.
- [41] O. Räsänen, M. Metsäranta, and S. Vanhatalo, "Development of a novel robust measure for interhemispheric synchrony in the neonatal EEG: Activation Synchrony Index (ASI)," *NeuroImage*, vol. 69, pp. 256–266, 2013.
- [42] N. Koolen, A. Dereymaeker, O. Räsänen, K. Jansen, J. Vervisch, V. Matic, G. Naulaers, M. De Vos, S. Van Huffel, and S. Vanhatalo, "Early development of synchrony in cortical activations in the human," *Neuroscience*, vol. 322, no. May, pp. 298–307, 2016.

- [43] N. Koolen, A. Dereymaeker, O. Räsänen, K. Jansen, J. Vervisch, V. Matic, M. De Vos, S. Van Huffel, G. Naulaers, and S. Vanhatalo, "Interhemispheric synchrony in the neonatal EEG revisited: activation synchrony index as a promising classifier," *Frontiers in Human Neuroscience*, vol. 8, p. 1030, 2014.
- [44] A. Tokariev, K. Palmu, A. Lano, M. Metsäranta, and S. Vanhatalo, "Phase synchrony in the early preterm EEG: Development of methods for estimating synchrony in both oscillations and events," *NeuroImage*, vol. 60, no. 2, pp. 1562–1573, 2012.
- [45] J. P. Lachaux, E. Rodriguez, J. Martinerie, and F. J. Varela, "Measuring phase synchrony in brain signals," *Human Brain Mapping*, vol. 8, no. 4, pp. 194–208, 1999.
- [46] C. J. Stam, G. Nolte, and A. Daffertshofer, "Phase lag index: Assessment of functional connectivity from multi channel EEG and MEG with diminished bias from common sources," *Human Brain Mapping*, vol. 28, no. 11, pp. 1178–1193, 2007.
- [47] M. Vinck, R. Oostenveld, M. Van Wingerden, F. Battaglia, and C. M. Pennartz, "An improved index of phase-synchronization for electrophysiological data in the presence of volume-conduction, noise and sample-size bias," *NeuroImage*, vol. 55, no. 4, pp. 1548–1565, 2011.
- [48] A. M. Bastos and J.-M. Schoffelen, "A Tutorial Review of Functional Connectivity Analysis Methods and Their Interpretational Pitfalls," *Frontiers in Systems Neuroscience*, vol. 9, p. 175, 2016.
- [49] A. Tokariev, S. Vanhatalo, and J. M. Palva, "Analysis of infant cortical synchrony is constrained by the number of recording electrodes and the recording montage," *Clinical Neurophysiology*, vol. 127, no. 1, pp. 310–323, 2016.
- [50] A. K. Engel, C. Gerloff, C. C. Hilgetag, and G. Nolte, "Intrinsic Coupling Modes: Multiscale Interactions in Ongoing Brain Activity," *Neuron*, vol. 80, no. 4, pp. 867–886, 2013.
- [51] R. C. Sotero, A. Bortel, S. Naaman, V. M. Mocanu, P. Kropf, M. Villeneuve, and A. Shmuel, "Laminar distribution of phase-amplitude coupling of spontaneous current sources and sinks," *Frontiers in Neuroscience*, vol. 9, no. DEC, p. 454, 2015.
- [52] S. Palva and J. M. Palva, "Discovering oscillatory interaction networks with M/EEG: Challenges and breakthroughs," *Trends in Cognitive Sciences*, vol. 16, no. 4, pp. 219–230, 2012.
- [53] P. D. Welch, "The Use of Fast Fourier Transform for the Estimation of Power Spectra: A Method Based on Time Averaging Over Short, Modified Periodograms," *IEEE Transactions on Audio and Electroacoustics*, vol. 15, no. 2, pp. 70–73, 1967.
- [54] G. Wang, H. Huang, H. Xie, Z. Wang, and X. Hu, "Multifractal analysis of ventricular fibrillation and ventricular tachycardia," *Medical Engineering and Physics*, vol. 29, no. 3, pp. 375–379, 2007.
- [55] Y. Zheng, J. Gao, J. C. Sanchez, J. C. Principe, and M. S. Okun, "Multiplicative multifractal modeling and discrimination of human neuronal activity," *Physics Letters, Section A: General, Atomic and Solid State Physics*, vol. 344, no. 2-4, pp. 253–264, 2005.
- [56] J. W. Kantelhardt, S. A. Zschiegner, E. Koscielny-Bunde, S. Havlin, A. Bunde, and H. E. Stanley, "Multifractal detrended fluctuation analysis of nonstationary time series," *Physica A: Statistical Mechanics and its Applications*, vol. 316, no. 1-4, pp. 87–114, 2002.

- [57] E. A. F. Ihlen, "Introduction to multifractal detrended fluctuation analysis in Matlab," *Frontiers in Physiology*, vol. 3, p. 141, 2012.
- [58] V. Matic, P. J. Cherian, N. Koolen, A. H. Ansari, G. Naulaers, P. Govaert, S. Van Huffel, M. De Vos, and S. Vanhatalo, "Objective differentiation of neonatal EEG background grades using detrended fluctuation analysis," *Frontiers in Human Neuroscience*, vol. 9, p. 198, 2015.
- [59] T. Zorick and M. A. Mandelkern, "Multifractal Detrended Fluctuation Analysis of Human EEG: Preliminary Investigation and Comparison with the Wavelet Transform Modulus Maxima Technique," *PLoS ONE*, vol. 8, no. 7, 2013.
- [60] L. Hellstrom Westas, I. Rosen, L. S. de Vries, and G. Greisen, "Amplitude-integrated EEG Classification and Interpretation in Preterm and Term Infants," *NeoReviews*, vol. 7, no. 2, pp. 76–87, 2006.
- [61] D. O'Reilly, M. A. Navakatikyan, M. Filip, D. Greene, and L. J. Van Marter, "Peak-to-peak amplitude in neonatal brain monitoring of premature infants," *Clinical Neurophysiology*, vol. 123, no. 11, pp. 2139–2153, 2012.
- [62] G. B. Boylan, L. Burgoyne, C. Moore, B. O'Flaherty, and J. M. Rennie, "An international survey of EEG use in the neonatal intensive care unit," *Acta Paediatrica, International Journal of Paediatrics*, vol. 99, no. 8, pp. 1150–1155, 2010.
- [63] L. Hellström-Westas and I. Rosén, "Continuous brain-function monitoring: State of the art in clinical practice," *Seminars in Fetal and Neonatal Medicine*, vol. 11, no. 6, pp. 503–511, 2006.
- [64] A. Wauquier, "EEG and Neuropharmacology," in *Electroencephalography: Basic Principles, Clinical Applications and Related Fields-Fifth Edition*, pp. 2730–2774, Baltimore: Williams & Wilkins, 1991.
- [65] M. A. Navakatikyan, D. O'Reilly, and L. J. Van Marter, "Automatic measurement of interburst interval in premature neonates using range EEG," *Clinical Neurophysiology*, vol. 127, no. 2, pp. 1233–1246, 2016.
- [66] R. Esteller, J. Echauz, T. Tcheng, B. Litt, and B. Pless, "Line length: An efficient feature for seizure onset detection," *Annual International Conference of the IEEE Engineering in Medicine and Biology-Proceedings*, vol. 2, pp. 1707–1710, 2001.
- [67] N. Koolen, K. Jansen, J. Vervisch, V. Matic, M. De Vos, G. Naulaers, and S. Van Huffel, "Line length as a robust method to detect high-activity events: Automated burst detection in premature EEG recordings," *Clinical Neurophysiology*, vol. 125, no. 10, pp. 1985–1994, 2014.
- [68] F. Wilcoxon, "Individual Comparisons by Ranking Methods," *Biometrics Bulletin*, vol. 1, no. 6, p. 80, 1945.
- [69] J. Hauke and T. Kossowski, "Comparison of values of Pearson's and Spearman's correlation coefficients on the same sets of data," *Quaestiones Geographicae*, vol. 30, pp. 87–93, 2011.
- [70] C. S. Gibbons J.D., "Nonparametric Statistical Inference," in *International Encyclopedia of Statistical Science*, pp. 977–979, Springer, 2011.
- [71] J. H. Zar, "Significance testing of the Spearman rank correlation coefficient," *Journal of the American Statistical Association*, vol. 67, pp. 578–580, 1972.

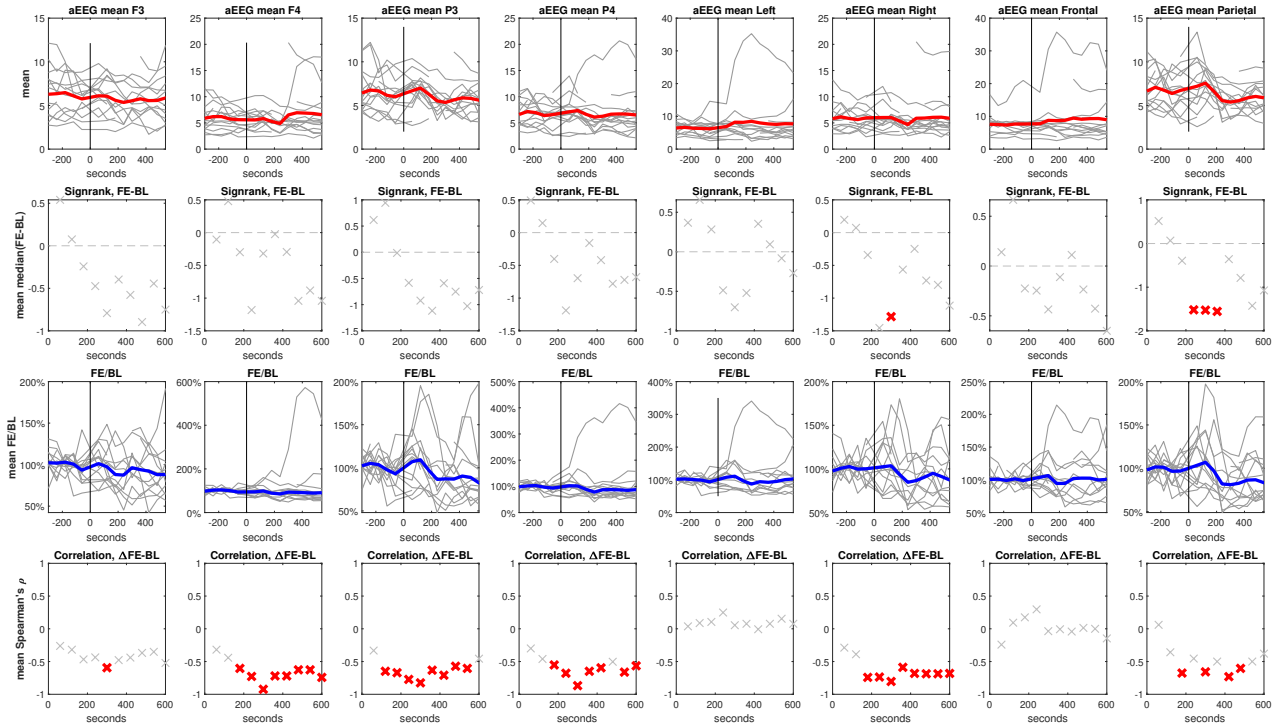
## A. Statistical Analysis Results

In this appendix is the complete collection of results for the statistical analyses introduced in Section 3.5. For clarity, explicit  $p$ -values have been omitted from the graphs. Instead, median values for the Wilcoxon signed rank test and correlation values for Spearman's rho have been marked with a red cross, if that value corresponded with a  $p$ -value that was below the significance threshold of 0.05. Otherwise, those values are marked with a gray cross.

All the Spearman's correlation coefficients and their corresponding  $p$ -values are attached as tables.

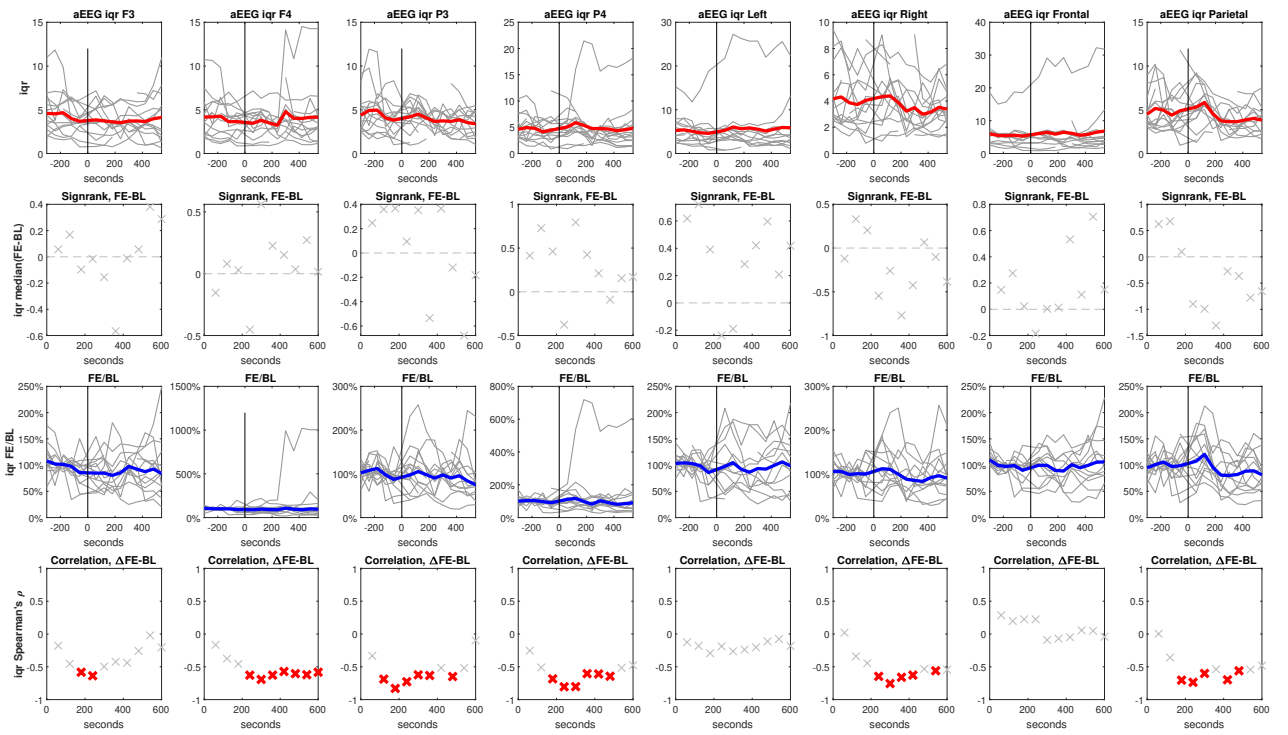
## aEEG

## mean



time after drug [s]	aEEG mean															
	F3		F4		P3		P4		Left		Right		Frontal		Parietal	
	CC	p														
0-120	-0.261538	0.366411	-0.318681	0.266785	-0.332143	0.226353	-0.3	0.276682	0.037363	0.899093	-0.287912	0.318193	-0.241758	0.426176	0.060714	0.832426
60-180	-0.318681	0.266785	-0.441758	0.113778	-0.648352	0.012144	-0.460714	0.086069	0.087912	0.775195	-0.389011	0.169217	0.093407	0.7615	-0.358242	0.208498
120-240	-0.467033	0.107609	-0.604396	0.028673	-0.67033	0.012166	-0.551648	0.040849	0.104895	0.745609	-0.741758	0.003701	0.174825	0.586824	-0.675824	0.011225
180-300	-0.436364	0.179665	-0.727273	0.011205	-0.772727	0.005299	-0.678322	0.015317	0.248485	0.488776	-0.736364	0.00976	0.29697	0.404702	-0.454545	0.160145
240-360	-0.594406	0.041521	-0.923077	1.86E-05	-0.825175	0.000951	-0.868132	0.000119	0.054545	0.873447	-0.804196	0.001615	-0.036364	0.915468	-0.657343	0.020185
300-420	-0.478022	0.09849	-0.71978	0.005536	-0.631868	0.020516	-0.648352	0.012144	0.076923	0.812183	-0.587912	0.034586	-0.006993	0.982792	-0.5	0.081864
360-480	-0.43956	0.13286	-0.71978	0.005536	-0.708791	0.006682	-0.595604	0.024613	-0.006993	0.982792	-0.681319	0.01034	-0.041958	0.896986	-0.730769	0.004548
420-540	-0.368132	0.215857	-0.626374	0.021989	-0.571429	0.041342	-0.503297	0.06656	0.076923	0.812183	-0.686813	0.009509	0.013986	0.96559	-0.604396	0.028673
480-600	-0.351648	0.2387	-0.626374	0.021989	-0.604396	0.028673	-0.661538	0.009975	0.153846	0.633091	-0.686813	0.009509	0	1	-0.5	0.081864
540-660	-0.521978	0.067292	-0.741758	0.003701	-0.456044	0.117283	-0.564835	0.03533	0.076923	0.812183	-0.681319	0.01034	-0.146853	0.648796	-0.379121	0.201406

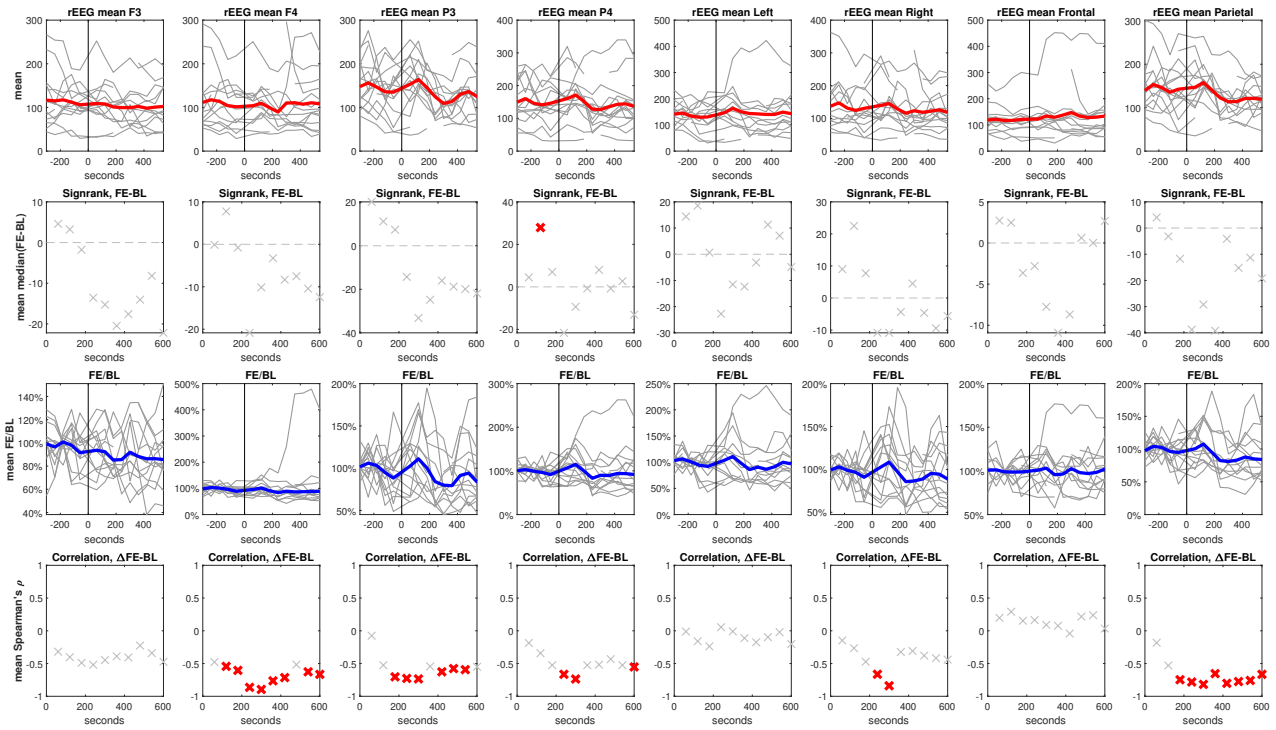
## IQR



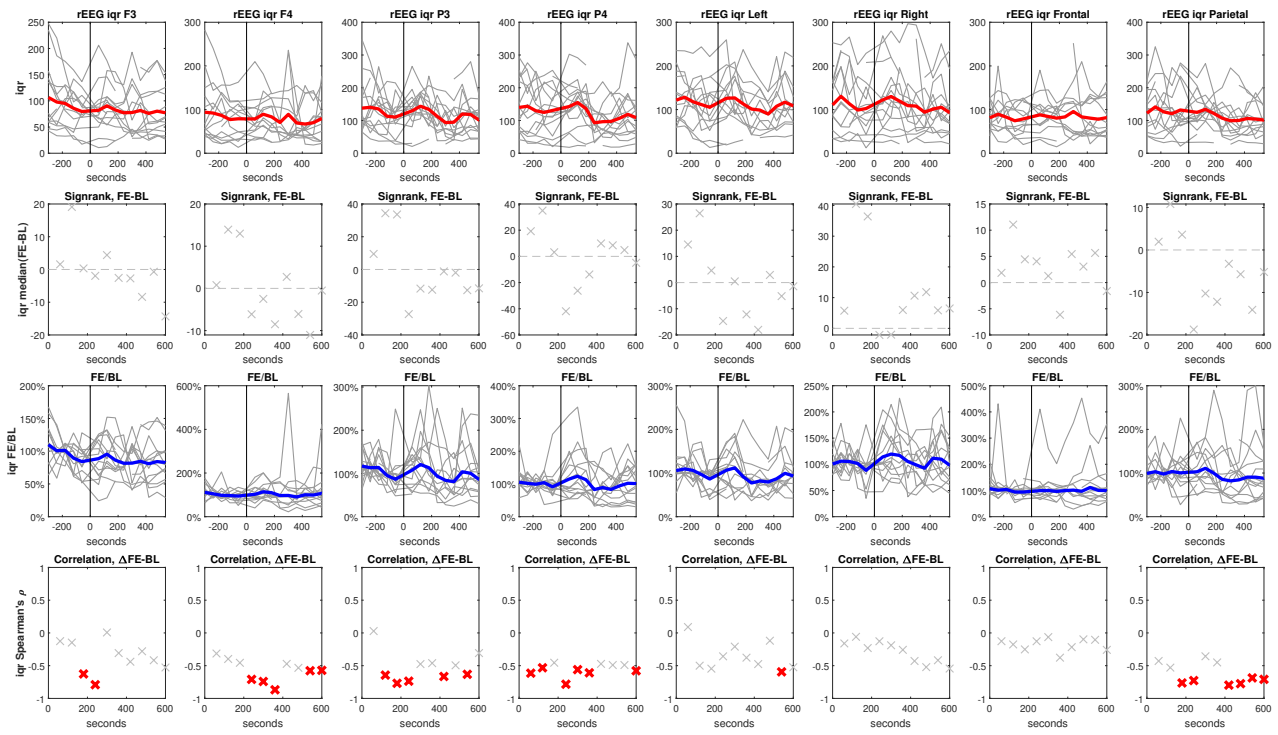
aEEG IQR										
time after drug [s]	F3		F4		P3		P4		Left	
	CC	p								
0-120	-0.178022	0.542597	-0.164835	0.573346	-0.332143	0.226353	-0.253571	0.360721	-0.125275	0.669582
60-180	-0.454945	0.102154	-0.375824	0.18541	-0.687912	0.00654	-0.510714	0.054296	-0.181319	0.553295
120-240	-0.582418	0.036741	-0.456044	0.117283	-0.82967	0.00045	-0.683516	0.007037	-0.293706	0.354148
180-300	-0.636364	0.035287	-0.627273	0.038845	-0.727273	0.011205	-0.804196	0.001615	-0.187879	0.603218
240-360	-0.496503	0.100603	-0.692308	0.012593	-0.622378	0.030676	-0.802198	0.000969	-0.263636	0.433441
300-420	-0.423077	0.149749	-0.626374	0.021989	-0.631868	0.020516	-0.604396	0.022057	-0.237762	0.456801
360-480	-0.43956	0.13286	-0.571429	0.041342	-0.516484	0.070749	-0.608791	0.020857	-0.202797	0.527302
420-540	-0.258242	0.394284	-0.604396	0.028673	-0.648352	0.016537	-0.643956	0.012942	-0.111888	0.729195
480-600	-0.021978	0.943186	-0.620879	0.023538	-0.516484	0.070749	-0.516484	0.058637	-0.076923	0.812183
540-660	-0.203297	0.505315	-0.582418	0.036741	-0.098901	0.747868	-0.476923	0.084648	-0.181818	0.571701

## rEEG

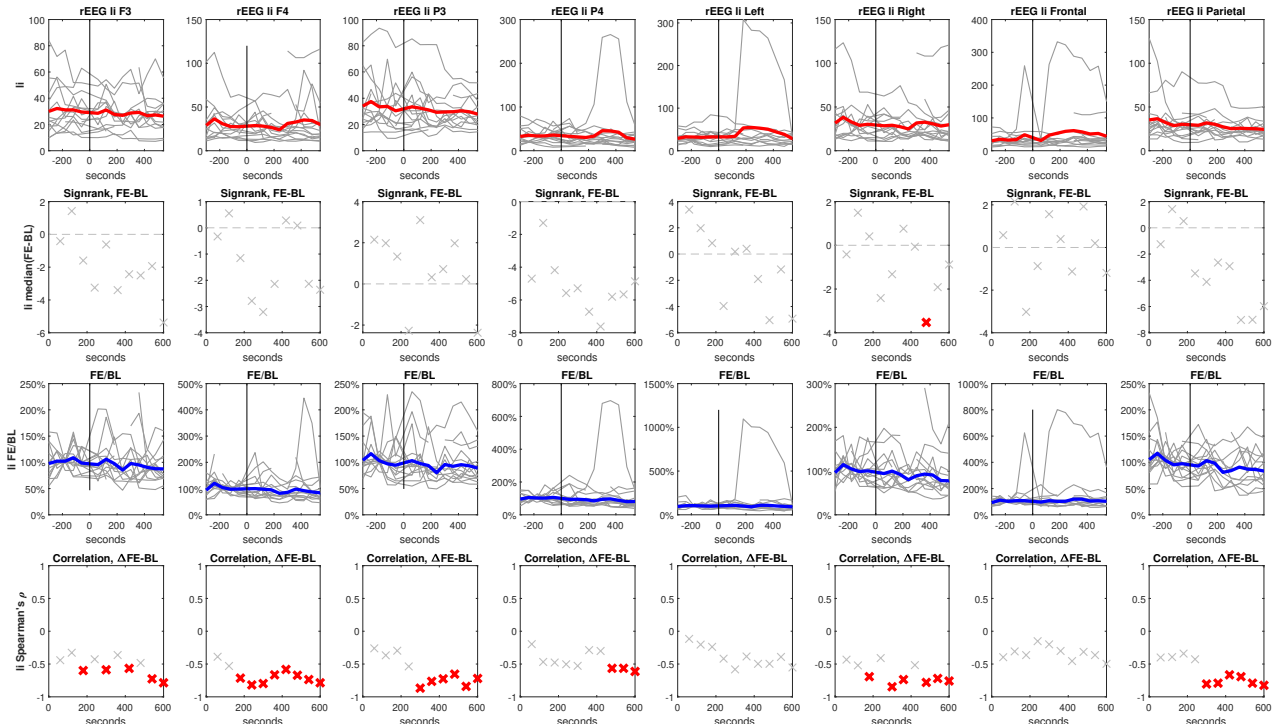
## mean



time after drug [s]	rEEG mean															
	F3		F4		P3		P4		Left		Right		Frontal		Parietal	
	CC	p														
0-120	-0.318681	0.266785	-0.476923	0.084648	-0.075	0.792571	-0.185714	0.506674	-0.010989	0.970258	-0.147253	0.615419	0.197802	0.517131	-0.182143	0.915061
60-180	-0.402198	0.153974	-0.542857	0.044864	-0.525275	0.053748	-0.342857	0.211	-0.159341	0.603088	-0.265934	0.358113	0.291209	0.334386	-0.52967	0.051417
120-240	-0.489011	0.089913	-0.604396	0.028673	-0.703297	0.007319	-0.525275	0.053748	-0.237762	0.456801	-0.472527	0.102981	0.153846	0.633091	-0.747253	0.003327
180-300	-0.518182	0.102492	-0.863636	0.000612	-0.727273	0.011205	-0.664336	0.018453	0.054545	0.881036	-0.663636	0.025984	0.163636	0.651477	-0.781818	0.004473
240-360	-0.447552	0.144586	-0.895105	8.37e-05	-0.734266	0.006543	-0.736264	0.004108	-0.009091	0.978837	-0.839161	0.000643	0.090909	0.790373	-0.818182	0.001143
300-420	-0.39011	0.187574	-0.763736	0.002377	-0.543956	0.054647	-0.525275	0.053748	-0.111888	0.729195	-0.324176	0.279882	0.076923	0.812183	-0.653846	0.015349
360-480	-0.406593	0.167978	-0.714286	0.006088	-0.626374	0.021989	-0.516484	0.058637	-0.174825	0.586824	-0.307692	0.306447	-0.041958	0.896986	-0.802198	0.000969
420-540	-0.225275	0.459305	-0.516484	0.070749	-0.576923	0.038993	-0.432967	0.12201	-0.097902	0.762122	-0.379121	0.201406	0.216783	0.498556	-0.774725	0.001871
480-600	-0.340659	0.254706	-0.626374	0.021989	-0.593407	0.032524	-0.525275	0.053748	-0.020979	0.948402	-0.417582	0.155675	0.237762	0.456801	-0.758242	0.002666
540-660	-0.472527	0.102981	-0.664835	0.013166	-0.549451	0.051771	-0.551648	0.040849	-0.202797	0.527302	-0.43956	0.13286	0.034965	0.914093	-0.664835	0.013166

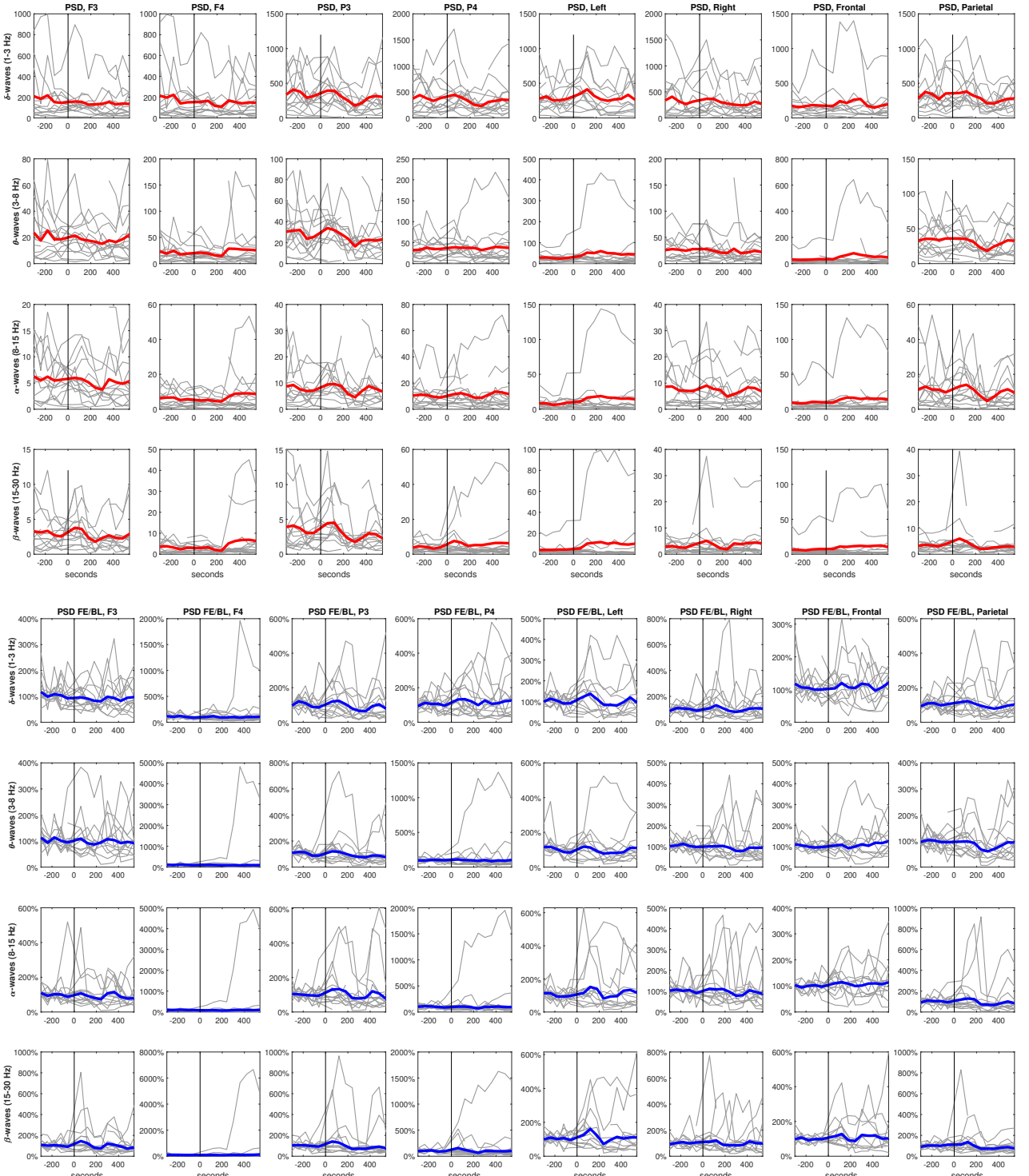
**IQR**

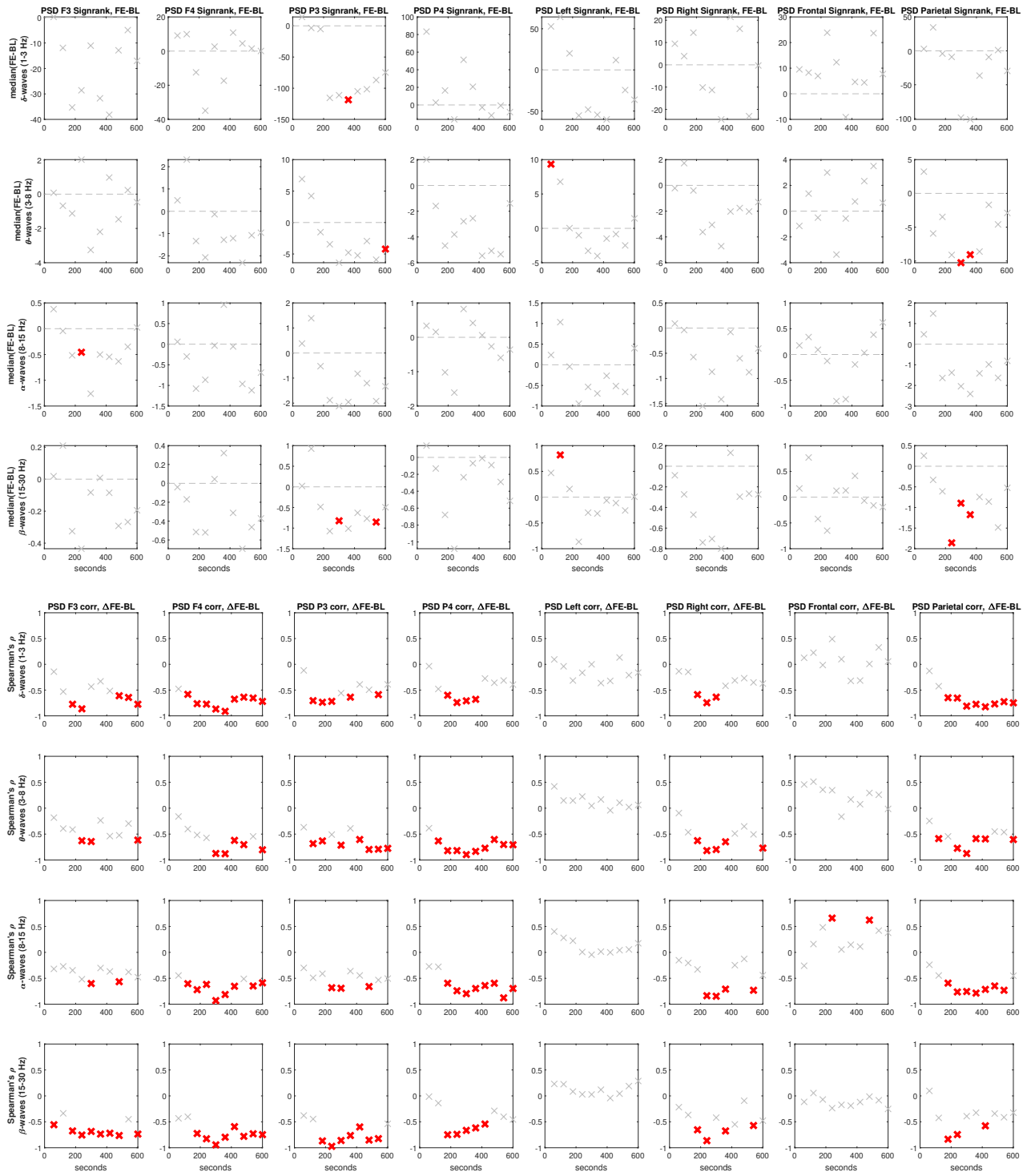
rEEG IQR										
time after drug [s]	F3		F4		P3		P4		Left	
	CC	p								
0-120	-0.125275	0.669582	-0.314286	0.273805	0.028571	0.923417	-0.614286	0.017076	0.09011	0.759339
60-180	-0.147253	0.615419	-0.397802	0.158951	-0.643956	0.012942	-0.532143	0.043792	-0.5	0.081864
120-240	-0.626374	0.021989	-0.456044	0.117283	-0.769231	0.002112	-0.454945	0.102154	-0.545455	0.066612
180-300	-0.790909	0.003746	-0.709091	0.014552	-0.736364	0.00976	-0.783217	0.002586	-0.357576	0.310376
240-360	0.006993	0.982792	-0.741259	0.005801	-0.475524	0.118176	-0.56044	0.046346	-0.209091	0.537221
300-420	-0.307692	0.306447	-0.868132	0.000119	-0.461538	0.112376	-0.608791	0.020857	-0.377622	0.226206
360-480	-0.43956	0.13286	-0.472527	0.102981	-0.664835	0.013166	-0.472527	0.087967	-0.475524	0.118176
420-540	-0.28022	0.353764	-0.532967	0.060737	-0.494505	0.085824	-0.49011	0.07522	-0.118881	0.712884
480-600	-0.417582	0.155675	-0.576923	0.038993	-0.631868	0.020516	-0.49011	0.07522	-0.594406	0.041521
540-660	-0.527473	0.063955	-0.571429	0.041342	-0.307692	0.306447	-0.57802	0.030383	-0.524476	0.080019

**II**

time after drug [s]	EEG LI															
	F3		F4		P3		P4		Left		Right		Frontal		Parietal	
	CC	p	CC	p	CC	p	CC	p	CC	p	CC	p	CC	p	CC	p
0-120	-0.428571	0.11263	-0.389011	0.169217	-0.260714	0.346928	-0.196429	0.481914	-0.116484	0.691691	-0.432967	0.12201	-0.395604	0.180889	-0.4	0.140762
60-180	-0.52967	0.051417	-0.52967	0.051417	-0.367033	0.196739	-0.467857	0.080851	-0.203297	0.505315	-0.520879	0.056154	-0.307692	0.306447	-0.393407	0.164032
120-240	-0.763736	0.002377	-0.714286	0.006088	-0.296703	0.324922	-0.476923	0.084648	-0.237762	0.456801	-0.692308	0.00873	-0.363636	0.245265	-0.340659	0.254706
180-300	-0.727273	0.011205	-0.818182	0.002083	-0.536364	0.088953	-0.503497	0.095157	-0.418182	0.229113	-0.409091	0.211545	-0.151515	0.676065	-0.427273	0.189944
240-360	-0.356643	0.255138	-0.797203	0.0019	-0.867133	0.00026	-0.527473	0.063955	-0.581818	0.06042	-0.846154	0.000521	-0.2	0.555445	-0.804196	0.001615
300-420	-0.450549	0.122332	-0.664835	0.013166	-0.763736	0.002377	-0.287912	0.318193	-0.384615	0.21702	-0.736264	0.004108	-0.300699	0.34226	-0.791209	0.001275
360-480	-0.796703	0.001114	-0.582418	0.036741	-0.725275	0.005023	-0.301099	0.0564835	-0.496503	0.100603	-0.496503	0.100603	-0.78022	0.001653	-0.454545	0.137658
420-540	-0.774725	0.001871	-0.67033	0.012166	-0.653846	0.015349	-0.564835	0.03533	-0.391608	0.208063	-0.71978	0.005536	-0.314685	0.319139	-0.692308	0.00873
480-600	-0.686813	0.009509	-0.736264	0.004108	-0.840659	0.000319	-0.564835	0.03533	-0.592448	0.062511	-0.758242	0.002666	-0.363636	0.245265	-0.791209	0.001275
540-660	-0.708791	0.006682	-0.785714	0.001454	-0.71978	0.005536	-0.613187	0.019706	-	-	-0.496503	0.100603	-0.824176	0.00053	-	-

PSD

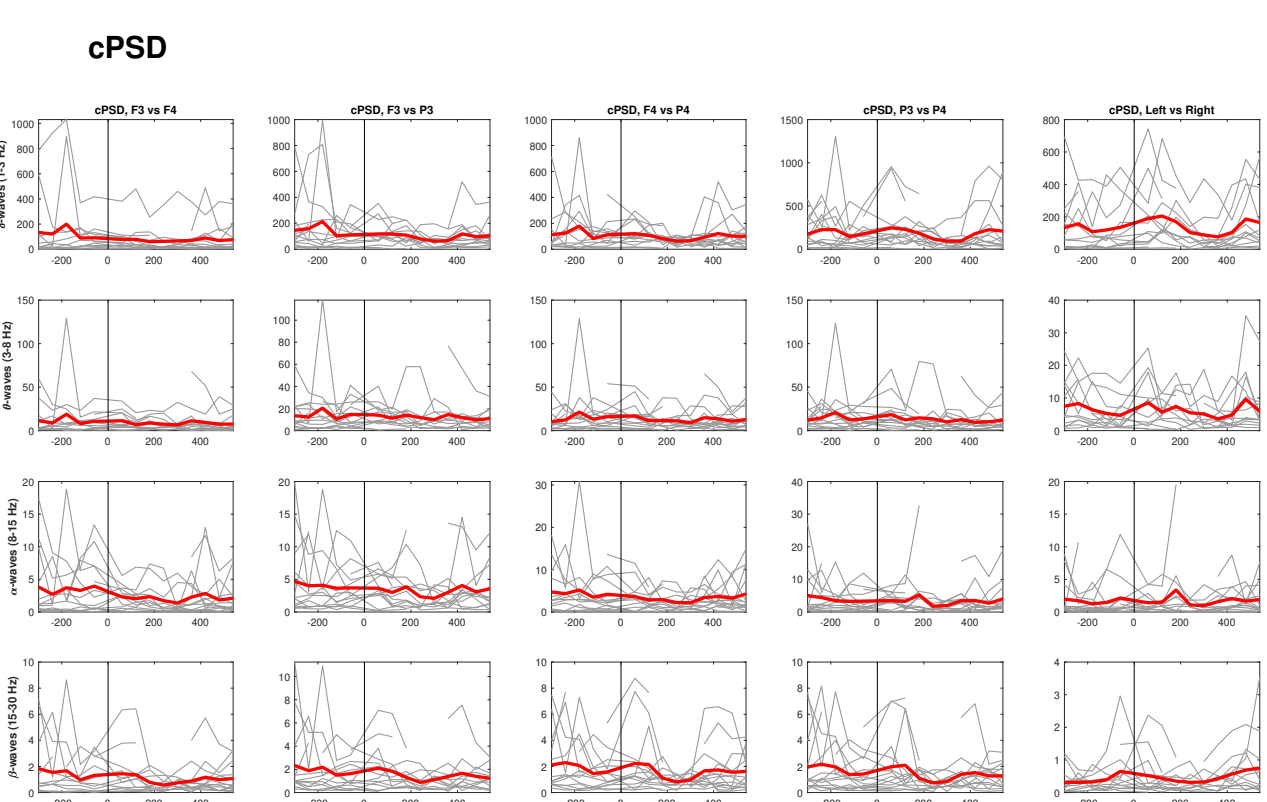


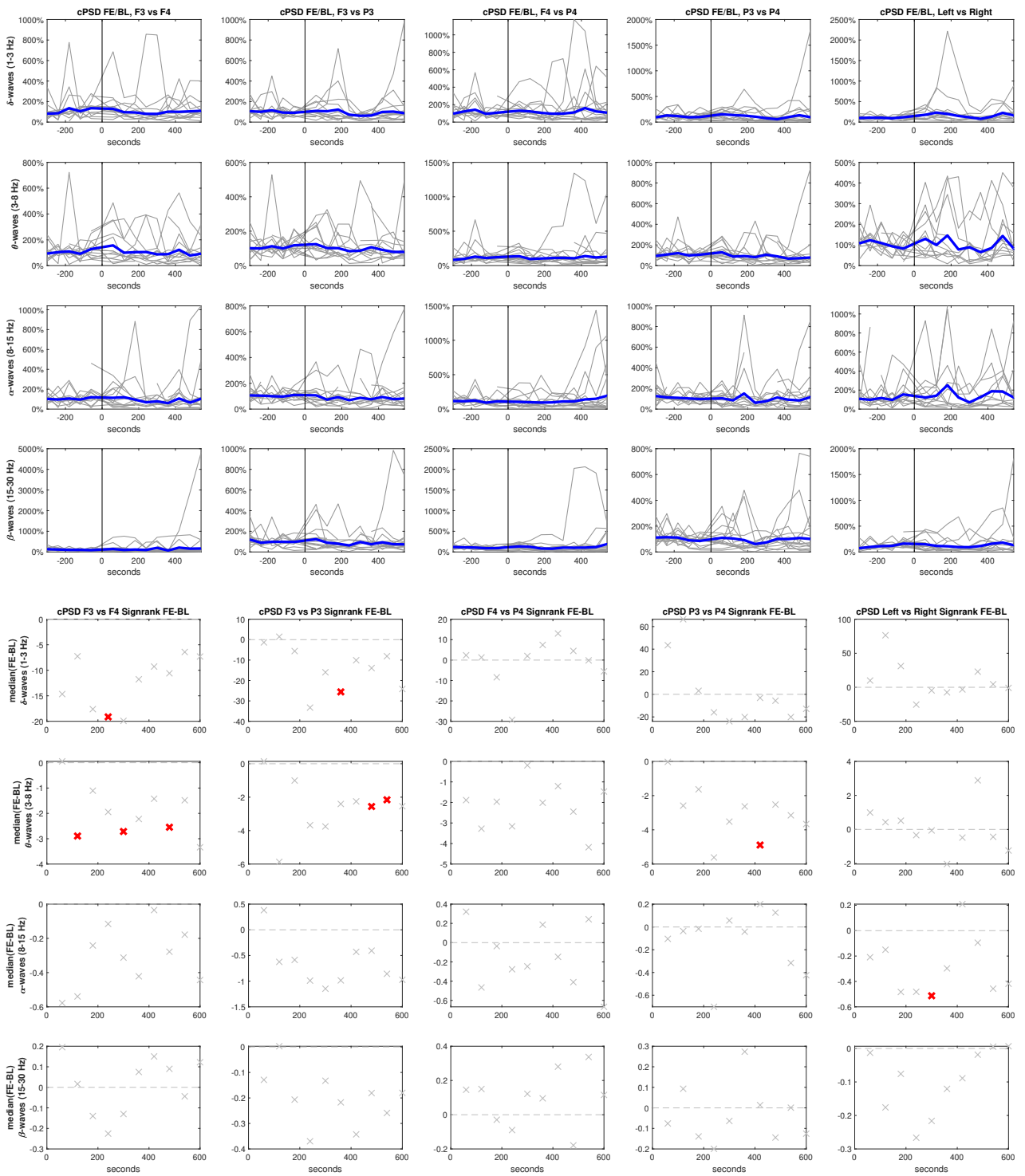


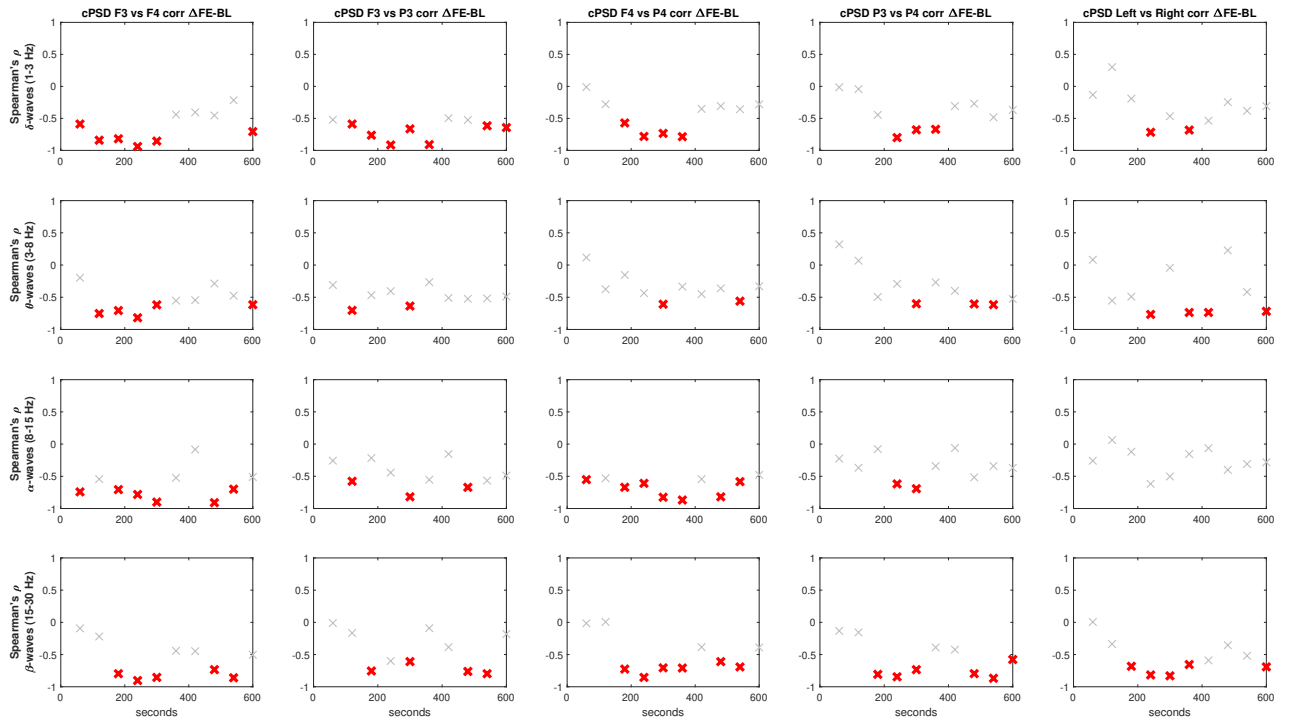
time after drug [s]	PSD 1-3 Hz															
	F3		F4		P3		P4		Left		Right		Frontal		Parietal	
CC	p	CC	p	CC	p	CC	p	CC	p	CC	p	CC	p	CC	p	
0-120	-0.142857	0.626117	-0.476923	0.084648	-0.117857	0.676305	-0.035714	0.903077	0.094505	0.747938	-0.134066	0.64772	0.126374	0.680785	-0.128571	0.648202
60-180	-0.52967	0.051417	-0.582418	0.028855	-0.705495	0.00482	-0.478571	0.073466	-0.038462	0.900724	-0.147253	0.615419	0.225275	0.459305	-0.424176	0.130637
120-240	-0.774725	0.001871	-0.763736	0.002377	-0.736264	0.004108	-0.6	0.023308	-0.314685	0.319139	-0.587912	0.034586	-0.013986	0.96559	-0.648352	0.016537
180-300	-0.863636	0.000612	-0.772727	0.005299	-0.718182	0.0128	-0.559441	0.058589	-0.708791	0.006682	0	1	-0.636364	0.026097	0.1	0.769875
240-360	-0.433566	0.159106	-0.867133	0.00026	-0.39011	0.187574	-0.741259	0.005801	-0.163636	0.651477	-0.745455	0.008455	0.490909	0.149656	-0.654545	0.028865
300-420	-0.32967	0.271335	-0.912088	1.4E-05	-0.637363	0.019118	-0.679121	0.007562	-0.363636	0.245265	-0.417582	0.155675	-0.321678	0.30791	-0.774725	0.001871
360-480	-0.516484	0.070749	-0.675824	0.011225	-0.39011	0.187574	-0.274725	0.34183	-0.321678	0.30791	-0.313187	0.297438	-0.314685	0.319139	-0.824176	0.00053
420-540	-0.60989	0.026878	-0.637363	0.019118	-0.494505	0.085824	-0.358242	0.208498	0.132867	0.680598	-0.269231	0.373733	0.006993	0.982792	-0.769231	0.002112
480-600	-0.642857	0.017792	-0.653846	0.015349	-0.587912	0.034586	-0.314286	0.273805	-0.20979	0.512841	-0.351648	0.2387	0.328671	0.296904	-0.725275	0.005023
540-660	-0.774725	0.001871	-0.71978	0.005536	-0.39011	0.187574	-0.393407	0.164032	-0.160839	0.617523	-0.373626	0.208554	0.055944	0.862898	-0.747253	0.003327

time after drug [s]	PSD 3-8 Hz								PSD 8-15 Hz								PSD 15-30 Hz															
	F3		F4		P3		P4		Left		Right		Frontal		Parietal		F3		F4		P3		P4		Left		Right		Frontal		Parietal	
	CC	p	CC	p	CC	p	CC	p	CC	p	CC	p	CC	p	CC	p	CC	p	CC	p	CC	p	CC	p	CC	p	CC	p				
0-120	-0.182418	0.532509	-0.16044	0.583753	-0.367857	0.177894	-0.385714	0.156528	0.41978	0.135101	-0.094505	0.747938	0.456044	0.117283	-0.246429	0.374825	-0.393407	0.202581	-0.463243	0.007037	0.148352	0.628609	-0.463736	0.094876	0.510989	0.074329	-0.586813	0.027384				
60-180	-0.393407	0.164032	-0.402198	0.153974	-0.683516	0.007037	-0.632143	0.013512	0.148352	0.628609	-0.463736	0.094876	0.510989	0.074329	-0.586813	0.027384	-0.246429	0.374825	-0.393407	0.202581	0.148352	0.628609	-0.463736	0.094876	0.510989	0.074329	-0.586813	0.027384				
120-240	-0.412088	0.161751	-0.516484	0.070749	-0.631868	0.020516	-0.81978	0.000331	0.146853	0.648796	-0.626374	0.021989	0.356643	0.255138	-0.543956	0.054647	-0.242727	0.328227	-0.772727	0.000201	0.167832	0.602099	-0.587912	0.034586	0.167832	0.602099	-0.587912	0.034586				
180-300	-0.627273	0.038845	-0.572727	0.065543	-0.509091	0.109737	-0.818182	0.001143	0.224242	0.533401	-0.818182	0.020283	0.345455	0.894427	-0.797203	0.0019	-0.163636	0.630685	-0.874126	0.000201	0.167832	0.602099	-0.587912	0.034586	0.167832	0.602099	-0.587912	0.034586				
240-360	-0.643357	0.024003	-0.874126	0.000201	-0.713287	0.009202	-0.895604	3.48E-05	0.045455	0.894427	-0.797203	0.0019	0.167832	0.602099	-0.587912	0.034586	-0.242727	0.328227	-0.772727	0.000201	0.167832	0.602099	-0.587912	0.034586	0.167832	0.602099	-0.587912	0.034586				
300-420	-0.236264	0.437084	-0.879121	7.54E-05	-0.39011	0.187574	-0.832967	0.000217	0.167832	0.602099	-0.648352	0.016537	0.167832	0.602099	-0.587912	0.034586	-0.242727	0.328227	-0.772727	0.000201	0.167832	0.602099	-0.587912	0.034586	0.167832	0.602099	-0.587912	0.034586				
360-480	-0.538462	0.057634	-0.620879	0.022358	-0.604396	0.028673	-0.714229	0.001233	0.604396	0.022057	0.104895	0.745609	-0.351648	0.2387	0.293706	0.354148	-0.450549	0.122332	0.521978	0.067292	-0.703297	0.007319	-0.604396	0.02198	-0.593407	0.032524	-0.593407	0.032524				
420-540	-0.521978	0.067292	-0.703297	0.007319	-0.796703	0.001114	-0.604396	0.022057	0.604396	0.022057	0.020979	0.948402	-0.505495	0.078033	-0.701099	0.001275	-0.604396	0.022057	0.521978	0.067292	-0.703297	0.007319	-0.604396	0.02198	-0.593407	0.032524	-0.593407	0.032524				
480-600	-0.296703	0.324922	-0.543956	0.054647	-0.791209	0.001275	-0.701099	0.001275	0.604396	0.022057	0.020979	0.948402	-0.505495	0.078033	-0.701099	0.001275	-0.604396	0.022057	0.521978	0.067292	-0.703297	0.007319	-0.604396	0.02198	-0.593407	0.032524	-0.593407	0.032524				
540-660	-0.615385	0.025167	-0.802198	0.000969	-0.774725	0.001871	-0.705495	0.00482	0.62937	0.845931	-0.769231	0.002112	-0.604396	0.022057	-0.701099	0.001275	-0.604396	0.022057	0.521978	0.067292	-0.703297	0.007319	-0.604396	0.02198	-0.593407	0.032524	-0.593407	0.032524				

time after drug [s]	PSD 3-8 Hz								PSD 8-15 Hz								PSD 15-30 Hz																	
	F3		F4		P3		P4		Left		Right		Frontal		Parietal		F3		F4		P3		P4		Left		Right		Frontal		Parietal			
	CC	p	CC	p	CC	p	CC	p	CC	p	CC	p	CC	p	CC	p	CC	p	CC	p	CC	p	CC	p	CC	p	CC	p						
0-120	-0.318681	0.266785	-0.446154	0.109807	-0.3	0.276682	-0.271429	0.326822	0.402198	0.153974	-0.151648	0.604791	-0.258242	0.394284	-0.239286	0.389235	-0.27033	0.349919	-0.604396	0.022057	-0.49011	0.07522	0.28022	0.353764	-0.204396	0.483346	0.159341	0.603088	-0.446154	0.109807				
60-180	-0.27033	0.349919	-0.604396	0.022057	-0.49011	0.07522	-0.278571	0.313812	0.223776	0.484452	-0.32967	0.271335	-0.482517	0.112109	-0.593407	0.032524	-0.27033	0.349919	-0.604396	0.022057	-0.49011	0.07522	0.28022	0.353764	-0.204396	0.483346	0.159341	0.603088	-0.446154	0.109807				
120-240	-0.346154	0.246625	-0.71978	0.005023	-0.412088	0.161751	-0.595604	0.024613	0.006061	0.986743	-0.836364	0.001333	0.606060	0.037588	-0.763636	0.006233	-0.346154	0.246625	-0.71978	0.005023	-0.412088	0.161751	-0.595604	0.024613	-0.006061	0.022057	0.986743	-0.836364	0.001333	0.606060	0.037588	-0.763636	0.006233	
180-300	-0.518182	0.102492	-0.618182	0.042646	-0.681818	0.020843	-0.741259	0.005801	0.006061	0.986743	-0.836364	0.001333	0.606060	0.037588	-0.763636	0.006233	-0.518182	0.102492	-0.618182	0.042646	-0.681818	0.020843	-0.741259	0.005801	-0.006061	0.022057	0.986743	-0.836364	0.001333	0.606060	0.037588	-0.763636	0.006233	
240-360	-0.601399	0.038588	-0.93007	1.17E-05	-0.692308	0.012593	-0.796703	0.001114	0.045455	0.894427	-0.405455	0.005629	0.13986	0.96559	-0.708791	0.006682	-0.368132	0.315608	-0.861317	0.000724	-0.636237	0.002377	-0.696703	0.005629	-0.174545	0.001860	-0.041958	0.01378	0.001860	0.118881	0.056737	-0.755245	0.004508	
300-420	-0.302198	0.315608	-0.813187	0.000724	-0.362637	0.223316	-0.696703	0.005629	0.118881	0.96559	-0.405455	0.005629	0.13986	0.96559	-0.708791	0.006682	-0.368132	0.315608	-0.861317	0.000724	-0.636237	0.002377	-0.696703	0.005629	-0.174545	0.001860	-0.041958	0.01378	0.001860	0.118881	0.056737	-0.755245	0.004508	
360-480	-0.368132	0.215857	-0.653846	0.015349	-0.446154	0.127524	-0.639596	0.01378	0.041958	0.896986	-0.247523	0.415405	0.111888	0.729195	-0.712727	0.611542	-0.368132	0.215857	-0.653846	0.015349	-0.446154	0.127524	-0.639596	0.01378	-0.041958	0.01378	0.041958	0.896986	-0.247523	0.415405	0.111888	0.729195	-0.712727	0.611542
420-540	-0.565934	0.043793	-0.510989	0.074329	-0.659341	0.014226	-0.595604	0.024613	0.041958	0.896986	-0.246376	0.415405	0.111888	0.729195	-0.712727	0.611542	-0.368132	0.215857	-0.653846	0.015349	-0.446154	0.127524	-0.639596	0.01378	-0.041958	0.01378	0.041958	0.896986	-0.246376	0.415405	0.111888	0.729195	-0.712727	0.611542
480-600	-0.379121	0.201406	-0.648352	0.016537	-0.78022	0.001653	-0.851648	0.000222	-0.287912	0.318193	0.041958	0.896986	-0.093407	0.7615	-0.013986	0.96559	-0.368132	0.215857	-0.653846	0.015349	-0.446154	0.127524	-0.639596	0.01378	-0.041958	0.01378	0.041958	0.896986	-0.246376	0.415405	0.111888	0.729195	-0.712727	0.611542
540-660	-0.736264	0.004108	-0.747253	0.003327	-0.538464	0.057634	-0.454945	0.102154	0.286713	0.366251	-0.478022	0.429919	-0.251748	0.429919	-0.593407	0.032524	-0.368132	0.215857	-0.653846	0.015349	-0.446154	0.127524	-0.639596	0.01378	-0.041958	0.01378	0.041958	0.896986	-0.246376	0.415405	0.111888	0.729195	-0.712727	0.611542





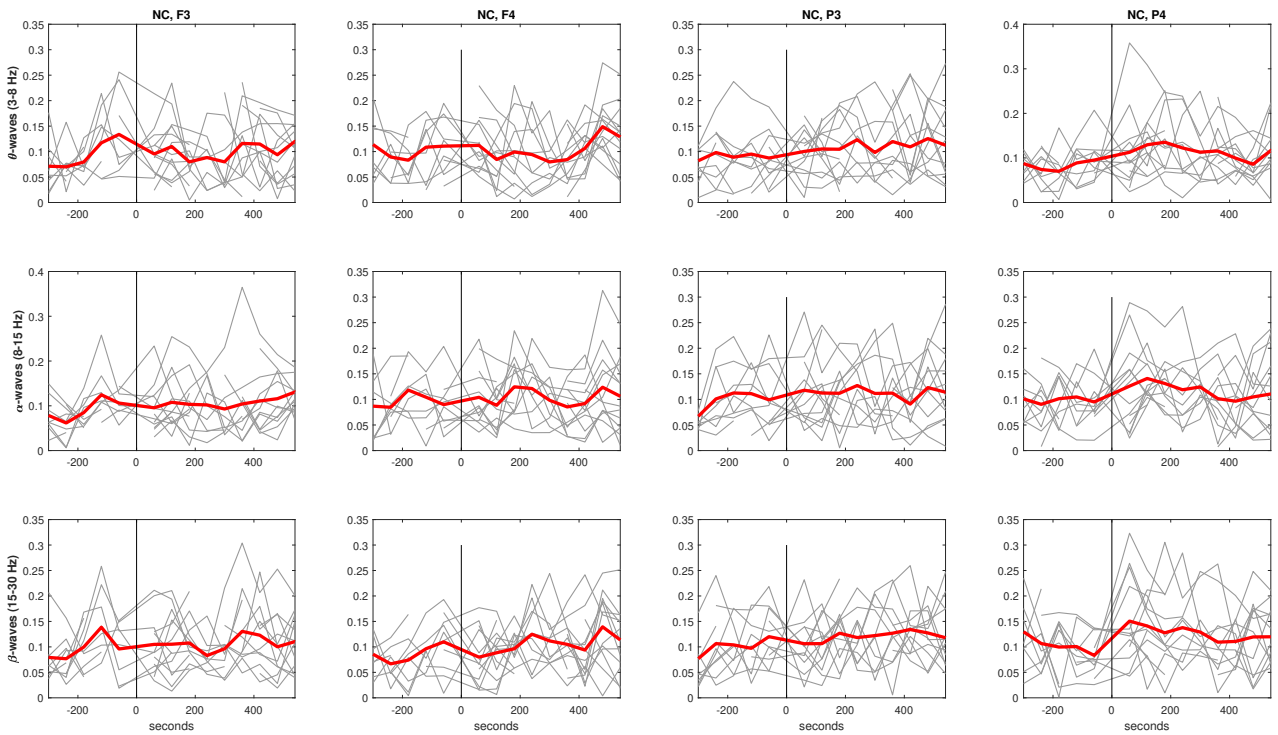


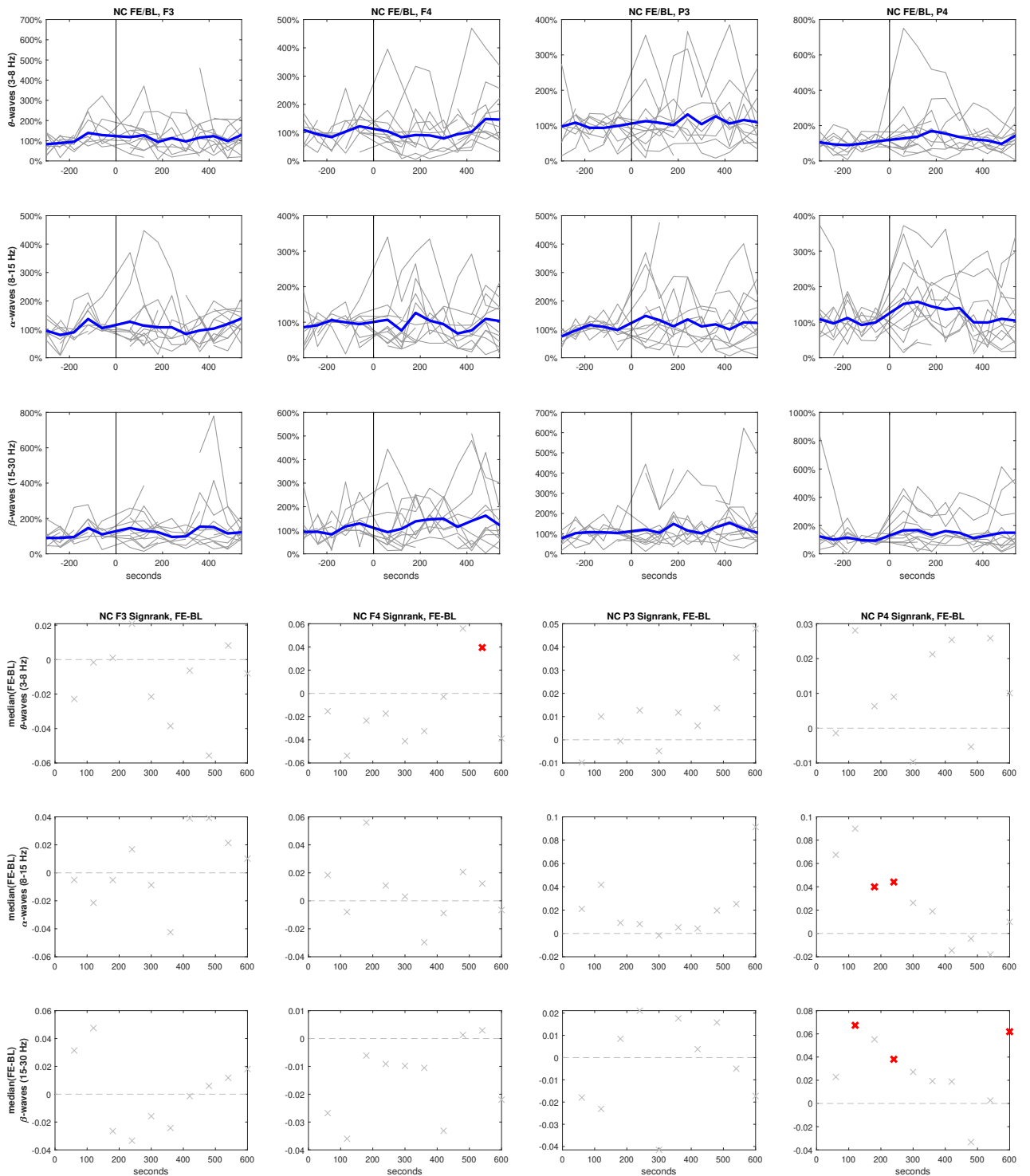
time after drug [s]	cPSD 1-3 Hz									
	F3 vs F4		F3 vs P3		F4 vs P4		P3 vs P4		Left vs Right	
	CC	p	CC	p	CC	p	CC	p	CC	p
0-120	-0.587912	0.034586	-0.520879	0.056154	-0.010989	0.970258	-0.014286	0.964222	-0.131868	0.667608
60-180	-0.840659	0.000319	-0.587912	0.034586	-0.279121	0.333845	-0.041758	0.887287	0.300699	0.34226
120-240	-0.818182	0.001143	-0.762238	0.00395	-0.571429	0.041342	-0.445055	0.127524	-0.190909	0.573913
180-300	-0.939394	5.48E-05	-0.915152	0.000204	-0.781818	0.004473	-0.8	0.00311	-0.716667	0.036866
240-360	-0.854545	0.000807	-0.663636	0.025984	-0.734266	0.006543	-0.678322	0.015317	-0.466667	0.173939
300-420	-0.440559	0.151735	-0.909091	4.19E-05	-0.785714	0.001454	-0.67033	0.012166	-0.681818	0.020843
360-480	-0.405594	0.190836	-0.496503	0.100603	-0.351648	0.2387	-0.307692	0.306447	-0.536364	0.088953
420-540	-0.454545	0.137658	-0.524476	0.080019	-0.307692	0.306447	-0.269231	0.373733	-0.245455	0.466922
480-600	-0.216783	0.498556	-0.615385	0.03317	-0.357143	0.23093	-0.483516	0.094135	-0.381818	0.24656
540-660	-0.706294	0.010245	-0.643357	0.024003	-0.28022	0.353764	-0.368132	0.215857	-0.309091	0.355028

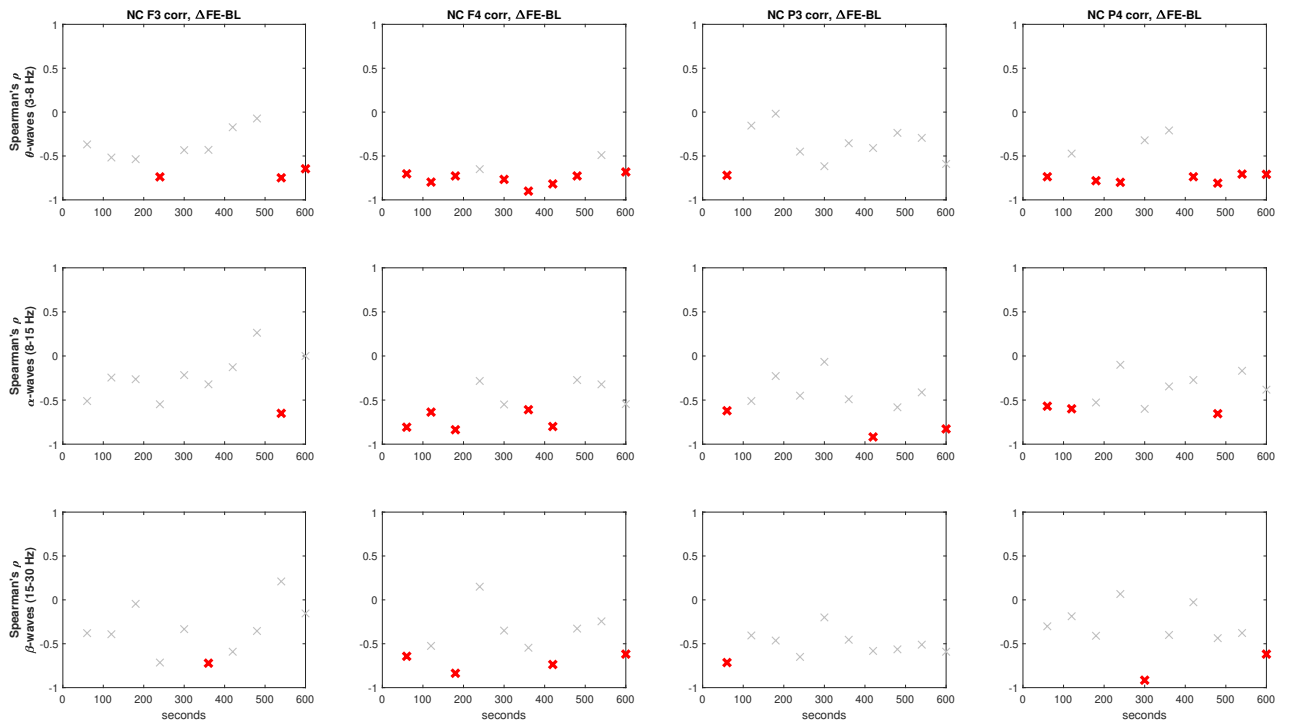
time after drug [s]	cPSD 3-8 Hz									
	F3 vs F4		F3 vs P3		F4 vs P4		P3 vs P4		Left vs Right	
	CC	p	CC	p	CC	p	CC	p	CC	p
0-120	-0.197802	0.517131	-0.30989	0.280933	0.116484	0.691691	0.321429	0.242415	0.082418	0.788951
60-180	-0.752747	0.002982	-0.703297	0.007319	-0.375824	0.18541	0.068132	0.816984	-0.552448	0.062511
120-240	-0.706294	0.010245	-0.468531	0.124455	-0.153846	0.615799	-0.494505	0.085824	-0.490909	0.125204
180-300	-0.818182	0.003815	-0.406061	0.244282	-0.436364	0.179665	-0.290909	0.385457	-0.766667	0.02139
240-360	-0.618182	0.042646	-0.636364	0.035287	-0.608392	0.035806	-0.601399	0.038588	-0.042424	0.907364
300-420	-0.552448	0.062511	-0.265734	0.403833	-0.335165	0.262943	-0.269231	0.373733	-0.736364	0.00976
360-480	-0.545455	0.066612	-0.51049	0.089914	-0.450549	0.122332	-0.401099	0.174357	-0.736364	0.00976
420-540	-0.286713	0.366251	-0.524476	0.080019	-0.362637	0.223316	-0.604396	0.028673	0.227273	0.501536
480-600	-0.475524	0.118176	-0.517483	0.084869	-0.56044	0.046346	-0.615385	0.025167	-0.418182	0.20057
540-660	-0.615385	0.03317	-0.48951	0.106252	-0.32967	0.271335	-0.527473	0.063955	-0.718182	0.0128

time after drug [s]	cPSD 8-15 Hz									
	F3 vs F4		F3 vs P3		F4 vs P4		P3 vs P4		Left vs Right	
	CC	p	CC	p	CC	p	CC	p	CC	p
0-120	-0.741758	0.003701	-0.257143	0.374812	-0.551648	0.040849	-0.225	0.41896	-0.258242	0.394284
60-180	-0.543956	0.054647	-0.576923	0.038993	-0.52967	0.051417	-0.367033	0.196739	0.062937	0.845931
120-240	-0.706294	0.010245	-0.216783	0.498556	-0.67033	0.012166	-0.076923	0.802763	-0.118182	0.729285
180-300	-0.781818	0.007547	-0.442424	0.200423	-0.609091	0.046696	-0.618182	0.042646	-0.616667	0.085725
240-360	-0.9	0.00016	-0.818182	0.002083	-0.825175	0.000951	-0.692308	0.012593	-0.50303	0.138334
300-420	-0.524476	0.080019	-0.552448	0.062511	-0.868132	0.000119	-0.340659	0.254706	-0.154545	0.650034
360-480	-0.083916	0.795415	-0.153846	0.633091	-0.543956	0.054647	-0.06044	0.844502	-0.063636	0.852539
420-540	-0.909091	4.19E-05	-0.671329	0.016831	-0.818681	0.000621	-0.516484	0.070749	-0.4	0.222868
480-600	-0.699301	0.011374	-0.566434	0.054842	-0.582418	0.036741	-0.340659	0.254706	-0.309091	0.355028
540-660	-0.51049	0.089914	-0.48951	0.106252	-0.478022	0.09849	-0.368132	0.215857	-0.281818	0.401145

time after drug [s]	cPSD 15-30 Hz									
	F3 vs F4		F3 vs P3		F4 vs P4		P3 vs P4		Left vs Right	
	CC	p	CC	p	CC	p	CC	p	CC	p
0-120	-0.093407	0.7615	-0.010989	0.970258	-0.015385	0.95837	-0.132143	0.638933	0.005495	0.985787
60-180	-0.21978	0.470615	-0.164835	0.590479	0.006593	0.982153	-0.156044	0.594235	-0.335664	0.286123
120-240	-0.797203	0.0019	-0.755245	0.004508	-0.725275	0.005023	-0.807692	0.000839	-0.681818	0.020843
180-300	-0.90303	0.000344	-0.6	0.066688	-0.854545	0.000807	-0.845455	0.001045	-0.816667	0.010769
240-360	-0.854545	0.000807	-0.609091	0.046696	-0.706294	0.010245	-0.734266	0.006543	-0.830303	0.00294
300-420	-0.440559	0.151735	-0.090909	0.778725	-0.708791	0.006682	-0.39011	0.187574	-0.654545	0.028865
360-480	-0.447552	0.144586	-0.384615	0.21702	-0.384615	0.194413	-0.423077	0.149749	-0.590909	0.055576
420-540	-0.734266	0.006543	-0.762238	0.00395	-0.60989	0.026878	-0.796703	0.001114	-0.354545	0.284693
480-600	-0.86014	0.000332	-0.797203	0.0019	-0.692308	0.00873	-0.868132	0.000119	-0.518182	0.102492
540-660	-0.503497	0.095157	-0.181818	0.571701	-0.39011	0.187574	-0.576923	0.038993	-0.690909	0.018565

**NC**



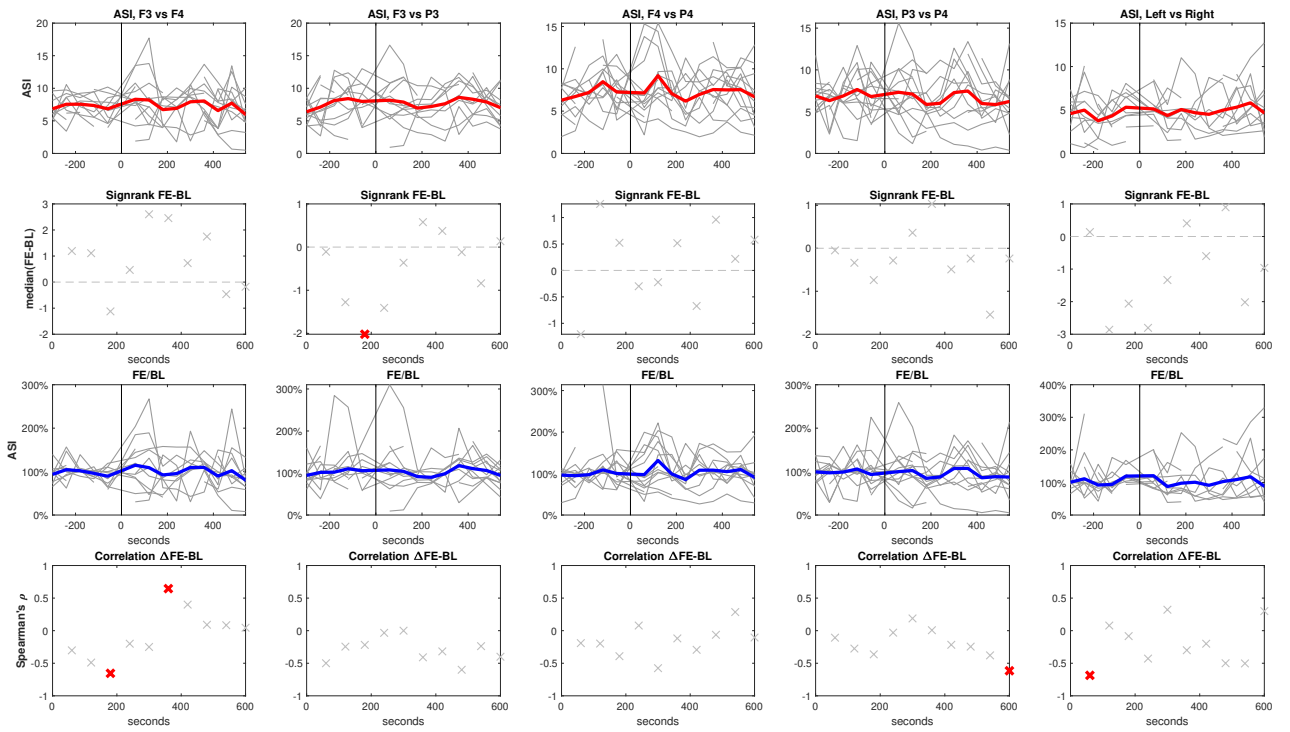


time after drug [s]	NC 3-8 Hz							
	F3		F4		P3		P4	
	CC	p	CC	p	CC	p	CC	p
0-120	-0.36813	0.215857	-0.7033	0.007319	-0.71978	0.005536	-0.73626	0.002676
60-180	-0.51748	0.084869	-0.7972	0.0019	-0.15385	0.633091	-0.47253	0.102981
120-240	-0.53636	0.088953	-0.72727	0.011205	-0.01818	0.957685	-0.78182	0.004473
180-300	-0.7381	0.045833	-0.65	0.066562	-0.45	0.229817	-0.8	0.013828
240-360	-0.43333	0.249917	-0.76667	0.02139	-0.61667	0.085725	-0.32121	0.365468
300-420	-0.4303	0.214492	-0.9	0.00016	-0.35455	0.284693	-0.20909	0.537221
360-480	-0.17273	0.611542	-0.81818	0.002083	-0.40909	0.211545	-0.73636	0.00976
420-540	-0.07273	0.831716	-0.72727	0.011205	-0.23636	0.484091	-0.80909	0.002559
480-600	-0.74825	0.005124	-0.48951	0.106252	-0.29371	0.354148	-0.70629	0.010245
540-660	-0.64545	0.031963	-0.68182	0.020843	-0.59091	0.055576	-0.70909	0.014552

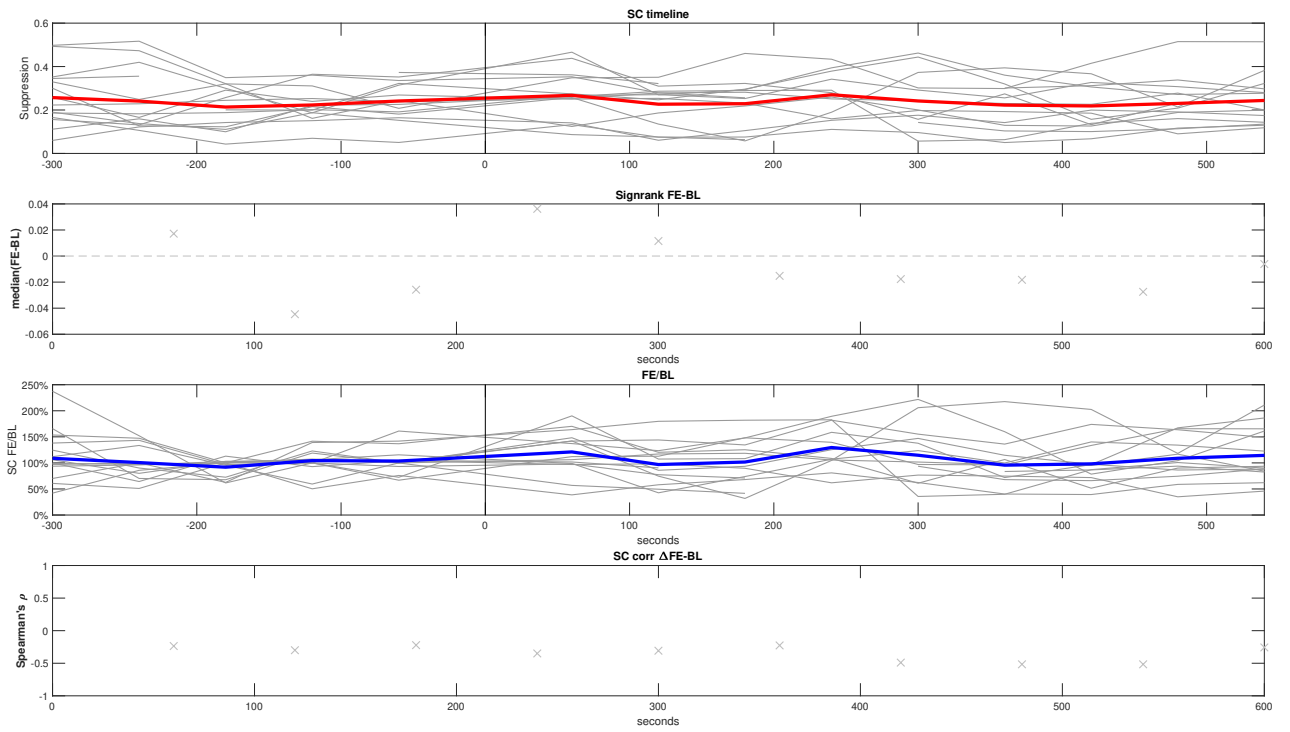
time after drug [s]	NC 8-15 Hz							
	F3		F4		P3		P4	
	CC	p	CC	p	CC	p	CC	p
0-120	-0.51099	0.074329	-0.80769	0.000839	-0.62088	0.023538	-0.56923	0.033619
60-180	-0.24476	0.443262	-0.63636	0.026097	-0.51049	0.089914	-0.5989	0.030554
120-240	-0.26364	0.433441	-0.83636	0.001333	-0.22727	0.501536	-0.52727	0.095565
180-300	-0.54762	0.170982	-0.28333	0.462991	-0.45	0.229817	-0.1	0.809981
240-360	-0.21667	0.580941	-0.55	0.132777	-0.06667	0.880093	-0.6	0.066688
300-420	-0.32121	0.365468	-0.60909	0.046696	-0.49091	0.125204	-0.34545	0.298089
360-480	-0.12727	0.709215	-0.8	0.003111	-0.91818	6.66E-05	-0.27273	0.417141
420-540	0.263636	0.433441	-0.27273	0.417141	-0.58182	0.06042	-0.65455	0.028865
480-600	-0.65035	0.022034	-0.32168	0.30791	-0.41259	0.182564	-0.16783	0.602099
540-660	0	1	-0.54545	0.082651	-0.82727	0.001677	-0.38182	0.24656

time after drug [s]	NC 15-30 Hz							
	F3		F4		P3		P4	
	CC	p	CC	p	CC	p	CC	p
0-120	-0.37912	0.201406	-0.64286	0.017792	-0.71429	0.006088	-0.3011	0.295514
60-180	-0.39161	0.208063	-0.52448	0.080019	-0.40559	0.190836	-0.18681	0.541124
120-240	-0.04545	0.894427	-0.83636	0.001333	-0.46364	0.150901	-0.40909	0.211545
180-300	-0.71429	0.057589	0.15	0.708069	-0.65	0.066562	0.066667	0.880093
240-360	-0.33333	0.385323	-0.35	0.358581	-0.2	0.613404	-0.91515	0.000204
300-420	-0.72121	0.018573	-0.54545	0.082651	-0.45455	0.160145	-0.4	0.222868
360-480	-0.59091	0.055576	-0.73636	0.00976	-0.58182	0.06042	-0.02727	0.936558
420-540	-0.35455	0.284693	-0.32727	0.325895	-0.56364	0.070952	-0.43636	0.179665
480-600	0.20979	0.512841	-0.24476	0.443262	-0.51049	0.089914	-0.37762	0.226206
540-660	-0.15455	0.650034	-0.61818	0.042646	-0.59091	0.055576	-0.61818	0.042646

## ASI



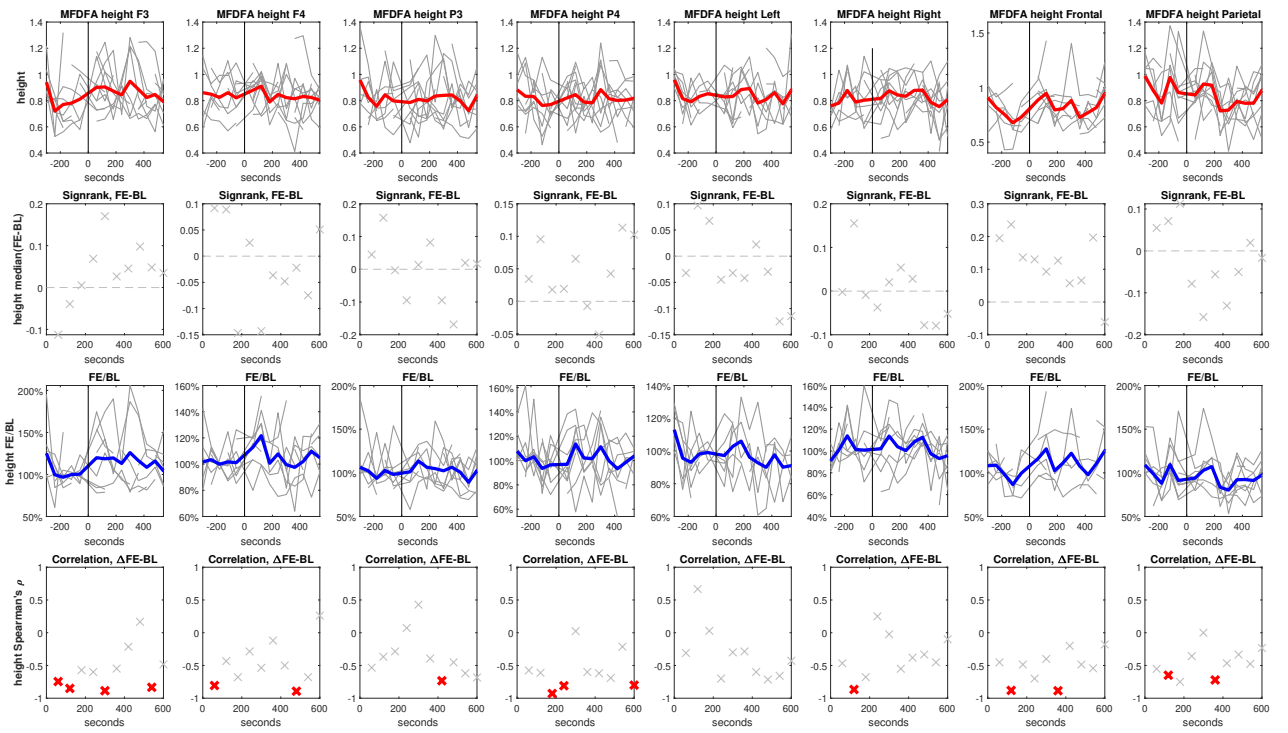
time after drug [s]	ASI									
	F3 vs F4		F3 vs P3		F4 vs P4		P3 vs P4		Left vs Right	
	CC	p	CC	p	CC	p	CC	p	CC	p
0-120	-0,302198	0,315608	-0,5	0,081864	-0,191209	0,512584	-0,107692	0,714031	-0,685315	0,013906
60-180	-0,48951	0,106252	-0,244755	0,443262	-0,197802	0,517131	-0,274725	0,363675	0,078788	0,828717
120-240	-0,654545	0,028865	-0,218182	0,519248	-0,391608	0,208063	-0,363636	0,245265	-0,083333	0,843182
180-300	-0,2	0,613404	-0,033333	0,948391	0,078788	0,828717	-0,030303	0,933773	-0,428571	0,353571
240-360	-0,25	0,520635	0	1	-0,575758	0,081553	0,187879	0,603218	0,321429	0,497619
300-420	0,645455	0,031963	-0,409091	0,211545	-0,118881	0,712884	0,006993	0,982792	-0,3	0,436624
360-480	0,4	0,222868	-0,318182	0,340298	-0,293706	0,354148	-0,216783	0,498556	-0,2	0,613404
420-540	0,090909	0,790373	-0,6	0,051003	-0,062937	0,845931	-0,244755	0,443262	-0,5	0,177662
480-600	0,083916	0,795415	-0,237762	0,456801	0,285714	0,344	-0,379121	0,201406	-0,50303	0,138334
540-660	0,045455	0,894427	-0,4	0,222868	-0,104895	0,745609	-0,615385	0,03317	0,3	0,436624

**SC**

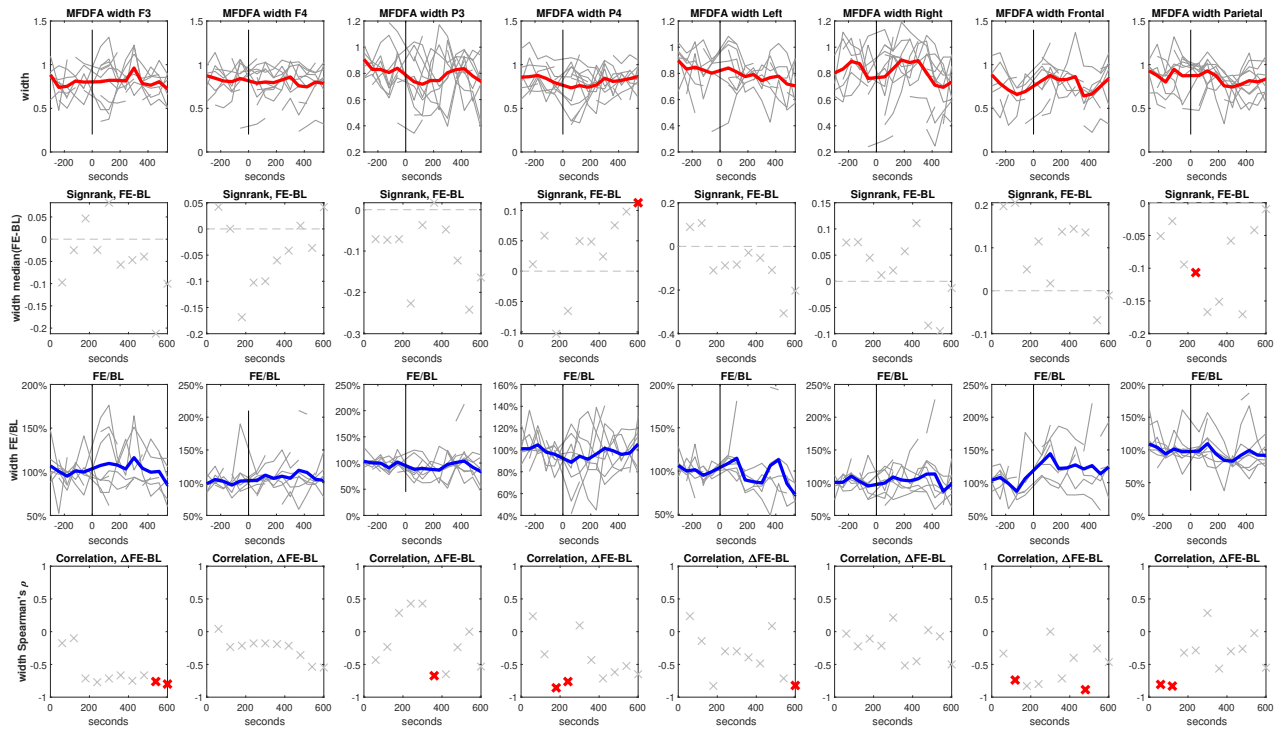
SC		
time after drug [s]	Whole brain	
	CC	p
0-120	-0.23571	0.396553
60-180	-0.3	0.276682
120-240	-0.22198	0.44563
180-300	-0.34965	0.265239
240-360	-0.30769	0.306447
300-420	-0.22637	0.436435
360-480	-0.49011	0.07522
420-540	-0.51648	0.058637
480-600	-0.51648	0.058637
540-660	-0.25714	0.374812

## MFDFA

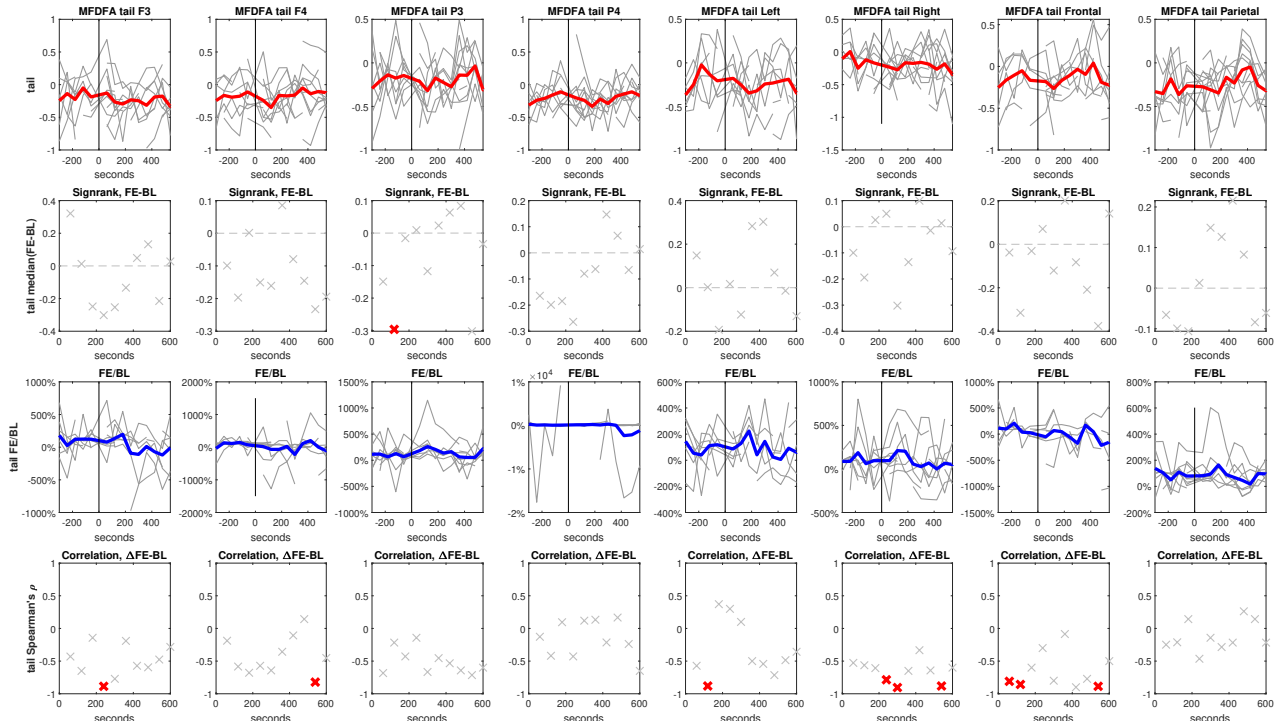
## height



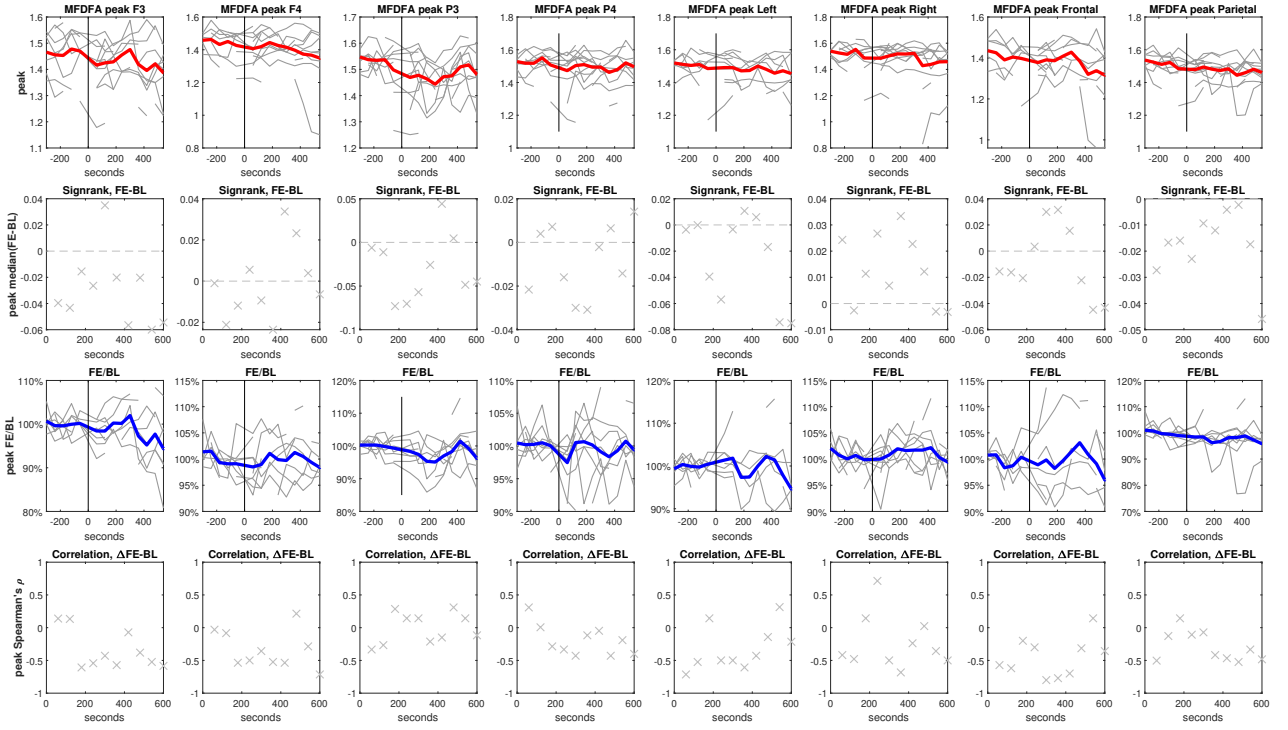
time after drug [s]	MFDFA height																	
	F3		F4		P3		P4		Left		Right		Frontal		Parietal			
	CC	p	CC	p	CC	p	CC	p	CC	p	CC	p	CC	p	CC	p		
0-120	-0.745455	0.01333	-0.806061	<b>0.004862</b>	-0.533333	0.147525	-0.575758	0.081553	-0.309524	0.461806	-0.466667	0.173939	-0.452381	0.26746	-0.551515	0.098401		
60-180	-0.85	<b>0.006074</b>	-0.433333	0.249917	-0.366667	0.33626	-0.612121	0.059972	0.666667	0.083085	-0.866667	<b>0.001174</b>	-0.880952	<b>0.007242</b>	-0.648485	0.04254		
120-240	-0.571429	0.2	-0.678571	0.109524	-0.285714	0.555952	0.071429	0.906349	-0.809524	<b>0.02232</b>	0.028571	1	-0.678571	0.109524	-0.485714	0.355556	-0.75	0.0627
180-300	-0.6	0.241667	-0.285714	0.555952	0.071429	0.906349	-0.809524	<b>0.02176</b>	-0.7	0.233333	0.25	0.594841	-0.7	0.233333	-0.357143	0.444444		
240-360	-0.885714	<b>0.033333</b>	-0.535714	0.235714	0.428571	0.299206	0.02381	0.976786	-0.3	0.683333	-0.02381	0.976786	-0.4	0.516667	0	1		
300-420	-0.547619	0.170982	-0.119048	0.793006	-0.393939	0.259998	-0.6	0.096798	-0.285714	0.555952	-0.55	0.132777	-0.885714	<b>0.033333</b>	-0.721212	<b>0.018573</b>		
360-480	-0.214286	0.661508	-0.5	0.266667	-0.733333	<b>0.031123</b>	-0.619048	0.11498	-0.6	0.241667	-0.380952	0.359871	-0.2	0.783333	-0.466667	0.212522		
420-540	0.166667	0.703323	-0.892857	<b>0.012302</b>	-0.452381	0.26746	-0.690476	0.069395	-0.714286	0.136111	-0.333333	0.427877	-0.485714	0.355556	-0.333333	0.427877		
480-600	-0.833333	<b>0.015377</b>	-0.678571	0.109524	-0.619048	0.11498	-0.214286	0.619097	-0.657143	0.175	-0.452381	0.26746	-0.542857	0.297222	-0.47619	0.243056		
540-660	-0.483333	0.1938	0.261905	0.536409	-0.683333	0.05032	-0.8	<b>0.013828</b>	-0.428571	0.353571	-0.1	0.809981	-0.178571	0.713095	-0.233333	0.551709		

**width**

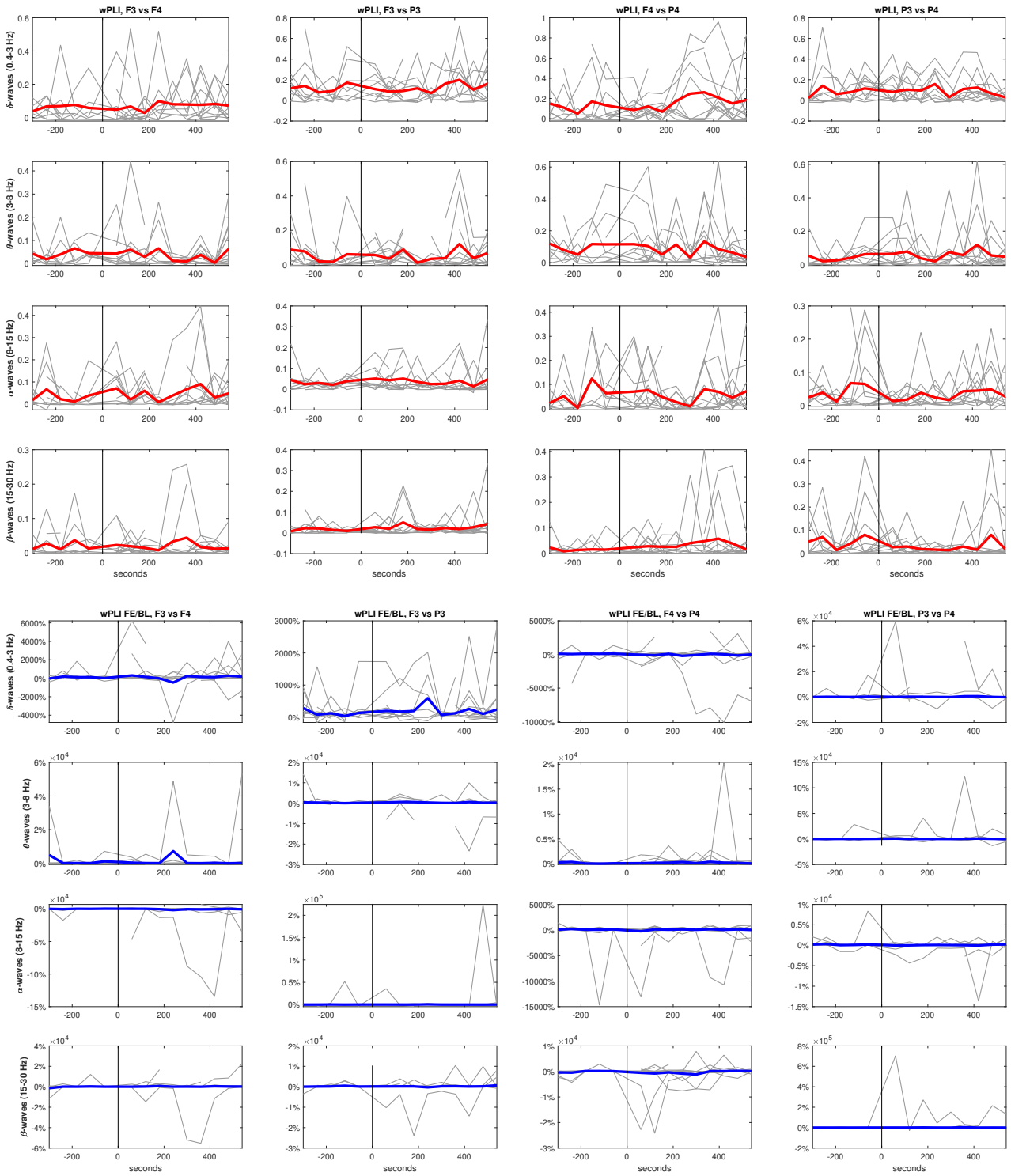
time after drug [s]	MFDFA width															
	F3		F4		P3		P4		Left		Right		Frontal		Parietal	
CC	p	CC	p	CC	p	CC	p	CC	p	CC	p	CC	p	CC	p	
0-120	-0.175758	0.627188	0.042424	0.907364	-0.433333	0.249917	0.236364	0.510885	0.238095	0.582143	-0.030303	0.933773	-0.333333	0.427877	-0.806061	0.004862
60-180	-0.1	0.809981	-0.233333	0.551709	-0.233333	0.551709	-0.345455	0.328227	-0.142857	0.752034	-0.224242	0.533401	-0.738095	0.045833	-0.830303	0.00294
120-240	-0.714286	0.088095	-0.214286	0.661508	0.285714	0.555952	-0.851743	0.010714	-0.828571	0.058333	-0.107143	0.839683	-0.828571	0.058333	-0.321429	0.497619
180-300	-0.771429	0.102778	-0.178571	0.713095	0.428571	0.353571	-0.761905	0.036756	-0.3	0.683333	-0.214286	0.661508	-0.8	0.133333	-0.285714	0.555952
240-360	-0.714286	0.136111	-0.178571	0.713095	0.428571	0.299206	0.095238	0.840129	-0.3	0.683333	0.214286	0.619097	0	1	0.285714	0.500794
300-420	-0.666667	0.083085	-0.190476	0.664583	-0.672727	0.033041	-0.433333	0.249917	-0.392857	0.395635	-0.516667	0.1618	-0.714286	0.136111	-0.563636	0.089724
360-480	-0.75	0.066677	-0.214286	0.661508	-0.65	0.066562	-0.714286	0.057589	-0.485714	0.355556	-0.452381	0.26746	-0.4	0.516667	-0.3	0.436624
420-540	-0.666667	0.083085	-0.357143	0.444444	-0.238095	0.582143	-0.619048	0.11498	0.085714	0.919444	0.02381	0.976786	-0.885714	0.033333	-0.261905	0.536409
480-600	-0.761905	0.036756	-0.535714	0.235714	0	1	-0.52381	0.196627	-0.714286	0.136111	-0.071429	0.881994	-0.257143	0.658333	-0.02381	0.976786
540-660	-0.8	0.013828	-0.547619	0.170982	-0.533333	0.147525	-0.65	0.066562	-0.821429	0.034127	-0.5	0.177662	-0.464286	0.302381	-0.55	0.132777

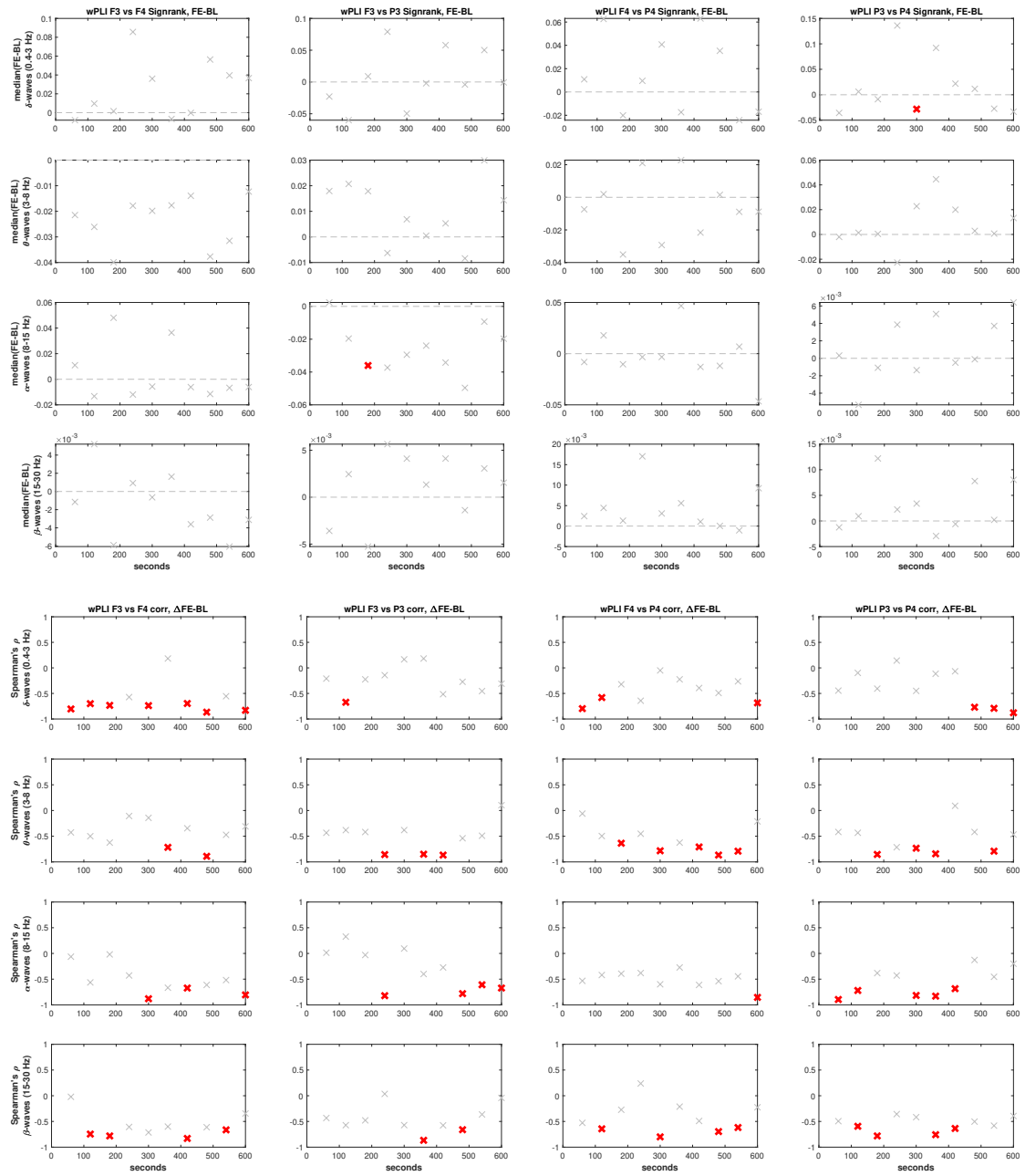
**tail**

time after drug [s]	MFdfa tail															
	F3		F4		P3		P4		Left		Right		Frontal		Parietal	
	CC	p	CC	p	CC	p	CC	p	CC	p	CC	p	CC	p	CC	p
0-120	-0.430303	0.214492	-0.187879	0.603218	-0.683333	0.05032	-0.127273	0.726057	-0.571429	0.151141	-0.527273	0.117308	-0.809524	0.021776	-0.248485	0.488776
60-180	-0.65	0.066562	-0.583333	0.107997	-0.216667	0.580941	-0.418182	0.229113	-0.880952	0.007242	-0.563636	0.089724	-0.857143	0.010714	-0.212121	0.556306
120-240	-0.142857	0.78254	-0.678571	0.109524	-0.428571	0.353571	0.095238	0.840129	0.371429	0.497222	-0.607143	0.166667	-0.6	0.241667	0.142857	0.78254
180-300	-0.885714	0.033333	-0.571429	0.2	-0.142857	0.78254	-0.428571	0.299206	0.3	0.683333	-0.785714	0.048016	-0.3	0.683333	-0.464286	0.302381
240-360	-0.771429	0.102778	-0.642857	0.138889	-0.666667	0.083085	0.119048	0.793006	0.1	0.95	-0.904762	0.004563	-0.8	0.133333	-0.142857	0.752034
300-420	-0.190476	0.664583	-0.357143	0.389385	-0.454545	0.186905	0.133333	0.743541	-0.5	0.266667	-0.65	0.066562	-0.808574	0.919444	-0.284848	0.425038
360-480	-0.571429	0.2	-0.107143	0.839683	-0.533333	0.147525	-0.214286	0.619097	-0.542857	0.297222	-0.333333	0.427877	-0.9	0.083333	-0.216667	0.580941
420-540	-0.595238	0.132292	0.142857	0.78254	-0.642857	0.096181	0.166667	0.703323	-0.714286	0.136111	-0.642857	0.096181	-0.771429	0.102778	0.261905	0.536409
480-600	-0.47619	0.243056	-0.821429	0.034127	-0.714286	0.057589	-0.238095	0.582143	-0.485714	0.355556	-0.880952	0.007242	-0.885714	0.033333	0.142857	0.752034
540-660	-0.283333	0.462991	-0.452381	0.26746	-0.6	0.096798	-0.65	0.066562	-0.357143	0.444444	-0.6	0.096798	-0.5	0.266667	-0.216667	0.580941

**peak**

time after drug [s]	MFdfa peak															
	F3		F4		P3		P4		Left		Right		Frontal		Parietal	
	CC	p	CC	p	CC	p	CC	p	CC	p	CC	p	CC	p	CC	p
0-120	0.139394	0.700932	-0.030303	0.933773	-0.333333	0.385323	0.309091	0.384841	-0.714286	0.057589	-0.418182	0.229113	-0.571429	0.151141	-0.50303	0.138334
60-180	0.133333	0.743541	-0.083333	0.843182	-0.266667	0.493331	0.006061	0.986743	-0.52381	0.196667	-0.478788	0.161523	-0.619048	0.11498	-0.127273	0.726057
120-240	-0.607143	0.166667	-0.535714	0.235714	0.285714	0.555952	-0.285714	0.500794	0.142857	0.802778	0.142857	0.78254	-0.2	0.713889	0.142857	0.78254
180-300	-0.542857	0.297222	-0.5	0.266667	0.142857	0.78254	-0.333333	0.427877	-0.5	0.45	0.714286	0.088095	-0.3	0.683333	-0.107143	0.839683
240-360	-0.428571	0.419444	-0.357143	0.444444	0.142857	0.752034	-0.428571	0.299206	-0.5	0.45	-0.5	0.216171	-0.8	0.133333	-0.071429	0.881994
300-420	-0.571429	0.151141	-0.52381	0.196627	-0.212121	0.556306	-0.116667	0.775628	-0.607143	0.166667	-0.683333	0.05032	-0.771429	0.102778	-0.418182	0.229113
360-480	-0.071429	0.906349	-0.535714	0.235714	-0.15	0.708069	-0.047619	0.934871	-0.428571	0.419444	-0.238095	0.582143	-0.7	0.233333	-0.466667	0.212522
420-540	-0.380952	0.359871	0.214286	0.661508	0.309524	0.461806	-0.428571	0.299206	-0.142857	0.802778	0.02381	0.976786	-0.314286	0.563889	-0.52381	0.196627
480-600	-0.52381	0.196627	-0.285714	0.555952	0.142857	0.752034	-0.190476	0.664583	0.314286	0.563889	-0.357143	0.389385	0.142857	0.802778	-0.333333	0.427877
540-660	-0.583333	0.107997	-0.714286	0.057589	-0.116667	0.775628	-0.4	0.291193	-0.214286	0.661508	-0.5	0.177662	-0.357143	0.444444	-0.483333	0.1938

**wPLI**

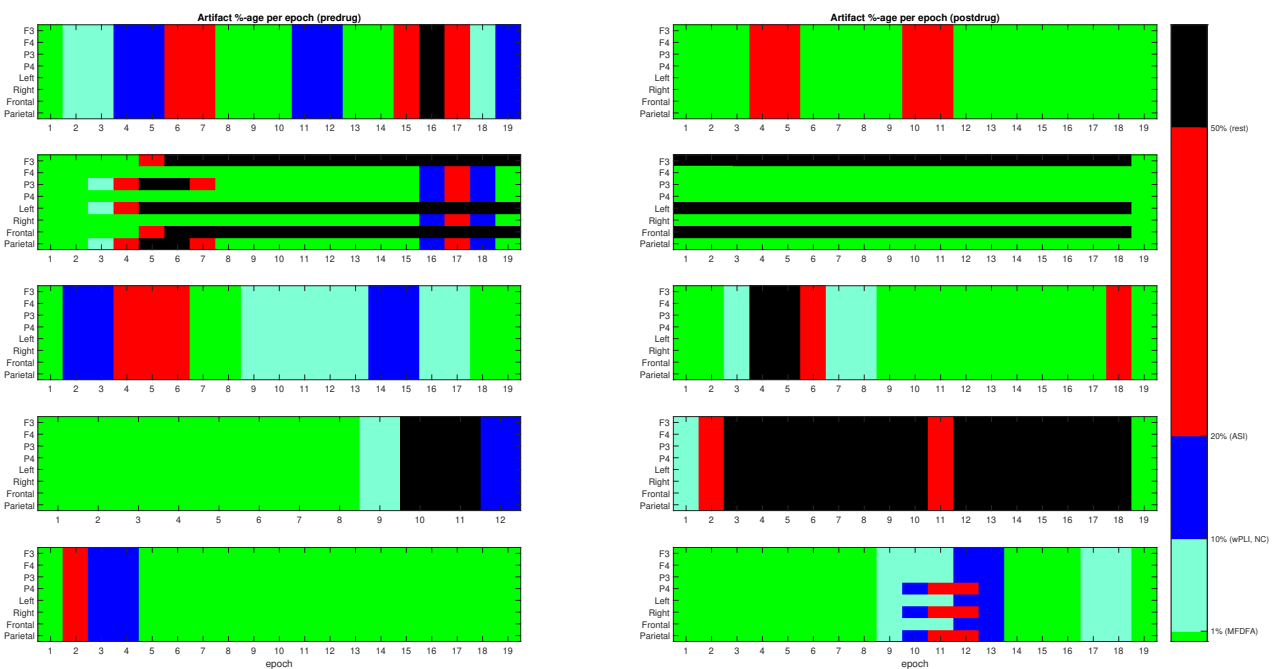


wPLI 1-3 Hz										wPLI 3-8 Hz									
time after drug [s]	F3 vs F4		F3 vs P3		F4 vs P4		P3 vs P4		time after drug [s]	F3 vs F4		F3 vs P3		F4 vs P4		P3 vs P4			
	CC	p	CC	p	CC	p	CC	p		CC	p	CC	p	CC	p	CC	p		
0-120	-0.8042	0.001615	-0.20979	0.512841	-0.7967	0.001114	-0.44505	0.127524	0-120	-0.42657	0.1667	-0.43357	0.159106	-0.06044	0.844502	-0.41758	0.155675		
60-180	-0.7	0.016471	-0.67273	0.023313	-0.58042	0.047856	-0.0979	0.762122	60-180	-0.5	0.117307	-0.38182	0.24656	-0.4965	0.100503	-0.43357	0.159106		
120-240	-0.73333	0.015801	-0.22424	0.533401	-0.32121	0.365468	-0.40606	0.244282	120-240	-0.62424	0.053718	-0.41818	0.229113	-0.63636	0.047912	-0.85455	0.001637		
180-300	-0.57143	0.2	-0.14286	0.78254	-0.64286	0.096181	0.142857	0.752034	180-300	-0.10714	0.839683	-0.85714	0.02381	-0.45238	0.26746	-0.71429	0.057589		
240-360	-0.7381	0.045833	0.166667	0.703323	-0.05	0.911618	-0.45	0.229817	240-360	-0.14286	0.752034	-0.38095	0.359871	-0.78333	0.017223	-0.73333	0.031123		
300-420	0.183333	0.64364	0.183333	0.64364	-0.22424	0.533401	-0.11515	0.75142	300-420	-0.71667	0.036866	-0.85	0.006074	-0.62424	0.053718	-0.84242	0.00222		
360-480	-0.69697	0.025097	-0.51515	0.127553	-0.39394	0.259988	-0.06667	0.854813	360-480	-0.34545	0.328271	-0.86667	0.001174	-0.70909	0.021666	-0.090909	0.802772		
420-540	-0.86667	0.001174	-0.27273	0.445838	-0.49091	0.149656	-0.7697	0.009222	420-540	-0.89091	0.000542	-0.53939	0.107593	-0.86667	0.001174	-0.41818	0.229113		
480-600	-0.55455	0.076652	-0.45455	0.160145	-0.26364	0.433441	-0.79091	0.003746	480-600	-0.47273	0.141999	-0.49091	0.125204	-0.79091	0.003746	-0.79091	0.003746		
540-660	-0.8303	0.00294	-0.30909	0.384841	-0.68485	0.028883	-0.67879	0.000814	540-660	-0.30909	0.384841	0.10303	0.776998	-0.21212	0.556306	-0.46667	0.173939		

wPLI 8-15 Hz										wPLI 15-30 Hz									
time after drug [s]	F3 vs F4		F3 vs P3		F4 vs P4		P3 vs P4		time after drug [s]	F3 vs F4		F3 vs P3		F4 vs P4		P3 vs P4			
	CC	p	CC	p	CC	p	CC	p		CC	p	CC	p	CC	p	CC	p		
0-120	-0.06294	0.845931	0.013986	0.96559	-0.53297	0.060737	-0.8956	3.48E-05	0-120	-0.02098	0.948402	-0.43357	0.159106	-0.52747	0.063955	-0.49451	0.085824		
60-180	-0.56364	0.070952	0.327273	0.325895	-0.41958	0.174519	-0.72028	0.00824	60-180	-0.74545	0.008455	-0.57273	0.065543	-0.64336	0.024003	-0.59441	0.041521		
120-240	-0.01818	0.96024	-0.0303	0.933773	-0.39394	0.259988	-0.38182	0.276205	120-240	-0.78182	0.007547	-0.47879	0.161523	-0.27273	0.445882	-0.78182	0.007547		
180-300	-0.42857	0.353571	-0.82143	0.0343127	-0.38095	0.359871	-0.42857	0.299206	180-300	-0.60714	0.166667	0.035714	0.963492	0.238095	0.582143	-0.35714	0.389385		
240-360	-0.88095	0.007242	0.095238	0.840129	-0.6	0.096798	-0.81667	0.010769	240-360	-0.71429	0.057589	-0.57143	0.151141	-0.8	0.013828	-0.41667	0.269582		
300-420	-0.66667	0.05889	-0.4	0.291193	-0.27273	0.445838	-0.8303	0.00294	300-420	-0.6	0.096798	-0.86667	0.004508	-0.21212	0.556306	-0.75758	0.011143		
360-480	-0.67273	0.033041	-0.27273	0.445838	-0.61212	0.059972	-0.68485	0.028883	360-480	-0.8303	0.00294	-0.57576	0.081553	-0.49091	0.149656	-0.63636	0.047912		
420-540	-0.61212	0.059972	-0.78182	0.007547	-0.53939	0.107593	-0.12727	0.726057	420-540	-0.61212	0.059972	-0.66061	0.037588	-0.69697	0.025097	-0.50303	0.138334		
480-600	-0.51818	0.102492	-0.60909	0.046696	-0.44545	0.169733	-0.45455	0.160145	480-600	-0.66364	0.025984	-0.36364	0.271638	-0.61818	0.042646	-0.58182	0.06042		
540-660	-0.80606	0.004862	-0.67273	0.033041	-0.85455	0.001637	-0.2	0.579584	540-660	-0.34545	0.328227	-0.04242	0.907364	-0.22424	0.533401	-0.39394	0.259998		

## B. Artifact Percentage Table

This appendix includes the visualization of the artifact percentage present in the data for all 15 subjects. These visualizations include all the available pre-drug epochs and the first 19 post-drug epochs. The artifact percentage thresholds are color-coded, and explained in the colorbar on the right. For example, epochs marked with green had less than 1 % of artifact-ridden samples, while those marked with black had more than 50% of the samples marked as unusable data.



Artifact Percentage Table

